



저작자표시-비영리-변경금지 2.0 대한민국

이용자는 아래의 조건을 따르는 경우에 한하여 자유롭게

- 이 저작물을 복제, 배포, 전송, 전시, 공연 및 방송할 수 있습니다.

다음과 같은 조건을 따라야 합니다:



저작자표시. 귀하는 원저작자를 표시하여야 합니다.



비영리. 귀하는 이 저작물을 영리 목적으로 이용할 수 없습니다.



변경금지. 귀하는 이 저작물을 개작, 변형 또는 가공할 수 없습니다.

- 귀하는, 이 저작물의 재이용이나 배포의 경우, 이 저작물에 적용된 이용허락조건을 명확하게 나타내어야 합니다.
- 저작권자로부터 별도의 허가를 받으면 이러한 조건들은 적용되지 않습니다.

저작권법에 따른 이용자의 권리는 위의 내용에 의하여 영향을 받지 않습니다.

이것은 [이용허락규약\(Legal Code\)](#)을 이해하기 쉽게 요약한 것입니다.

[Disclaimer](#)

Doctoral Thesis

Synthesis of Mussel-Inspired Functional Materials for Surface Modification

Eeseul Shin

Department of Chemistry

Graduate School of UNIST

2019

Synthesis of Mussel-Inspired Functional Materials for Surface Modification

Eeseul Shin

Department of Chemistry

Graduate School of UNIST

Synthesis of Mussel-Inspired Functional Materials for Surface Modification

A thesis/dissertation
submitted to the Graduate School of UNIST
in partial fulfillment of the
requirements for the degree of
Doctor of Philosophy

Eeseul Shin

05/24/2019 of submission

Approved by



Advisor

Dong Woog Lee

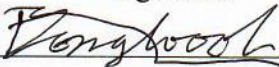
Synthesis of Mussel-Inspired Functional Materials for Surface Modification

Eeseul Shin

This certifies that the thesis/dissertation of Eeseul Shin is approved.

05/24/2019 of submission

signature



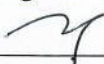
Advisor: Dong Woog Lee

signature




Byeong-Su Kim: Thesis Committee Member #1

signature



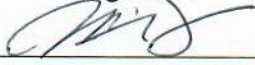
Young S. Park: Thesis Committee Member #2

signature



Chaenyung Cha: Thesis Committee Member #3

signature



Soo-Hyung Choi: Thesis Committee Member #4;

Abstract

Mussel enables surface independent wet adhesion with the secretion of mussel foot protein. Mussel foot protein contains a unique amino acid, Dopa, as the key of adhesion. Catechol functional group of Dopa introduces robust and durable adhesion properties, hence, catechol is attracted the intensive interest as a universal anchoring block for surface modification. The catechol-functionalized materials are applied for a wide range of applications such as biomedical, energy storage and environmental applications. In this regard, this thesis describes the synthesis of catechol-functionalized materials and the use of the materials for various applications.

This thesis divided into three part; (1) catechol-functionalized dental primer, (2) antifouling coating of catechol functionalized polymer (3) wet-adhesion of catechol-amine functionalized polymer.

In the first part, the catecholic primer with (meth)acrylate group was synthesized. The catecholic primers effectively crosslink the glass substrate and polymer-based resin matrix with a simple drop-casting method. The composite resin containing the catecholic primers exhibited improved mechanical properties comparable with commercial silane primers.

The second part introduced catechol-functionalized block copolymer initiated by polyethylene glycol (PEG). The catechol anchoring block offers a binding ability to substrate while PEG shows antifouling effect. The antifouling effect according to the various composition and conformation was studied using quartz crystal microbalance. (QCM) and surface force apparatus (SFA).

Finally, the wet-adhesion of Dopa and lysine of mussel foot protein was translated to polyether system. The protected catechol and azide functionalized epoxide were synthesized and copolymer was prepared with different composition. The surface interaction of copolymers was investigated by SFA to reveal the synergistic adhesion of catechol and amine.

Contents

Contents	I
List of Figures	III
List of Tables	VII
Chapter 1. Background and introduction	1
1.1 Mussel foot protein	1
1.2. Catechol Chemistry.....	2
1.3. Catechol incorporated polymer preparation.....	7
1.4. Applications of catechol-functionalized polymers.....	9
1.5. References.....	12
Chapter. 2. Bioinspired Catecholic Primers for Rigid and Ductile Dental Resin Composites	16
2.1 Introduction.....	16
2.2. Materials and methods	19
2.3. Results and discussion	22
2.4. Conclusion	31
2.5. References.....	32
Chapter 3. Bioinspired Bifunctional Block-Copolymers with superior antifouling properties	36
3.1. Introduction.....	36
3.2. Materials and methods	37
3.3. Results and discussion	42
3.4. Conclusion	58
3.5. References.....	59
Chapter 4. Synergistic adhesion properties of catechol and amine functionalized polyether	63
4.1 Introduction.....	63
4.2. Materials and methods	65
4.3. Results and discussion	70
4.4. Conclusion	75

4.5. References.....	76
Chapter 5. Summary	78
Lists of publications	79

List of Figures

Chapter 1.

Figure 1.1. (a) The structure of mussel byssus. (b) The distribution of mussel foot proteins in the byssal plaque.

Figure 1.2. The amino acid sequence and composition of mussel foot protein in the adhesive plaque.

Figure 1.3. The versatility of catechol-based chemistry. (a, b) Reversible reduction/oxidation. (c) Coordination with metal ion. (d) pH-responsive catechol-boronate complex. (e) π - π stacking with aromatic rings (f) Coordination bonds with inorganic surface. (g) Cation- π interaction (h, i) Hydrogen bonding (j) Schiff base reaction (k) Michael-type addition with thiols (l, m) amine or other catechol (n) dimer.

Figure 1.4. Catechol-functionalized materials based on non-covalent interaction. (a) Self-healing hydrogel. (b) Hydrogel actuators. (c) pH-responsive drug delivery system. (d) Mechanically improved polymeric fibers

Figure 1.5. (a) Covalent interaction of o-quinone and amine. (b) Proposed progressive assembly for polydopamine coating.

Figure 1.6. Schematic illustration of the strategies for the synthesis of catechol incorporated polymers

Figure 1.7. Biomedical applications of catechol-functionalized polymers (a) Wet adhesion of mussel and catechol-functionalized polymer poly[(3,4-dimethoxystyrene)-co-(styrene)]. (b) Catechol-functionalized polymer loops for lubrication antifouling properties. (c) Catechol-functionalized dental adhesive polymer (d) pH-responsive self-healing hydrogel using the boronate ester.

Chapter 2.

Figure 2.1. (a) A schematic cartoon of mussel byssal threads, which are produced in the mussel foot to adhere to mineral substrates. (b) Synthetic pathways of catecholic primers (catechol acrylate primer (CAP) and catechol methacrylate primer (CMP)) derived from eugenol.

Figure 2.2. ^1H NMR spectra of (a) acrylate primer (CAP) and (b) methacrylate primer (CMP).

Figure 2.3. (a) Representative AFM images of bare silicon wafer and silane-, catechol acrylate (CAP)- and catechol methacrylate (CMP)-primed surfaces with corresponding line scan profiles. (b) Static contact angles of the bare and the primed glass substrates.

Figure 2.4. (a) A photograph of the knife shear test and schematic representation of catecholic primer bridging (coupling) between glass and PMA resin. (b) Knife shear strength of methacrylate primer in various concentrations (0.07 – 10 mg/mL) and solvents (methanol and acetone). (c) Comparison of the knife shear strength of catecholic primers (concentration: 0.15 mg/mL). Bars with the different letters are significantly different according to Turkey's HSD.

Figure 2.5. Schematic of sample preparation for the knife shear test.

Figure 2.6. Surface roughness in our terms of "RMS" consisted of square pyramid valleys of base area 1 nm^2 and nm height denoted by "RMS". Each square grid is a section of the total nanoparticle surface area, which is also denoted. To quantify surface roughness, we approximated "RMS" as a height of square pyramid valleys in the glass surface. Each catechol-methacrylate molecule is assumed to occupy 1 nm^2 on the substrate surface, for the hydrogen bonding employed by catechol creates a dynamic system that occupies space as such. Through stoichiometric calculations, we prepared solutions as follows: RMS 10 nm (0.07 mg/mL), RMS 20 nm (0.15 mg/mL), RMS 40 nm (0.30 mg/mL), RMS 100 nm (0.78 mg/mL), RMS 1200 nm (10 mg/mL).

Figure 2.7. Compression tests of dental composites. (a) A schematic representation of the compression test. (b) Images of the silane, CAP, and CMP composite samples during the compression test. (c) Representative stress-strain curves for the dental composites. (d) Elastic modulus and (e) ultimate stress (left), strain at failure (middle), and toughness (right) of all dental composites prepared. Bars with the different letters are significantly different according to Turkey's HSD.

Figure 2.8. A stress-strain curve shows compressive stress (σ in MPa) of a material responding to displacement (strain, ε in %). A slope of elastic region (elastic modulus, yellow), the cross-sectional area under the stress-strain curve (toughness, red), highest stress withheld by the specimen (ultimate strength, green) and strain at complete breakage (strain at failure, blue) were calculated.

Figure 2.9. (a) Optical microscopy images of L929 cells seeded on the priming surfaces using various primer solutions for 24 h (conc. 0.15 mg/mL). (b) Relative cell viability on the priming surfaces. The cell viability of the control group was normalized to 100%.

Chapter 3.

Figure 3.1. Fabrication of catechol-functionalized polymer films presenting the antifouling effect. (a) Synthesis of acetonide-protected catechol functionalized triblock copolymer. (b) ^1H NMR spectra of CAG and catechol functionalized triblock copolymer (L10K-10). (c) Schematic illustration of antifouling polymer coated surfaces.

Figure 3.2. Synthesis of acetonide-protected catechol functionalized monomer (CAG)

Figure 3.3. ^{13}C NMR spectrum of CAG

Figure 3.4. COSY NMR spectrum of CAG

Figure 3.5. ^1H NMR spectra of homopolymerization of CAG using CsOH at high temperature

Figure 3.6. ^1H NMR spectrum of *L10K-10

Figure 3.7. SEC trace of bare PEG and catechol functionalized polymers in DMF at 40 °C

Figure 3.8. (a) The molecular weight of ethylene oxide and CAG. (b) MALDI-TOF spectrum of *L10K-10. (c) MALDI-TOF spectrum of CAG homopolymer

Figure 3.9. (a) TGA of catechol-functionalized triblock copolymers (b) T_g of various catechol functionalized polymers

Figure 3.10. PEG hydrolysis test. (a) SEC trace and (b) molecular weight obtained by SEC

Figure 3.11. The UV-Vis spectra of protected (*L10K-10) and deprotected (L10K-10) polymer in pH 8.5 aqueous solution. Inset shows the protected polymer solution (left) and deprotected solution (right).

Figure 3.12. (a) Topographic AFM images and section plots of *L10K-10, L10K-10, and B5K-10 coating on silicon wafer (polymer concentration: 10 mg mL⁻¹). (b) The static water contact angle of various bare surfaces, L10K-10 treated surfaces, and B5K-10 treated surfaces

Figure 3.13. Static water contact angle after polymer coating

Figure 3.14. Schematics depicting antifouling study of polymer films using surface force apparatus (SFA) and force-distance profile between two polymer films. Force-distance profiles between (a) L10K-10 and (b) B5K-10 films with different buffers; 10 mM PBS, BSA solution with 1 h incubation,

and 10 mM PBS

Figure 3.15. The semi-log plot of the approach curves of (a) L10K-10 and (b) B5K-10. The solid line indicates the measured decay length.

Figure 3.16. (a) Schematic illustration of antifouling test by QCM-D (b) Frequency and dissipation shift associated with the adsorption of polymer (L10K-10) and protein on gold sensor. (c) Adsorption of polymers on bare gold surfaces. (d) Adsorption of BSA on bare and polymer immobilized gold surfaces.

Figure 3.17. $\Delta D/\Delta F/n$ plot of the adsorption of L10K-10

Figure 3.18. Cell attachment on each surface

Chapter 4.

Figure 4.1. (a) Primary sequence of mfp-5 and Structure of mussel-inspired functional epoxide monomers. (b) Synthesis of amine and catechol functionalized copolymer. (c) ^1H NMR spectra of amine and catechol functionalized copolymer (AC1)

Figure 4.2. ^1H NMR spectrum of AHGE

Figure 4.3. ^{13}C NMR spectrum of AHGE

Figure 4.4. ^1H - ^1H COSY NMR spectrum of AHGE

Figure 4.5. ^1H NMR spectrum of AC1 before deprotection

Figure 4.6. (a) Schematic representation of adhesion and cohesion mechanism of amine and catechol functionalized polymer with mica substrate. (b) Representative force-distance curves of AC1 (0.1 mg mL⁻¹). Effect of pH and contact time on Interaction energy of AC polymers with different catechol contents in (c) symmetric mode and (d) asymmetric mode.

Figure 4.7. Representative force-distance curves of AC1 (0.1 mg mL⁻¹) with different pH.

List of Tables

Chapter 2.

Table 2.1. Polymerization-induced shrinkage of resin composites

Chapter 3.

Table 3.1. Characterization of PCAG homopolymer using CsOH

Table 3.2. Characterization of the catechol-functionalized polymers

Table 3.3. Dry mass and surface grafting density of catechol-functionalized polymer

Chapter 4.

Table 4.1 Characterization of azide and protected catechol-functionalized polymers

Chapter 1. Background and introduction

1.1 Mussel foot protein

Mussel is a marine organism which attaches to various surfaces under salty and wet environment. Mussel attaches to wetted surface using byssal threads, which is secreted under acidic condition and rapidly matured in water.¹ Because wet-adhesion is still remains an issue for most synthetic adhesive, strong wet adhesion properties of mussel attracted much interest.² Marine mussels secrete a various kinds of mussel foot proteins (Mfp) and form adhesive plaques to attach to a wide range of substrates. At least nine mfps have been identified from several species of mussel, and the sequence of amino acid of some Mfp was investigated.^{3,4} The unique feature of mussel protein is high content of a catecholic amino acid, 3,4-dihydroxyphenylalanine (Dopa), which is the result from posttranslational modification of tyrosine.⁵ The catechol functional group of Dopa offers the surface-independent and water-resistant adhesion properties which can be used as versatile platform for surface modification.

As shown in **Figure 1.1**, Mfps contain various amount of Dopa and they contribute to curing plaque or interfacial binding. Mfp-1 is a high molecular protein that compose the cuticle and serves to protect adhesive plaques from the external environment, whereas from Mfp-2 to Mfp-6 is located inside the plaques.³ Mfp-2 is abundant protein within the plaques and contains more cysteine residues (6 mol %) than other proteins.⁶ Mfp-4 contains high contents of histidine and achieve coupling with transition metal ion. It also distributed between the byssal thread and the adhesive plaques to linking plaque proteins. Mfp-3, 5, and 6 located in the area where the plaques interact with the surface, that is, the center of wet adhesion (**Figure 1.2**). Mfp-3 contains a large amount of glycine and asparagine and it can be categorized into Mfp-3f and Mfp-3s.⁷ Especially, Mfp-3f contains a high portion of Dopa (21 mol%) and cationic amino acid. Mfp-3s, on the other hand, contain relatively low contents of Dopa (5-10 mol) and have a small charge of density. Mfp-3s can delay the oxidation of Dopa in seawater with basic pH, which renders the diverse chemistry with reduced catechol. Mfp-5 contains the highest portion of Dopa and cationic amino acids.³ Moreover, it contains post-translationally modified phosphoserine, which contributes interfacial binding with the calcareous mineral surface.⁸ While Mfp-6 contains lower amount of Dopa, it contains 11 mol % of cysteine. The role of Mfp-6 is to link the interfacial protein and plaque protein. Moreover, the antioxidant thiolate protects Dopa of mfp-3 and mfp-5 from oxidation.

Although each protein has a different amino acid content depending on its role and location, there is a common characteristic of Mfp is the presence of Dopa. Dopa is involved in various areas from

surface adhesion to curing. The catechol chemistry which renders this fascinating property is discussed in the following section.

1.2. Catechol Chemistry

The catechol functional group of Dopa offers the strong adhesion onto various surface or cohesion with catechol-containing adhesives. Therefore, the chemical structure and binding mechanism of catechol have been studied. As shown in Figure 1.3, catechol forms reversible non-covalent interaction or irreversible covalent interaction.

1.2.1. Non-covalent interaction

The aromatic ring of catechol form π - π stacking interaction which can be attributed to the cohesion with catechol-based materials and attached to the aromatic-rich surfaces such as polystyrene and gold.⁹ Moreover, the aromatic ring achieve cation- π interaction which enables binding to the charged surface and contributes to the cohesive interaction of functional materials which contains both cationic and aromatic moieties.^{10,11} The dihydroxyl functionality of catechol form hydrogen bond with mucosal tissue and hydroxyapatite surface.^{12,13}

The catechol can form a coordination bond with a metal ion (Ca^{2+} , Cu^{2+} , Fe^{3+} , Mn^{3+} , Ti^{4+}) with various stoichiometry depending on the valency of metal ion and pH.^{14,15} The increment of pH enables the higher-order coordination (tris-complexes) which gives more stability. Therefore, the catechol-metal coordination improves high extensibility, hardness, and self-healing property of mussel byssus cuticle.¹⁶ In addition to the metal ions, catechol form an interfacial bond with metal or metal oxide surfaces (Al_2CO_3 , Fe_3O_4 , SiO_2) which can be utilized as a versatile surface modification agent.¹⁷

Moreover, the catechol and boronic acid form a reversible catechol-boronate complex which is pH-responsive.¹⁸ These pH-responsive, self-healing properties from non-covalent interaction of catechol have been employed to create self-healing hydrogel, hydrogel actuators, pH-responsive drug delivery system and mechanically improved polymeric fibers.¹⁹⁻²²

1.2.2 Covalent interaction

Catechol can be oxidized by basic pH, oxidizing agent (IO_4^- , H_2O_2) and enzyme (tyrosinase, peroxidase).²³ The one-electron oxidation of catechol to the *o*-semiquinone radical and disproportionation reaction of two radical to *o*-quinone has been reported.²⁴ *o*-Quinone is unstable intermediates and highly reactive in various organic species such as amine and thiol. The between *o*-quinones and amines, such as Michael-type addition, Schiff base reaction, and Strecker degradation was shown in Figure 1.5a. The reaction mechanism of *o*-quinones and amine is determined by the structure of amine, such as Michael-type addition with aromatic amines and Schiff base reaction with aliphatic amines.²⁵

In the case of Michael-type addition, amine attack quinone to form quinone-amine species. Even though the reaction mechanism is unclear, the existence of stable covalent dopa-N bond was revealed.²⁶ The reaction rate of Michael addition is affected by pH, the structure of catechol functional group, and the basicity of amine. The reaction rate of Michael addition can be highly affected by pH, by adjusting the protonation state of amine. Therefore, the rate constant of Michael addition reaction increased with increasing pH. The structure of catechol moieties also affects the Michael addition reaction. The reaction constant of 4-methylcatechol is lower than catechol, due to the steric hindrance of the methyl group.²⁷ Moreover, the high concentration of nucleophile accelerates the reaction rate, hence the aromatic amine undergoes Michael addition even at acidic pH.²³

Schiff base reaction is also a reaction between *o*-quinone and amine. Although the reaction mechanism is not fully understood, the product of the Schiff base reaction was identified. The reaction occurs faster under higher pH. It also affected by the aliphatic chain length of amine, because longer chain decreases the basicity of $\alpha\text{-NH}_2$, which enables the reaction performed at lower pH.²⁸

Especially in the case of dopamine where catechol and free amine exist at the same molecule, they can self-polymerized by intramolecular cyclization.²⁹ Polydopamine, the polymeric form of dopamine can attach to various substrates and extensively studied for biomedical applications such as surface modification, antifouling coatings.³⁰ Despite the extensive research using the versatility of polydopamine was performed, the challenge to reveal the molecular mechanism is still remained. As shown in Figure 1.5b, the polydopamine is composed of covalently bonded oligomers and physically assembled.³¹

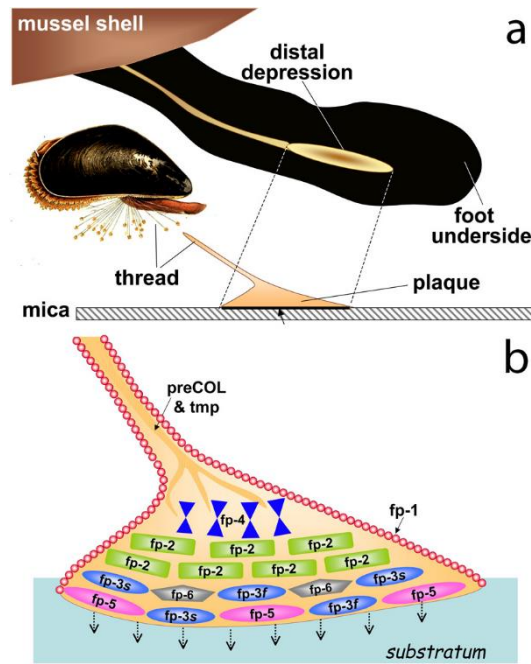


Figure 1.1. (a) The structure of mussel byssus. (b) The distribution of mussel foot proteins in the byssal plaque. Reprinted with permission from ref³². Copyright 2012 Taylor & Francis Group.

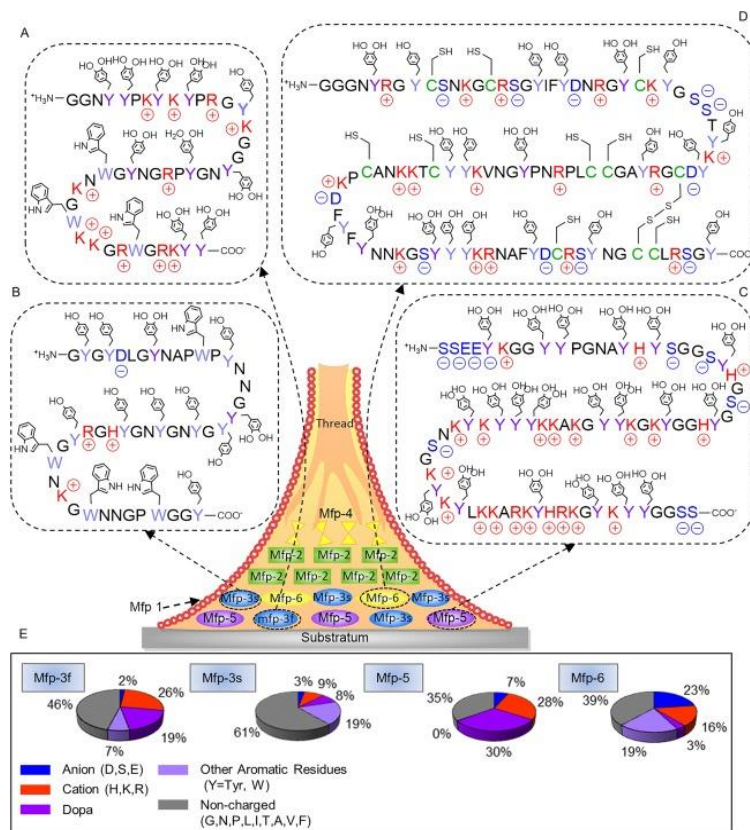


Figure 1.2. The amino acid sequence and composition of mussel foot protein in the adhesive plaque. Reprinted with permission from ref³³. Copyright 2017 Wiley.

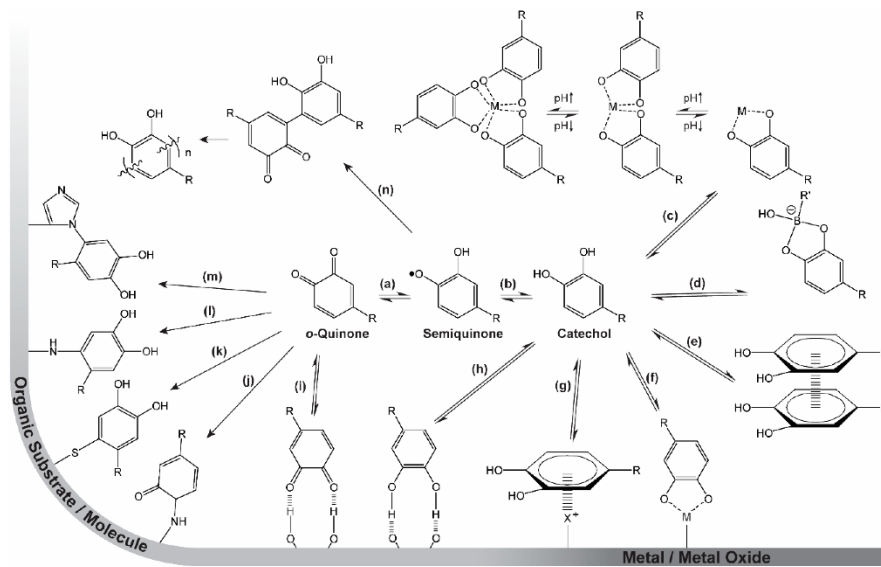


Figure 1.3. The versatility of catechol-based chemistry (a-b) Reversible reduction/oxidation. (c) Coordination with metal ion. (d) pH-responsive catechol-boronate complex (e) π - π stacking with aromatic moieties (f) Coordination bonds with inorganic surface. (g) Cation- π interaction. (h, i) Hydrogen bonding. (j) Schiff base reaction (k) Michael-type addition with thiols (l, m) amine or other catechol (n) dimer. Reprinted with permission of ref³⁴. Copyright 2019 MDPI

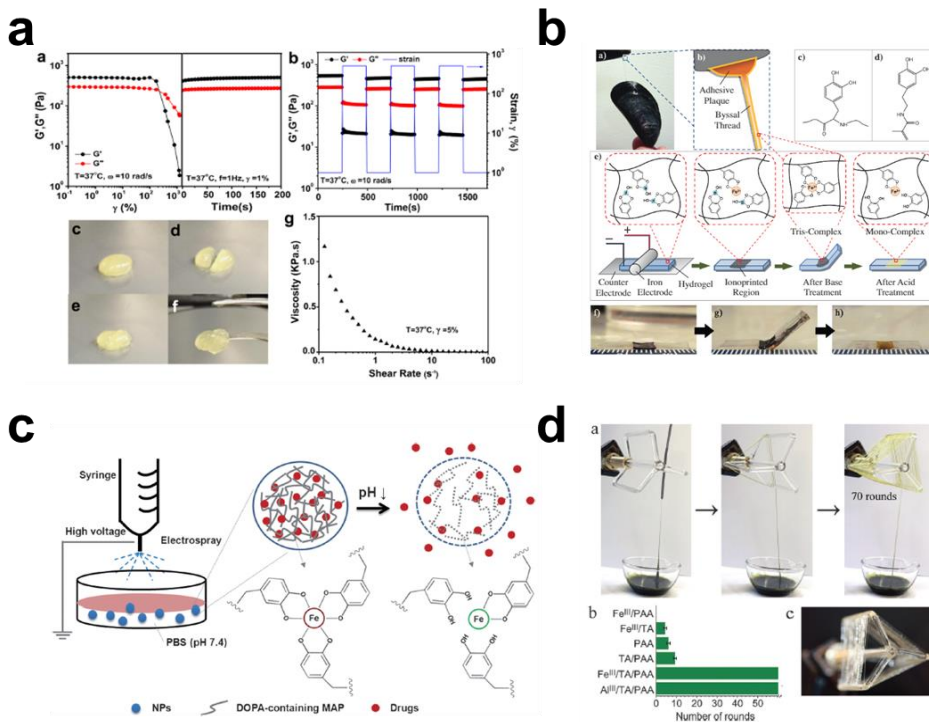


Figure 1.4. Catechol-functionalized materials based on non-covalent interaction. (a) Self-healing hydrogel. Reprinted with permission from ref¹⁹. Copyright 2017 American Chemical Society (b) Hydrogel actuators. Reprinted with permission from ref²⁰. Copyright 2014 Wiley. (c) pH-Responsive drug delivery system. Reprinted with permission from ref²¹. Copyright 2015 Wiley. (d) Mechanically improved polymeric fibers. Reprinted with permission from ref²². Copyright 2014 Royal Society of Chemistry.

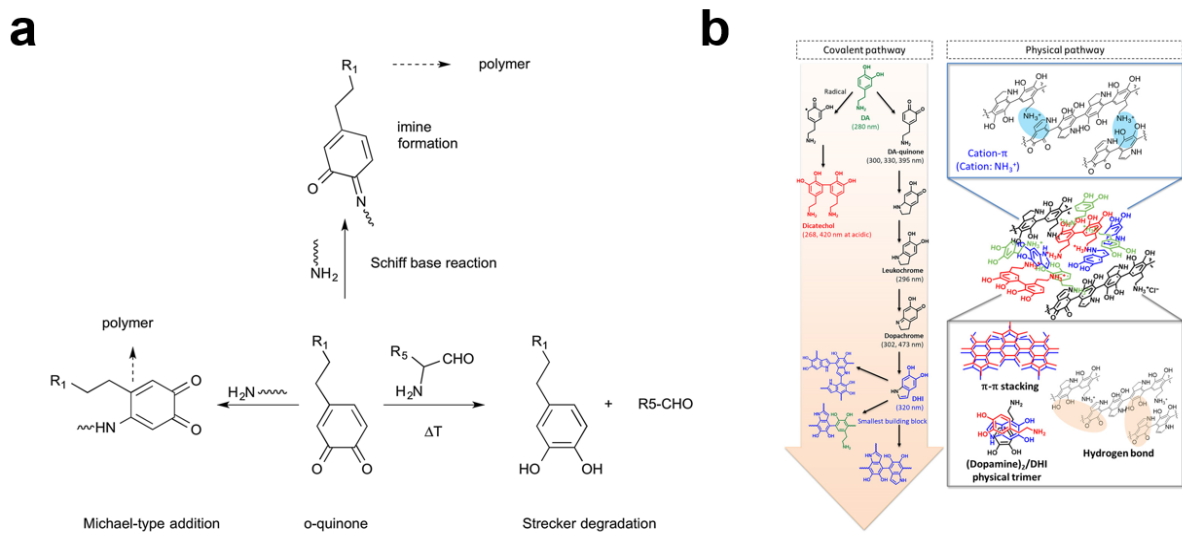


Figure 1.5. (a) Covalent interaction of *o*-quinone and amine. Reprinted with permission from ref³⁵. Copyright 2014 Royal Society of Chemistry. (b) Proposed progressive assembly for polydopamine coating. Reprinted with permission from ref³¹. Copyright 2018 Science.

1.3. Catechol incorporated polymer preparation

Inspired by the versatility of the catechol moieties, catechol has been adapted to synthetic polymer system to develop strong wet adhesive properties and curing. There are three strategies to synthesis catechol incorporated polymer; direct functionalization of polymers with catechol-containing compound, polymerization of catechol-functionalized monomer, and polymerization using the catechol-functionalized initiator (Figure 1.6).

The catechol functional group such as dopamine and eugenol can be conjugated to the polymer by forming amide, urethane, ester and thiol-ene chemistry.^{36,37} The strategy can be adapted to polymers with various architecture and functionality and the resulting polymers can obtain the binding ability of catechol functional group. Especially, the biopolymer which contains numerous reactive functional groups can be easily modified and employed for biomedical applications. Lee et al modified chitosan using catechol functional group.³⁸ The chitosan-catechol rapidly interact with blood protein and exhibits hemostatic ability.

Catechol containing initiator can be utilized to end-functionalization with binding ability. Hyperbranched polyglycerol synthesized using catechol functionalized initiator and adapted to surface modification of manganese oxide (MnO) nanoparticle.³⁹ The hydrophilicity of polyglycerol enhances the water solubility and biocompatibility of MnO nanoparticle, render the potential as a contrast agent for MRI measurement.

The catechol-functionalized polymer can be prepared using catechol-functionalized monomer, which enables a broad range of molecular weight, catechol contents. The most of catechol-functionalized monomer based on the radical polymerization of a vinyl monomer. For example, Patil et al polymerized protected dopamine (meth)acrylamide monomers (ADA and ADMA) and polymerized with (methacryl)amide monomer with pendent PEG chain.⁴⁰ The hydrophilic PEG chains effectively inhibited the protein adsorption while the catechol group immobilized the polymer on the substrate.

The dopamine (meth)acrylamide monomer also copolymerized with 2-aminoethylmethacrylamide hydrochloride (AMEA) using free-radical polymerization.⁴¹ After deprotection of the polymer, the elevation of pH and addition of sodium periodate (NaIO₄) induce the crosslinking of free amine and o-quinone using Schiff-base reaction and Michael-type addition. The polymer film, which comes from water-soluble precursor was stable and highly adhesive to a glass substrate.

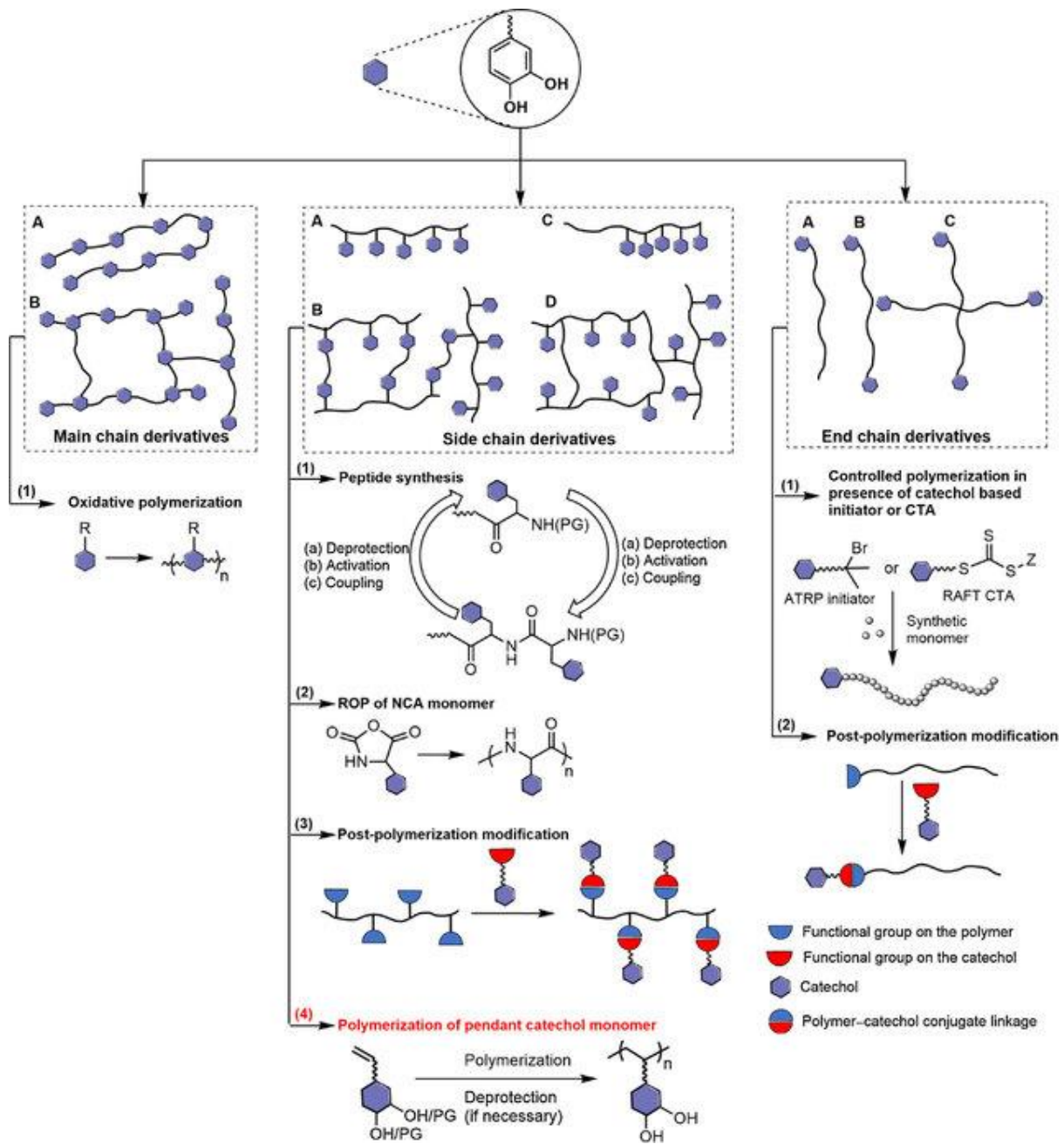


Figure 1.6. Schematic illustration of the strategies for the synthesis of catechol incorporated polymers. Reprinted with permission from ref⁴². Copyright 2018 Elsevier

1.4. Applications of catechol-functionalized polymers

1.4.1 Polymer adhesive

Inspired by the adhesion ability of mussel-foot protein, catechol-functionalized polymers have been utilized as adhesives. The various catechol-functionalized polymers with different molecular weight and composition were applied to surface coating.

The underwater adhesion is still challenging in synthetic adhesive system. To translate the wet-adhesion ability of catechol, poly[(3,4-dihydroxystyrene)-co-styrene] was synthesized.⁴³ The adhesion strength was examined with various molecular weight and composition. The underwater bonding of poly[(3,4-dihydroxystyrene)-co-styrene] was measured and adhesion strength exhibited outstanding property under wet and salty environment when it compared to commercial adhesives.

In mussel adhesion, the coacervate formation of polyelectrolyte proteins forms dense fluid with low interfacial energy and reduced viscosity. The self-coacervation of mfp-3s was translated into a polymer system, and a series of the ampholytic copolymer was prepared to study the microphase behavior.⁴⁴ The mfp-3s mimetic copolyacrylate reported the strong wet-cohesion, which surpass the cohesion of mussel foot proteins.

1.4.2 Surface modification

The catechol functional group has been introduced to a polymer system to anchor the functional polymer onto the surface.

The antifouling polymer can be grafted to various surfaces and inhibit the adhesion of biomaterials, such as protein, cell, and marine organisms. The catechol moiety was functionalized at the chain end of poly(ethylene glycol) (PEG) using thiol-ene chemistry as anchoring blocks.⁴⁵ The triblock copolymers form loop conformation, which enhances the antifouling property of PEG and lubrication. The poly-2-ethyl-2-oxazoline (PEOXA) with loop conformation and cyclic conformation was achieved using nitro catechol group.⁴⁶ The cyclic conformation effectively improved the antifouling property rather than loop conformation, which deduce the potential for biomedical applications.

Immobilization of biomolecules has also been explored for various biomedical applications. The copolymerization of polydopamine (PDA) and hexamethylenediamine (HD) gives cytocompatibility and tissue compatibility to the surface of 316L SS implants.⁴⁷ The primary amine groups of the PDAM/HD coated surface enables the heparin conjugation with biological activity.

One interesting use of catechol-functionalized polymer is a dental primer. The catechol-functionalized polymer, poly(DMA-MEA) was prepared as a dental adhesive by free radical

polymerization of dopamine-methacrylate (DMA) and 2-methoxyethyl acrylate (MEA).⁴⁸ This dental adhesive was successfully bonded onto the saliva contaminated dental surface. Additionally, Fe³⁺ additive reinforces the adhesion strength by formation of Fe-catechol complex. The Fe-catechol complex prevents the leakage of the bonding interface even in the presence of saliva, which exhibits potential as a dental primer. The bifunctional catechol primer molecule was also synthesized and compared with traditional silane-based primers.^{49,50} The bioinspired primer treated glass filler was adopted to the composite resin system and enhanced both of toughness and rigidity with a simple process.

1.4.3 Hydrogel

A significant amount of research has been achieved to prepare hydrogel, which is a highly hydrated three-dimensional polymer network. Due to the physical properties which are similar to human tissues, it offers potentials for biomedical applications.

The pH-responsive smart adhesive hydrogel which form the adhesive polymeric network was synthesized using a catechol-boronate complex.⁵¹ The catechol-boronate complex is stable under neutral or basic pH, which gives a strong adhesion. The incorporation of anionic moiety requires a higher pH for complexation and enhance the binding property at a neutral or basic pH.

Boronate ester, the result of the catechol-boronate complex is reversible with pH which offers the self-healing properties to the hydrogel. The benzoxaborole-containing zwitterionic copolymer (poly(MPC-st-MAABO) and catechol-containing zwitterionic copolymer (poly(MPC-st-DMA) were synthesized using free-radical polymerization.⁵² The hydrogel was crosslinked by benzoxaborole-catechol complexation and fast self-healing property and biocompatibility.

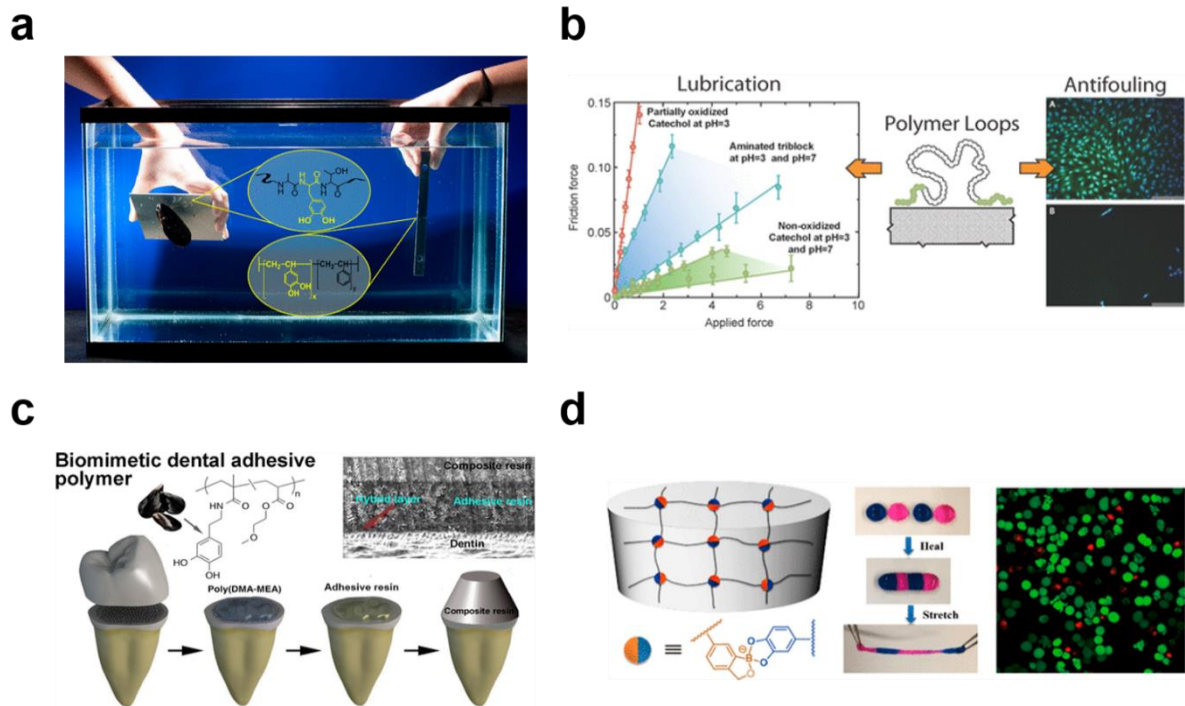


Figure 1.7. Biomedical applications of catechol-functionalized polymers (a) Wet adhesion of mussel and catechol-functionalized polymer poly[(3,4-dimethoxystyrene)-co-(styrene)]. Reprinted with permission from ref⁴³. Copyright 2017 American Chemical Society. (b) Catechol-functionalized polymer loops for lubrication antifouling properties. Reprinted with permission from ref⁴⁵. Copyright 2015 American Chemical Society. (c) Catechol-functionalized dental adhesive polymer. Reprinted with permission from ref⁴⁸. Copyright 2015 American Chemical Society. (d) pH-responsive self-healing hydrogel using boronate ester. Reprinted with permission from ref⁵². Copyright 2018 American Chemical Society.

1.5. References

1. Coyne, K. J.; Qin, X. X.; Waite, J. H. Extensible Collagen in Mussel Byssus: A Natural Block Copolymer. *Science* (80-.). **1997**, *277*, 1830–1832.
2. Bordes, M.; Davies, P.; Cognard, J. Y.; Sohier, L.; Sauvant-Moynot, V.; Galy, J. Prediction of Long Term Strength of Adhesively Bonded Steel/Epoxy Joints in Sea Water. *Int. J. Adhes. Adhes.* **2009**, *29*, 595–608.
3. Zhao, H.; Waite, J. H. Linking Adhesive and Structural Proteins in the Attachment Plaque of *Mytilus Californianus*. *J. Biol. Chem.* **2006**, *281*, 26150–26158.
4. Wei, W.; Yu, J.; Broomell, C.; Israelachvili, J. N.; Waite, J. H. Hydrophobic Enhancement of Dopa-Mediated Adhesion in a Mussel Foot Protein. *J. Am. Chem. Soc.* **2013**, *135*, 377–383.
5. Hammer, M. U.; Danner, E. W.; Kan, Y.; Waite, J. H.; Israelachvili, J. N. Adhesion of Mussel Foot Protein Mefp-5 to Mica: An Underwater Superglue. *Biochemistry* **2012**, *51*, 6511–6518.
6. Rzepecki, L. M.; Hansen, K. M.; Waite, J. H. Characterization of a Cystine-Rich Polyphenolic Protein Family from the Blue Mussel *Mytilus Edulis* L. *Biol. Bull.* **2007**, *183*, 123–137.
7. Zhao, H.; Robertson, N. B.; Jewhurst, S. A.; Waite, J. H. Probing the Adhesive Footprints of *Mytilus Californianus* Byssus. *J. Biol. Chem.* **2006**, *281*, 11090–11096.
8. Waite, J. H.; Qin, X. Polyphosphoprotein from the Adhesive Pads of *Mytilus Edulis*. *Biochemistry* **2001**, *40*, 2887–2893.
9. Waite, J. H. Reverse Engineering of Bioadhesion in Marine Mussels. *Ann. N. Y. Acad. Sci.* **1999**, *875*, 301–309.
10. Das, S.; Rodriguez, N. R. M.; Wei, W.; Waite, J. H.; Israelachvili, J. N. Peptide Length and Dopa Determine Iron-Mediated Cohesion of Mussel Foot Proteins. *Adv. Funct. Mater.* **2015**, *25*, 5840–5847.
11. Gallivan, J. P.; Dougherty, D. A. A Computational Study of Cation- π Interactions vs Salt Bridges in Aqueous Media: Implications for Protein Engineering. *J. Am. Chem. Soc.* **2000**, *122*, 870–874.
12. Schnurrer, J.; Lehr, C. M. Mucoadhesive Properties of the Mussel Adhesive Protein. *Int. J. Pharm.* **1996**, *141*, 251–256.
13. Chirdon, W. M.; O'Brien, W. J.; Robertson, R. E. Adsorption of Catechol and Comparative Solutes on Hydroxyapatite. *J. Biomed. Mater. Res. - Part B Appl. Biomater.* **2003**, *66*, 532–538.
14. Sever, M. J.; Wilker, J. J. Absorption Spectroscopy and Binding Constants for First-Row Transition Metal Complexes of a DOPA-Containing Peptide. *Dalt. Trans.* **2006**, *14*, 813–822.

15. Xu, Z. Mechanics of Metal-Catecholate Complexes: The Roles of Coordination State and Metal Types. *Sci. Rep.* **2013**, *3*, 7–9.
16. Kummert, R.; Stumm, W. The Surface Complexation of Organic Acids on Hydrous γ -Al₂O₃. *J. Colloid Interface Sci.* **1980**, *75*, 373–385.
17. Lee, B. P.; Chao, C. Y.; Nelson Nunalee, F.; Motan, E.; Shull, K. R.; Messersmith, P. B. Rapid Gel Formation and Adhesion in Photocurable and Biodegradable Block Copolymers with High DOPA Content. *Macromolecules* **2006**, *39*, 1740–1748.
18. Pizer, R.; Babcock, L. Mechanism of the Complexation of Boron Acids with Catechol and Substituted Catechols. *Inorg. Chem.* **1977**, *16*, 1677–1681.
19. Li, L.; Yan, B.; Yang, J.; Huang, W.; Chen, L.; Zeng, H. Injectable Self-Healing Hydrogel with Antimicrobial and Antifouling Properties. *ACS Appl. Mater. Interfaces* **2017**, *9*, 9221–9225.
20. Lee, B. P.; Konst, S. Novel Hydrogel Actuator Inspired by Reversible Mussel Adhesive Protein Chemistry. *Adv. Mater.* **2014**, *26*, 3415–3419.
21. Kim, B. J.; Cheong, H.; Hwang, B. H.; Cha, H. J. Mussel-Inspired Protein Nanoparticles Containing Iron(III)-DOPA Complexes for PH-Responsive Drug Delivery. *Angew. Chemie - Int. Ed.* **2015**, *54*, 7318–7322.
22. Krogsgaard, M.; Andersen, A.; Birkedal, H. Gels and Threads: Mussel-Inspired One-Pot Route to Advanced Responsive Materials. *Chem. Commun.* **2014**, *50*, 13278–13281.
23. McDowell, L. M.; Burzio, L. A.; Waite, J. H.; Schaeffer, J. Detection of Cross-Links Formed in Mussel Byssus under High Flow Stress. *J. Biol. Chem.* **1999**, *274*, 20293–20295.
24. Felix, C.; Sealy, R. C. FORMATION OF SEMIQUINONE RADICALS AND THEIR COMPLEXATION WITH. *Photochem. Photobiol.* **1981**, *34*, 423–429.
25. Manthey, M. K.; Pyne, S. G.; Truscott, R. J. W. Addition of Aliphatic and Aromatic Amines to Catechol in Aqueous Solution under Oxidizing Conditions. *Aust. J. Chem.* **1989**, *42*, 365–373.
26. Dalsin, J. L.; Hu, B. H.; Lee, B. P.; Messersmith, P. B. Mussel Adhesive Protein Mimetic Polymers for the Preparation of Nonfouling Surfaces. *J. Am. Chem. Soc.* **2003**, *125*, 4253–4258.
27. Khalafi, L.; Rafiee, M.; Shahbak, M.; Shirmohammadi, H. Kinetic Study of the Oxidation of Catechols in the Presence of N-Methylaniline. *J. Chem.* **2013**, *2013*.
28. Aveldano, M. I.; Sprecher, H. Very Long Chain (C₂₄ to C₃₆) Polyenoic Fatty Acids of the n - 3 and n - 6 Series in Dipolyunsaturated Phosphatidylcholines from Bovine Retina. *J. Biol. Chem.* **1987**, *262*, 1180–1186.
29. Dreyer, D. R.; Miller, D. J.; Freeman, B. D.; Paul, D. R.; Bielawski, C. W. Elucidating the Structure of Poly(Dopamine). *Langmuir* **2012**, *28*, 6428–6435.
30. Kang, S. M.; Hwang, N. S.; Yeom, J.; Park, S. Y.; Messersmith, P. B.; Choi, I. S.; Langer, R.;

- Anderson, D. G.; Lee, H. One-Step Multipurpose Surface Functionalization by Adhesive Catecholamine. *Adv. Funct. Mater.* **2012**, *22*, 2949–2955.
31. Hong, S.; Wang, Y.; Park, S. Y.; Lee, H. Progressive Fuzzy Cation- Assembly of Biological Catecholamines. *Sci. Adv.* **2018**, *4*, 1–11.
 32. Davidson, I.; Scianni, C.; Hewitt, C.; Everett, R.; Holm, E.; Tamburri, M.; Ruiz, G. Mini-Review: Assessing the Drivers of Ship Biofouling Management – Aligning Industry and Biosecurity Goals. *Biofouling* **2016**, *32*, 411–428.
 33. Kord Forooshani, P.; Lee, B. P. Recent Approaches in Designing Bioadhesive Materials Inspired by Mussel Adhesive Protein. *J. Polym. Sci. Part A Polym. Chem.* **2017**, *55*, 9–33.
 34. Andersen, A.; Chen, Y.; Birkedal, H. Bioinspired Metal – Polyphenol Materials : Self-Healing and Beyond. *Biomimetics* **2019**, *4*, 30.
 35. Yang, J.; Cohen Stuart, M. A.; Kamperman, M. Jack of All Trades: Versatile Catechol Crosslinking Mechanisms. *Chem. Soc. Rev.* **2014**, *43*, 8271–8298.
 36. Jeong, Y.; Kim, K. A.; Kang, S. M. Effect of Catechol Content in Catechol-Conjugated Dextrans on Antiplatelet Performance. *Polymers (Basel)*. **2017**, *9*.
 37. Kim, H. S.; Ham, H. O.; Son, Y. J.; Messersmith, P. B.; Yoo, H. S. Electrospun Catechol-Modified Poly(Ethyleneglycol) Nanofibrous Mesh for Anti-Fouling Properties. *J. Mater. Chem. B* **2013**, *1*, 3940.
 38. Shin, M.; Ryu, J. H.; Kim, K.; Kim, M. J.; Jo, S.; Lee, M. S.; Lee, D. Y.; Lee, H. Hemostatic Swabs Containing Polydopamine-like Catecholamine Chitosan-Catechol for Normal and Coagulopathic Animal Models. *ACS Biomater. Sci. Eng.* **2018**, *4*, 2314–2318.
 39. Thomas, A.; Bauer, H.; Schilman, A. M.; Fischer, K.; Tremel, W.; Frey, H. The “Needle in the Haystack” Makes the Difference: Linear and Hyperbranched Polyglycerols with a Single Catechol Moiety for Metal Oxide Nanoparticle Coating. *Macromolecules* **2014**, *47*, 4557–4566.
 40. Patil, N.; Falentin-Daudré, C.; Jérôme, C.; Detrembleur, C. Mussel-Inspired Protein-Repelling Ambivalent Block Copolymers: Controlled Synthesis and Characterization. *Polym. Chem.* **2015**, *6*, 2919–2933.
 41. Velders, A. H.; Bos, I.; Yang, J.; Cohen Stuart, M. A.; Pranger, W.; Kamperman, M.; Stuijver, A. A Clear Coat from a Water Soluble Precursor: A Bioinspired Paint Concept. *J. Mater. Chem. A* **2016**, *4*, 6868–6877.
 42. Patil, N.; Jérôme, C.; Detrembleur, C. Recent Advances in the Synthesis of Catechol-Derived (Bio)Polymers for Applications in Energy Storage and Environment. *Prog. Polym. Sci.* **2018**, *82*, 34–91.
 43. North, M. A.; Del Grosso, C. A.; Wilker, J. J. High Strength Underwater Bonding with Polymer Mimics of Mussel Adhesive Proteins. *ACS Appl. Mater. Interfaces* **2017**, *9*, 7866–

- 7872.
44. Seo, S.; Das, S.; Zalicki, P. J.; Mirshafian, R.; Eisenbach, C. D.; Israelachvili, J. N.; Waite, J. H.; Ahn, B. K. Microphase Behavior and Enhanced Wet-Cohesion of Synthetic Copolyampholytes Inspired by a Mussel Foot Protein. *J. Am. Chem. Soc.* **2015**, *137*, 9214–9217.
 45. Kang, T.; Banquy, X.; Heo, J.; Lim, C.; Lynd, N. A.; Lundberg, P.; Oh, D. X.; Lee, H. K.; Hong, Y. K.; Hwang, D. S.; *et al.* Mussel-Inspired Anchoring of Polymer Loops That Provide Superior Surface Lubrication and Antifouling Properties. *ACS Nano* **2016**, *10*, 930–937.
 46. Morgese, G.; Trachsel, L.; Romio, M.; Divandari, M.; Ramakrishna, S. N.; Benetti, E. M. Topological Polymer Chemistry Enters Surface Science: Linear versus Cyclic Polymer Brushes. *Angew. Chemie - Int. Ed.* **2016**, *55*, 15583–15588.
 47. Yang, Y.; Qi, P.; Ding, Y.; Maitz, M. F.; Yang, Z.; Tu, Q.; Xiong, K.; Leng, Y.; Huang, N. A. Biocompatible and Functional Adhesive Amine-Rich Coating Based on Dopamine Polymerization. *J. Mater. Chem. B* **2015**, *3*, 72–81.
 48. Lee, S. B.; González-Cabezas, C.; Kim, K. M.; Kim, K. N.; Kuroda, K. Catechol-Functionalized Synthetic Polymer as a Dental Adhesive to Contaminated Dentin Surface for a Composite Restoration. *Biomacromolecules* **2015**, *16*, 2265–2275.
 49. Seo, S.; Lee, D. W.; Ahn, J. S.; Cunha, K.; Filippidi, E.; Ju, S. W.; Shin, E.; Kim, B.-S.; Levine, Z. A.; Lins, R. D.; *et al.* Significant Performance Enhancement of Polymer Resins by Bioinspired Dynamic Bonding. *Adv. Mater.* **2017**, *29*.
 50. Shin, E.; Ju, S. W.; An, L.; Ahn, E.; Ahn, J. S.; Kim, B. S.; Ahn, B. K. Bioinspired Catecholic Primers for Rigid and Ductile Dental Resin Composites. *ACS Appl. Mater. Interfaces* **2018**, *10*, 1520–1527.
 51. Narkar, A. R.; Lee, B. P. Incorporation of Anionic Monomer to Tune the Reversible Catechol-Boronate Complex for PH-Responsive, Reversible Adhesion. *Langmuir* **2018**, *34*, 9410–9417.
 52. Asha, A. B.; Chen, Y.; Peng, Y.-Y.; Hall, D. G.; Narain, R.; Wu, D.; Ishihara, K.; Diaz-Dussan, D.; Wang, W. Bioinspired Self-Healing Hydrogel Based on Benzoxaborole-Catechol Dynamic Covalent Chemistry for 3D Cell Encapsulation. *ACS Macro Lett.* **2018**, *7*, 904–908.

Chapter. 2. Bioinspired Catecholic Primers for Rigid and Ductile Dental Resin Composites

2.1 Introduction

Dental restoration is a treatment of the dental caries to restore the function, integrity and morphology of teeth. Filling the missing parts of a tooth such as caries is the most common method of dental restoration. A variety of materials such as amalgam, glass ionomers, and resins have been used for dental restorations. Polymethacrylate (PMA) resin composites have been the most popular with several clinical advantages such as aesthetics, repairability, and versatility.

PMA resins, however, have some issues in that they shrink during photoinitiated free radical polymerization and are much softer than human teeth. Therefore, dental PMA composites contain up to 80 wt% glass fillers to reduce the volume shrinkage during the curing of the resin composites and thereby avoid marginal leakage and secondary caries associated with interfacial adhesion failure between the tooth and resin composite, as well as to increase the elastic modulus (rigidity) of the restoration. Despite their popularity and clinical advances, several challenges remain for restorative resin composite materials, and the short lifetime of dental restorations (less than several years or months) causes the need for repeated-restoration treatments followed by a dental crown and eventual tooth loss. Therefore, demand for more durable and tougher restoration is high.

Currently the most common approach to increasing the rigidity of polymer composites is to incorporate hard domains in the soft matrix; in dental composites, glass fillers are added to the PMA resin matrix due to their economical and esthetic advantages. However, in this state-of-the-art approach, an increase in hardness or rigidity often sacrifices their flexibility (strain at fracture), which leads to a decrease in toughness. For more durable dental restorations, tougher resin composites are required to reduce the risk of issues with restorations such as marginal adhesion failure, staining, sensitivity, recurrent caries, and catastrophic fracture. In our previous paper, we presented strong adhesion of a bioinspired catecholic primer to various minerals and PMA composites.¹⁴ In this work, we have conducted further systematic studies in continuation of our endeavor in the development of practical dental applications.

In state-of-the-art dental resin composite technologies, surface modification of clean glass filler using a silane coupling agent is essential to increase the wetting of inorganic fillers and to provide a

* Chapter 2 is reproduced in part with permission of "ACS Appl. Mater. Interfaces 2018, 10, 1520". Copyright 2017 American Chemical Society.

chemical bond between the dissimilar materials (e.g. glass and PMA resin).¹⁵⁻¹⁷ Without the surface treatment, the filler content cannot be higher than 30 wt% due to poor mixing. To date, silane-based primers (or silane coupling agents) have been the most popular and primarily used for inorganic fillers because they can bind covalently to various inorganic surfaces such as metal oxides and oxide minerals. However, only 10 to 20% of the chains of silanes chemically bind to the surfaces, and their hydrolytic stability still remains an issue for dental applications.

Our approach to provide more durable bonding between glass and resin surfaces is inspired by the adhesion mechanism of marine mussels and mussel foot proteins (mfp's). One of the unique features of interfacial mfp's - that mussels use as surface primer prior to applying their bulk mfp's (Figure 2.1a) - is their high content of phenolic residues, especially 3,4-dihydroxyphenyl-L-alanine (DOPA) or catechol moieties. A majority of catechol functional residues exists in the interfacial mfp's up to 30 mol %, mussels use the catechol moieties as one of the key functional groups for surface adhesion. Despite extensive research on the use of catechol moieties for synthetic adhesives in the past decade, only a few studies have applied this catechol chemistry for surface priming. For example, a recent report by Seo et al. demonstrated that mussel-inspired dynamic bonds can overcome the challenges associated with the current silane-based priming in a load-bearing polymer composite. It proposed that catecholic primer can be an alternative to the conventional silane coupling agent which cannot bind to mineral surfaces without using toxic chemicals.⁸ The previous study showed that the synthetic catecholic primers from eugenol (used in a traditional temporary dental restoration) can enhance the adhesion performance and mechanical properties.¹⁴ In contrast to the previous study using acrylic primers as potential alternative of silane primers, here we employ methacrylate primers, which is clinically and economically more viable than the acrylic primers, and optimize the priming process for practical dental applications. Coupling effect of the catechol-functionalized methacrylate primers via a simple dip-coating process was investigated for dental resin composite applications, and the results were compared to a conventional silane primer. In addition, the treatment conditions such as processing time, concentration, and shrinkage rate were carefully optimized. The standard knife shear and compression tests were also performed to evaluate the mechanical properties of the dental resin composites. Finally, the biocompatibility of the primed surfaces was studied via cell attachment assay.

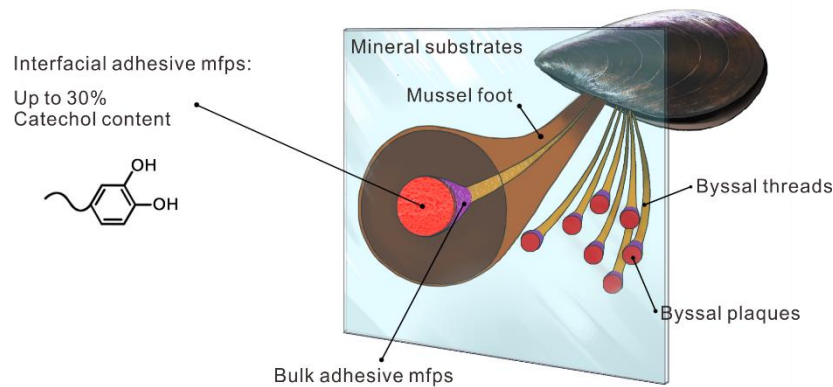
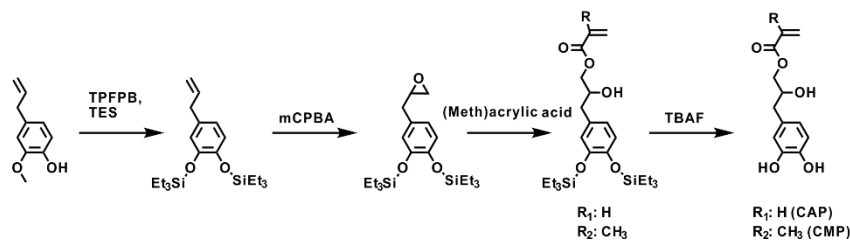
a Biological primers**b** Synthetic primer from eugenol

Figure 2.1. (a) A schematic cartoon of mussel byssal threads, which are produced in the mussel foot to adhere to mineral substrates. (b) Synthetic pathways of catecholic primers (catechol acrylate primer (CAP) and catechol methacrylate primer (CMP)) derived from eugenol.

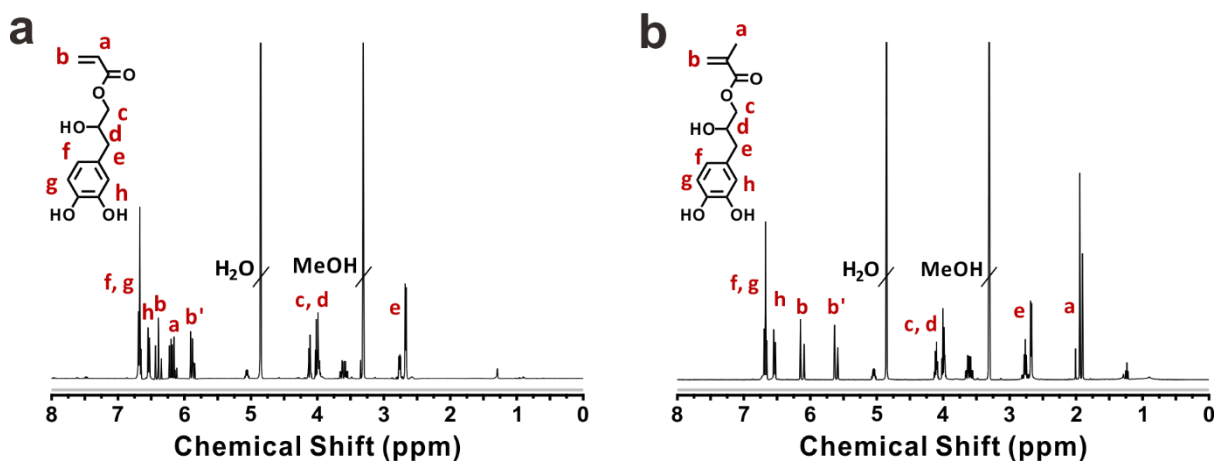


Figure 2.2. 1H NMR spectra of (a) acrylate primer (CAP) and (b) methacrylate primer (CMP).

2.2. Materials and methods

Reagents. 1.0 M of tetrabutylammonium fluoride (TBAF) solution in tetrahydrofuran (THF), 3-(trimethoxysilyl) propyl acrylate, bisphenol A glycerolate dimethacrylate (Bis-GMA), triethylene glycol dimethacrylate (TEGDMA), 2-(dimethylamino)ethyl methacrylate (DMAEMA), and camphorquinone (CQ) were obtained from Sigma-Aldrich. Triethylsilane-protected eugenol acrylate and triethylsilane-protected eugenol methacrylate were provided by Osaka Organic Chemical Industry LTD (Japan). Polysiloxane-coated barium glass powder (0.7 μm diameter) and bare barium glass powder were provided by Sukgyung AT (South Korea). Methanol, hexane, diethyl ether, and THF were purchased from Sigma Aldrich (USA). Glass slides (25 mm \times 75 mm) were obtained from Fisher Scientific (USA). All chemicals were analytical reagent grade and used without purification unless otherwise indicated.

Instruments. ^1H NMR spectra were recorded at 298 K with a VNMRs 400 spectrometer operating at 400 MHz using CDCl_3 and CD_3OD . The surface morphologies of the primed surfaces were examined using an atomic force microscope (AFM, Dimension D3100, Veeco, USA). Contact angles were obtained using a contact angle analyzer (DSA 100, KRUSS, Germany). Cell attachment was observed using an inverted microscope (IX73, OLYMPUS, Japan). A Servo-hydraulic Universal Testing Machine (MTS 810, MTS System Corp., USA) was used for compressive fracture tests.

Synthesis of catechol-functionalized primers. All reactions were carried out under argon unless otherwise noted. 3-(3,4-dihydroxyphenyl)-2-hydroxypropyl acrylate (catechol acrylate primer, **CAP**) was prepared by deprotection of triethylsilane-protected eugenol acrylate. Triethylsilane-protected eugenol acrylate (0.30 g, 0.643 mmol, 1.0 equiv) was dissolved in 40 mL of dry THF. Subsequently, TBAF solution (0.516 mL, 0.8 equiv) was slowly added and stirred for 1 h at room temperature. The solvent was removed using a rotary evaporator and the crude material was purified using silica gel flash column chromatography with methanol to remove triethylfluorosilane. The product was further purified by silica gel flash column chromatography with hexane/ethyl acetate (1:1 v/v) to provide 121 mg (79.3% yield) of slightly brownish liquid. The product purity was verified by ^1H NMR. ^1H NMR (600MHz, CDCl_3): = 6.77 (d, 1H, Ar-H), 6.69 (d, 1H, Ar-H), 6.64 (q, 1H, Ar-H), 6.16 (d, 1H, -CH=CH₂), 6.17 (q, 1H, -CH=CH₂), 5.86 (d, 1H, -CH=CH₂), 4.24 (q, 1H, -CH₂OOC-), 4.08 (q, 1H, -CH₂OOC-), 2.72 (m, 2H, -CH₂CH(OH)-), 2.20 (d, 1H, -CH(OH)-), 1.03 (t, 18H, -Si-CH₂CH₃), 0.78 (q, 12H, -Si-CH₂CH₃). ^{13}C NMR (600 MHz, CDCl_3): = 166.19, 146.76, 145.65, 131.19, 128.04, 122.15., 121.66, 120.47, 70.77, 67.56, 39.31, 6.62, 5.07 ppm. ESI-MS, m/z = 489.25 [M^+Na^+]. The purity of the product is 95.8% by HPLC analysis.

3-(3,4-dihydroxyphenyl)-2-hydroxypropyl methacrylate (catechol methacrylate primer, CMP) was prepared by deprotection of triethylsilane-protected eugenol methacrylate. Triethylsilane-protected eugenol methacrylate (1.0 g, 2.080 mmol, 1.0 equiv) was dissolved in 40 mL of dry THF. After that, TBAF (1.664 mL, 0.8 equiv) was slowly added and stirred for 1 h at room temperature. The solvent was removed using a rotary evaporator and the crude material was purified using silica gel flash column chromatography with methanol to remove triethylfluorosilane. The product was further purified by silica gel flash column chromatography with hexane/ethyl acetate (1:1 v/v) to provide 211 mg (40.0% yield) of light brownish liquid. The product purity was verified by ¹H NMR. ¹H NMR (600MHz, CDCl₃): = 6.77 (d, 1H, Ar-*H*), 6.69 (d, 1H, Ar-*H*), 6.64 (q, 1H, Ar-*H*), 6.13 (d, 1H, -CH₂C(CH₃)=CH₂), 5.58 (d, 1H, -CH₂C(CH₃)=CH₂), 4.22 (q, 1H, -CH₂OOC-), 4.10 (q, 1H, -CH₂OOC-), 2.72 (m, 2H, -CH₂CH(OH)-), 2.20 (d, 1H, -CH(OH)-), 1.95 (d, 3H, -C(CH₃)=CH₂), 1.03 (t, 18H, -Si-CH₂CH₃), 0.78 (q, 12H, -Si-CH₂CH₃). ¹³C NMR (600 MHz, CDCl₃): = 166.19, 146.76, 145.65, 131.19, 128.04, 122.15., 121.66, 120.47, 70.77, 67.56, 39.31, 6.62, 5.07 ppm. ESI-MS, m/z = 503.26 [M⁺Na⁺]. The purity of the product is 96.1 % by HPLC analysis.

Static contact angle measurement. The static contact angles of water on the priming substrates were measured to analyze surface hydrophilicity. The glass substrates were cleaned prior to use and primer solutions (0.15 mg/mL) were spread over a glass surface and incubated for 5 min at room temperature. 10 μL of deionized water was dropped onto the substrate and all samples were analyzed in triplicate.

Knife shear test. The adhesive ability of each primer was determined based on ISO 10477 and ISO 11405 using a material testing system (MTS). Glass slides were cleaned using sonication in acetone prior to testing. The primer solutions at various concentrations were spread over glass surfaces and incubated for 5 min at room temperature. After that, the surfaces were naturally dried. A PMA monomer blend, composed of triethylene glycol dimethacrylate (TEGDMA) 49.5 wt%, bisphenol A glycerolate dimethacrylate (bis-GMA) 49.5 wt%, 2-dimethylaminoethyl methacrylate (DMAEMA) 0.66 wt% and camphorquinone (CQ) 0.33 wt%, was filled into a gelatin capsule (size 4, Torpac Inc., USA) and placed upon the primer treated glass slide. The PMA monomer blend was cured for 3 min using a portable dental curing lamp (3M™, Elipar™ DeepCure-S LED Curing Light LY-A180, 430-480 nm, 1,470 mW·cm⁻²). The adhesive stress was measured by the materials testing system and converted to knife shear adhesion in Pascals. Each experimental set was repeated at least 10 times (*n* = 10) and the average and standard deviation were calculated.

Compression test. To prepare the surface treated glass fillers, 0.21 mg of CAP or CMP were dissolved in 10 mL of methanol and 5 g of bare glass fillers was added and stirred for 1 h at room

temperature. The solvent was evaporated using a rotary evaporator and dried under vacuum. During mixing of the fillers with the PMA resin blend (same as described in the previous section), the PMA monomer blend was placed on a 75 °C hot plate to reduce its viscosity, and dried glass fillers were added gradually at 70 wt%. The filler-PMA mixtures were filled into 8 mm cylindrical plastic molds and light-cured for 5 min. The top and bottom sides of the specimens were ground and polished for an accurate measurement, and the height and diameter of the samples were measured before testing. Composites with conventional silane grafted fillers were also made using the same method. The knife shear stress was measured based on ISO 6873 using materials testing system. Each experimental set was repeated at least 10 times ($n = 10$) and the average and standard deviation were calculated.

Polymerization shrinkage test. Linear mold shrinkage was determined by comparing the length of resin composites after polymerization. The PMA monomer blend and filler-PMA blend mixture were filled into 15.85 mm cylindrical plastic molds and light-cured for 5 min. The heights of the specimens were measured after polymerization and the shrinkage rate was calculated.

Cell attachment test. The cell adhesion test was performed using L929 mammalian fibroblast cells on the primer treated glass substrates ($1 \times 1 \text{ cm}^2$). Each glass substrate was placed on a 24-well cell culture plate, sterilized by 70% ethanol solution, and UV irradiated for 30 min. After being equilibrated in phosphate-buffered saline (PBS) and media for 30 min, L929 cells were seeded onto the glass substrates at a density of 1×10^5 cells per substrate. The substrates were incubated for 24 h in 5% CO_2 at 37 °C. After 24 h, the substrates were transferred to new culture plates and washed three times with PBS to remove any non-adherent cells. Three glass slides were prepared for each primer (silane, CAP, and CMP) and the number of live cells was counted from three random locations on each slide. The bare glass slide without any modification served as a control.

Statistical Analysis. Knife shear test and compression test data were analyzed by a one-way ANOVA analysis with level of statistical significance ($\alpha = 0.05$) using the software of Microsoft Excel 2016. In case of that statistical differences were found, all pairwise comparisons were performed using Tukey's honest significant difference (HSD) test. The statistical evaluations were performed to determined significance differences on the 5% ($\alpha < 0.05$).

2.3. Results and discussion

2.3.1. Synthesis of catechol-functionalized primer

Catechol can form a bidentate hydrogen bond to oxide mineral and metal surfaces.²² The binding lifetime of catechol's bidentate hydrogen bonding is 10^6 times longer than monodentate hydrogen bonding, and thus provides stronger and more durable adhesion.³⁰ The catecholic bifunctional monomers have been shown to form a uniform self-assembled monolayer whereas silane forms ill-defined multilayer films.²⁷

Catecholic primers were synthesized from naturally abundant and commercially available eugenol,²⁹ and the four-step synthesis is straightforward and inexpensive. Dihydroxyl groups were protected by triethylsilane during the synthesis due to the oxidation instability of catecholic moieties and removed by TBAF prior to surface priming (see the synthetic scheme shown in Figure 2.1b). The vinyl group of eugenols was epoxidized to provide a reaction site for acrylate or methacrylate via a nucleophilic S_N2 reaction of methacrylic acid. The successful synthesis of two different catecholic primers functionalized with acrylate (CAP) and methacrylate (CMP) was confirmed by 1H NMR spectra (Figure 2.2). We hypothesized in this study that the difference between the methacrylate and acrylate end groups affects the bonding and mechanical performance of the primers due to their reactivity difference during free radical polymerization.³¹

2.3.2. Surface morphology of primed surfaces

To compare the adsorption of the primer molecules to a silica surface, the morphology of each surface before and after the primer treatments was investigated using AFM on a silicon wafer. Figure 2.3a demonstrates that the height of molecular adsorption patches on the silica surfaces is less than 4 nm, which does not exceed the contour length of single primer molecules. Once the successful adsorption of the primers on the surface was confirmed, the static water contact angle was also measured to characterize the wettability of each surface. As shown in Figure 2.3b, the contact angle of bare glass was $35.2 \pm 1.2^\circ$, whereas the contact angle of the silane- and catechol-treated surfaces increased up to $62.1 \pm 5.9^\circ$ after the surface treatment. This significant increase in contact angle demonstrates the successful coating of primers and the increased hydrophobicity of the primed layer compared to the bare glass slide.

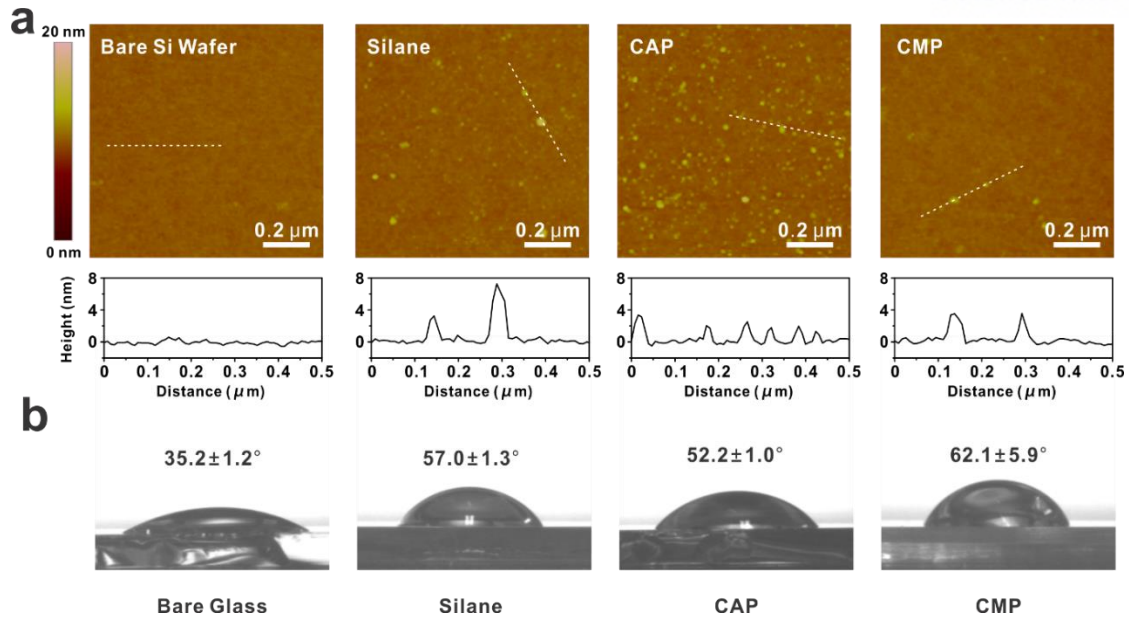


Figure 2.3. (a) Representative AFM images of bare silicon wafer and silane-, catechol acrylate (CAP)- and catechol methacrylate (CMP)-primed surfaces with corresponding line scan profiles. (b) Static contact angles of the bare and the primed glass substrates.

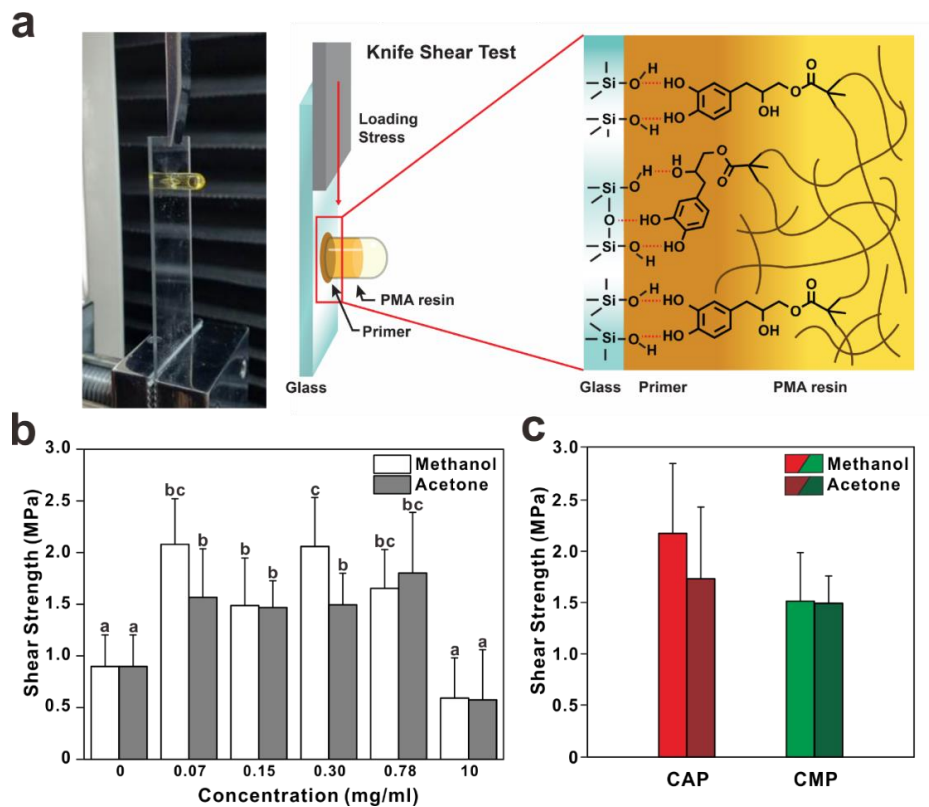


Figure 2.4. (a) A photograph of the knife shear test and schematic representation of catecholic primer bridging (coupling) between glass and PMA resin. (b) Knife shear strength of methacrylate primer in various concentrations (0.07 – 10 mg/mL) and solvents (methanol and acetone). (c) Comparison of the knife shear strength of catecholic primers (concentration: 0.15 mg/mL). Bars with the different letters are significantly different according to Turkey's HSD.

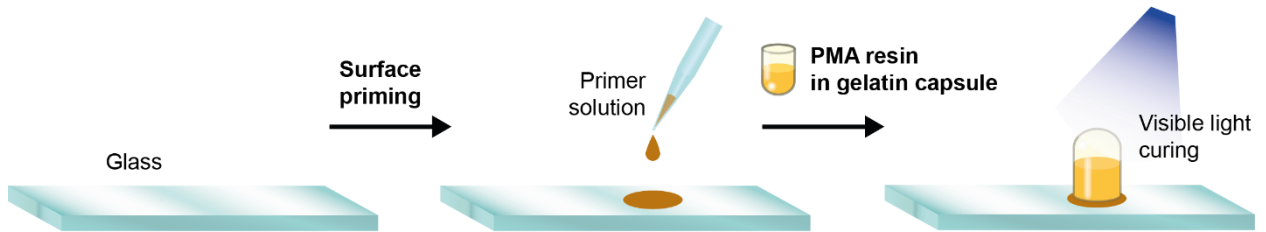


Figure 2.5. Schematic of sample preparation for the knife shear test.

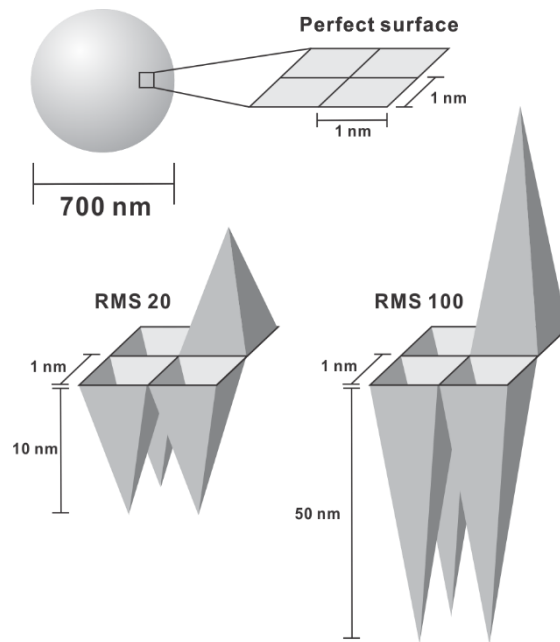


Figure 2.6. Surface roughness in our terms of “RMS” consisted of square pyramid valleys of base area 1 nm^2 and nm height denoted by “RMS”. Each square grid is a section of the total nanoparticle surface area, which is also denoted. To quantify surface roughness, we approximated “RMS” as a height of square pyramid valleys in the glass surface. Each catechol-methacrylate molecule is assumed to occupy 1 nm^2 on the substrate surface, for the hydrogen bonding employed by catechol creates a dynamic system that occupies space as such. Through stoichiometric calculations, we prepared solutions as follows: RMS 10 nm (0.07 mg/mL), RMS 20 nm (0.15 mg/mL), RMS 40 nm (0.30 mg/mL), RMS 100 nm (0.78 mg/mL), RMS 1200 nm (10 mg/mL).

2.3.3. Knife shear test

The knife shear bonding test is a common method for evaluating the bonding performance of dental resins.³² We carried out the knife shear stress test to evaluate the bonding performance related to possible crosslinking of the bifunctional primer at the interface between the glass and PMA resin, and also to optimize the treatment conditions. We primed the glass surface by drop-casting the primer solutions onto the glass substrate, and left the primers self-assemble and the solvent evaporate completely for 5 min at ambient condition (Figure 2.5). While the catechol moieties bind to the glass surface, the methacrylic end groups can face outwards during the self-assembly as similarly demonstrated in the molecular dynamic simulation in our previous study (see also the schematic representation in Figure 2.4a). Subsequently, the dental PMA resin was applied and cured over the surface. During the visible light curing, the methacrylic end groups are crosslinked with other methacrylic groups in the PMA resin blend.

In our previous study, the self-assembly priming process involved multiple rinses to remove the excess primer molecules and drying steps prior to applying resins.¹⁴ For practical dental applications, an improved processing method is required because treatment time is critical to clinicians and patients in clinical situations. In addition, the effect of different reactivities between the acrylate groups of the polymerization was not studied in the previous work.²³

We aimed in this work to minimize the processing steps and to investigate the effect of methacrylic end groups in the catecholic primer as well. To enable the one-step priming process for practical dental applications, we reduced the concentration of the primer solutions to eliminate the rinsing and drying steps. For this, we assumed that each catecholic primer occupies 1.0 nm² on the substrate surface based on the molecular dynamic simulation in the previous report.²⁷ Based on this assumption, we estimated the concentration and amount of each solution to be applied per area, with the surface area calculated based on the root-mean-squared (RMS) roughness (Figure 2.6). According to this calculation, we prepared the primer solutions as follows: RMS 10 nm (0.07 mg/mL), RMS 20 nm (0.15 mg/mL), RMS 40 nm (0.30 mg/mL), RMS 100 nm (0.78 mg/mL), and RMS 1200 nm (10 mg/mL). In addition, we prepared the primer solutions in two different solvents, i.e., acetone and methanol, to compare the effects of self-assemblies related to solubility and rapid drying via azeotropic removal of water molecules from the surface. Further, we prepared more practical dental PMA composites containing 70 wt% of glass fillers as in conventional dental PMA composites in comparison to the PMA composite containing 30 wt% of the fillers in the previous study.¹⁴

The average shear strengths of the different concentrations are shown in Figure 2.4b. The concentration range 0.07 – 0.78 mg/mL exhibited similar knife shear strengths. However, the knife shear strength was doubled when compared to the pristine glass control, which indicates that the CMP enhances the shear bonding performance by chemical bridging or coupling between the glass substrate

and the PMA resin. In the case of a high concentration of primer solution (10 mg/mL), the maximum shear stress dropped to ~0.5 MPa, which is half that of the control experiment. This result suggests that the unbound inordinate catecholic molecules on the substrate interfere with the coupling of the PMA resin to the surface-bound primers.

We also compared the shear strengths of CMP and CAP. Due to the reactivity difference between acrylate and methacrylate during the polymerization,³¹ we expected that it would affect the crosslinking of primers with PMA resin which, in turn, contributes to the difference in adhesion and shear bonding strength. However, as shown in Figure 2.4c, the knife shear bonding test results did not show a statistically significant difference. We speculate that surface adhesion of the catechol groups plays a more important role in the bonding performance than that arising from crosslinking between acrylate and methacrylate groups.

2.3.4. Compressive test

We extended our study to produce the actual dental restorative composite using the catecholic methacrylate primers compared to previously reported acrylate primers and silane coupling agents.¹⁴ The mechanical properties of dental composites were determined by a compressive test using a material testing system (Figure 2.7a and 2.7b). In this study, we evaluated five different dental resin composites as follows: one without filler (no filler), one with bare glass filler (no primer), one with commercial silane-treated filler (silane), and two catecholic primer treated glass fillers (CAP and CMP). Figure 2.7 shows a representative stress-strain curve for each composite sample. The mechanical properties of each resin composite were also determined from the stress-strain curve (Figure 2.8).

The key advantage of glass fillers is reducing polymerization-induced shrinkage of dental PMA resin composites, which is critical in practical situations because shrinkage is directly related to marginal leakage and secondary caries.^{8, 33} The high filler contents occupy the free volume of the composite resin to help reduce this shrinkage.³⁴ The linear shrinkage of resin composites after the photopolymerization is shown in Table 2.1. As expected, the resin composite containing both catechol and silane priming fillers shows a 7-fold lower shrinkage rate (0.43%) compared to the no filler composite (3.12%). This significantly lower shrinkage of resin composite suggests a very close packing between catecholic priming filler and PMA resin, which is associated with better wetting and coupling effects between the dissimilar surfaces (filler and resin).

Because the composite without the filler showed a too high shrinkage rate as well as a too low elastic modulus (less than 1.5 GPa) to be used for dental restorations, we further limit our discussion

only the composite containing fillers. In case of the no primer composite, as expected, the mechanical properties of the composite became worse due to the incongruities between glass filler and polymer resin. In a clear contrast, primer treated glass fillers demonstrated much higher elastic modulus and toughness compared to that of bare glass filler due to the efficient mixing of fillers with PMA resin. When the PMA resin composite containing primed fillers is compared to the resin composite without the primer, the mechanical properties of primed resin composite show up to 4.2 times the elastic modulus, 3.7 times the toughness, and 3.8 times the ultimate stress. However, the silane composite exhibited a decrease in strain-at-failure because high rigidity usually compromises extensibility or flexibility. As a result, an increase in the rigidity of the resin composites often compromises a reduce in the toughness. By the introduction of dynamic bonding at the interface between filler and resin surfaces, we have successfully diminished the trade-off, and catecholic surface primed glass filler-containing composites exhibited high toughness while maintaining a high rigidity (~3 GPa). Interestingly, the stress-strain curve of catecholic primer treated composite (CAP and CMP) showed a ductility in contrast to the silane treated filler-containing composite (Silane in Figure 2.7c). As also shown in Figure 2.7b, the silane treated filler-containing resin composite was completely destroyed, whereas the catechol treated filler-containing composite withstood and maintained its structure for a much longer time and at higher load. We believe the origin of these tough mechanical properties of the catecholic primer is the presence of abundant sacrificial hydrogen bonds. In other words, the energy dissipation associated with the gradual bond breakage is the key difference from the reliance on covalent coupling present in the silane composite. As seen in the shear bonding test, both CAP and CMP composites exhibited statistically similar properties in the compression test.

2.3.5. Cell attachment test

To further assess the possibility of using catecholic priming surfaces for practical dental applications, we studied the cell attachment and viability of L929 fibroblasts on the priming surfaces. After 24 h of incubation, the morphology of the cells on the bare glass slide and priming surfaces was investigated as shown in Figure 2.9. All surfaces showed that a significant number of cells were attached to the surface and grew without noticeable changes in the cell morphology. These results indicate that the priming surfaces did not have any toxic effects on the fibroblast cells. Considering the high biocompatibilities of the primers developed in this study, we suggest that these catecholic primers can potentially be used in a real clinical setting.

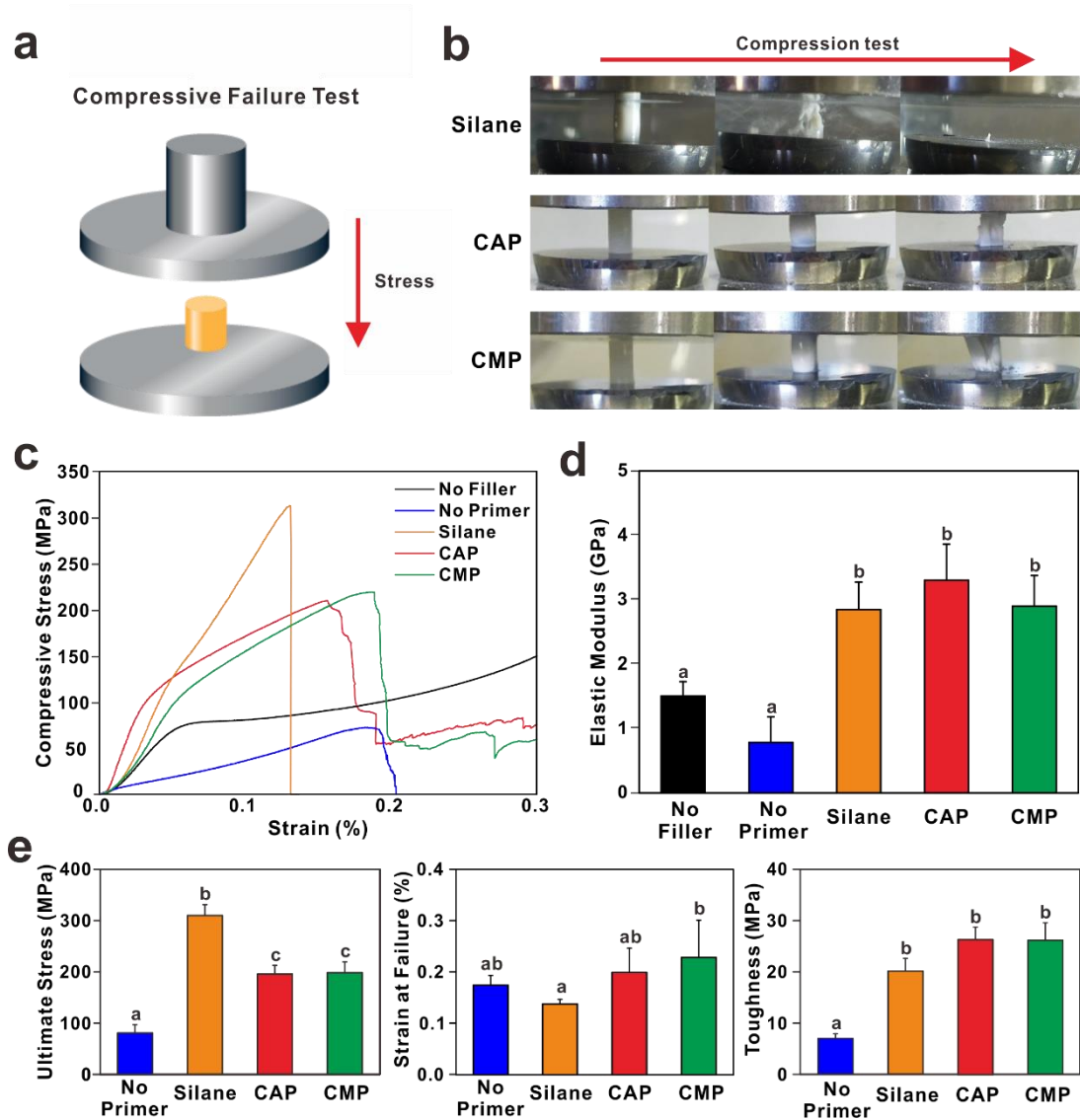


Figure 2.7. Compression tests of dental composites. (a) A schematic representation of the compression test. (b) Images of the silane, CAP, and CMP composite samples during the compression test. (c) Representative stress-strain curves for the dental composites. (d) Elastic modulus and (e) ultimate stress (left), strain at failure (middle), and toughness (right) of all dental composites prepared. Bars with the different letters are significantly different according to Turkey's HSD.

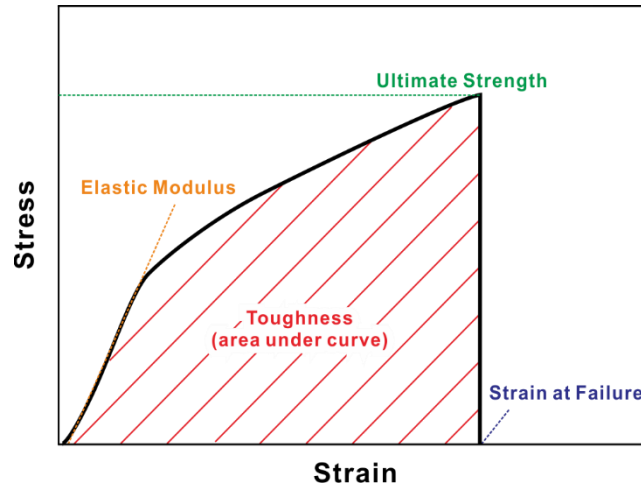


Figure 2.8. A stress-strain curve shows compressive stress (σ in MPa) of a material responding to displacement (strain, ϵ in %). A slope of elastic region (elastic modulus, yellow), the cross-sectional area under the stress-strain curve (toughness, red), highest stress withheld by the specimen (ultimate strength, green) and strain at complete breakage (strain at failure, blue) were calculated.

Table 2.1. Polymerization-induced shrinkage of resin composites

No Filler				With Filler			
Trial	L (mm)	L_0-L (mm)	Shrinkage	Trial	L (mm)	L_0-L (mm)	Shrinkage
1	15.37	0.48	3.03	1	15.78	0.07	0.44
2	15.34	0.51	3.22	2	15.79	0.06	0.38
3	15.36	0.49	3.09	3	15.79	0.06	0.38
4	15.35	0.50	3.15	4	15.77	0.08	0.50
5	15.36	0.49	3.09	5	15.78	0.07	0.44
Ave.	15.36	0.49	3.12	Ave.	15.78	0.07	0.43
Std.	0.01	0.01	0.07	Std.	0.01	0.01	0.05

Shrinkage of dental composites were measured by comparison the length of resin composites after polymerization.

L_0 = Length of cylindrical plastic mold, 15.85 mm

L = Length of resin composite after polymerization

$$\text{Linear shrinkage} = \frac{L_0 - L}{L_0} \times 100$$

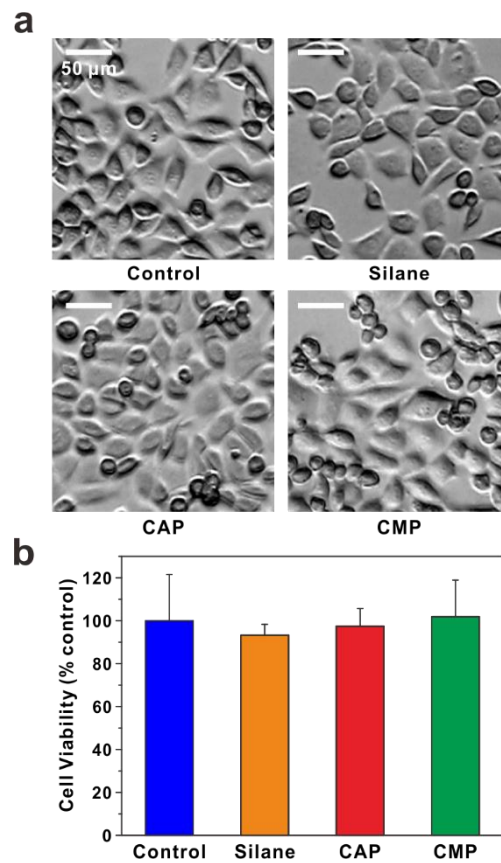


Figure 2.9. (a) Optical microscopy images of L929 cells seeded on the priming surfaces using various primer solutions for 24 h (conc. 0.15 mg/mL). (b) Relative cell viability on the priming surfaces. The cell viability of the control group was normalized to 100%.

2.4. Conclusion

In summary, catechol functionalized methacrylate primer (catechol-spacer-methacrylate) was developed for dental resin composites. In addition, we reduced the processing time and steps for the sake of clinical, industrial, and environmental viabilities. The synthesis of the primers was characterized by ^1H NMR and GC/MS, and the adsorption of the primers onto SiO_2 surfaces such as silicon wafer and glass substrates was confirmed by AFM and contact angle measurements. Catechol moieties can bind to the surface during their self-assembly, while methacrylate groups crosslink with dental polymethacrylate resin. These bifunctional molecules enhanced the binding of glass filler and polymeric resin matrix as a coupling agent, which in turn improved the mechanical performance of the dental PMA resin composite. Despite the difference between the chain end groups of CAP and CMP regarding their different reactivities, their mechanical performance was similar in dental resin. Both catecholic primers CAP and CMP show higher toughness compared to the conventional silane-based primers with similarly high rigidity and low shrinkage rate. In addition, the excellent biocompatibility of the primed surfaces clearly demonstrated their significant potential for dental and biomedical applications.

2.5. References

1. Eakle, W. S. Fracture Resistance of Teeth Restored with Class II Bonded Composite Resin. *J. Dent. Res.* **1986**, *65*, 149–153.
2. Erfan, M.; Jafarzadeh-Kashi, T. S.; Ghadiri, M.; Rakhshan, V. The Effects of Dentin Bonding Agent Formulas on Their Polymerization Quality, and Together with Tooth Tissues on Their Microleakage and Shear Bond Strength: An Explorative 3-Step Experiment. *J. Adv. Prosthodont.* **2014**, *6*, 333–345.
3. Rekow, E. D.; Bayne, S. C.; Carvalho, R. M.; Steele, J. G. What Constitutes an Ideal Dental Restorative Material? *Adv. Dent. Res.* **2013**, *25*, 18–23.
4. Stein, P. S.; Sullivan, J.; Haubenreich, J. E.; Osborne, P. B. Composite Resin in Medicine and Dentistry. *J. Long. Term. Eff. Med. Implants* **2005**, *15*, 641–654.
5. Peutzfeldt, A. Resin Composites in Dentistry: The Monomer Systems. *Eur. J. Oral Sci.* **1997**, *105*, 97–116.
6. Kuehn, K. D.; Ege, W.; Gopp, U. Acrylic Bone Cements: Composition and Properties. *Orthop. Clin. North Am.* **2005**, *36*, 17–28.
7. de Gee, A. F.; Feilzer, A. J.; Davidson, C. L. True Linear Polymerization Shrinkage of Unfilled Resins and Composites Determined with a Linometer. *Dent. Mater.* **1993**, *9*, 11–14.
8. Moszner, N.; Salz, U. New Developments of Polymeric Dental Composites. *Prog. Polym. Sci.* **2001**, *26*, 535–576.
9. Braem, M.; Finger, W.; Van Doren, V. E.; Lambrechts, P.; Vanherle, G. Mechanical Properties and Filler Fraction of Dental Composites. *Dent. Mater.* **1989**, *5*, 346–349.
10. Nedeljkovic, I.; Teughels, W.; De Munck, J.; Van Meerbeek, B.; Van Landuyt, K. L. Is Secondary Caries with Composites a Material-Based Problem? *Dent. Mater.* **2015**, *31*, 247–277.
11. Mjor, I. A.; Toffenetti, F. Secondary Caries: A Literature Review with Case Reports. *Quintessence Int.* **2000**, *31*, 165–179.
12. Cocco, A. R.; Rosa, W. L.; Silva, A. F.; Lund, R. G.; Piva, E. A Systematic Review about Antibacterial Monomers Used in Dental Adhesive Systems: Current Status and Further Prospects. *Dent. Mater.*, **2015**, *31*, 1345–1362.

13. Demarco, F. F.; Corrêa, M. B.; Cenci, M. S.; Moraes, R. R.; Opdam, N. J. Longevity of Posterior Composite Restorations: Not Only a Matter of Materials. *Dent. Mater.* **2012**, *28*, 87–101.
14. Seo, S.; Lee, D. W.; Ahn, J. S.; Cunha, K.; Filippidi, E.; Ju, S. W.; Shin, E.; Kim, B. S.; Levine, Z. A.; Lins, R. D.; Israelachvili, J. N.; Waite, J. H.; Valentine, M. T.; Shea, J. E.; Ahn, B. K. Significant Performance Enhancement of Polymer Resins by Bioinspired Dynamic Bonding. *Adv. Mater.* **2017**. DOI: 10.1002/adma.201703026
15. Heo, J.; Kang, T.; Jang, S. G.; Hwang, D. S.; Spruell, J. M.; Killops, K. L.; Waite, J. H.; Hawker, C. J. Improved Performance of Protected Catecholic Polysiloxanes for Bioinspired Wet Adhesion to Surface Oxides. *J. Am. Chem. Soc.* **2012**, *134*, 20139–20145.
16. Nishiyama, N.; Ishizaki, T.; Horie, K.; Tomari, M.; Someya, M. Novel Polyfunctional Silanes for Improved Hydrolytic Stability at the Polymer–silica Interface. *J. Biomed. Mater. Res.* **1991**, *25*, 213–221.
17. Debnath, S.; Wunder, S. L.; McCool, J. I.; Baran, G. R. Silane Treatment Effects on Glass/resin Interfacial Shear Strengths. *Dent. Mater.* **2003**, *19*, 441–448.
18. Das, S.; Lee, B. H.; Linstadt, R. T.; Cunha, K.; Li, Y.; Kaufman, Y.; Levine, Z. A.; Lipshutz, B. H.; Lins, R. D.; Shea, J. E.; Heeger, A. J.; Ahn, B. K. Molecularly Smooth Self-Assembled Monolayer for High-Mobility Organic Field-Effect Transistors. *Nano Lett.* **2016**, *16*, 6709–6715.
19. Gooding, J. J.; Ciampi, S. The Molecular Level Modification of Surfaces: From Self-Assembled Monolayers to Complex Molecular Assemblies. *Chem. Soc. Rev.* **2011**, *40*, 2704–2718.
20. Arksornnukit, M.; Takahashi, H.; Nishiyama, N. Effects of Silane Coupling Agent Amount on Mechanical Properties and Hydrolytic Durability of Composite Resin after Hot Water Storage. *Dent. Mater.* **2004**, *23*, 31–36.
21. Roeters, J. J.; Shortall, A. C.; Opdam, N. J. Can a Single Composite Resin Serve All Purposes? *Br. Dent. J.* **2005**, *199*, 73–79.
22. Yu, J.; Kan, Y.; Rapp, M.; Danner, E.; Wei, W.; Das, S.; Miller, D. R.; Chen, Y.; Waite, J. H.; Israelachvili, J. N. Adaptive Hydrophobic and Hydrophilic Interactions of Mussel Foot Proteins with Organic Thin Films. *Proc. Natl. Acad. Sci. U. S. A.* **2013**, *110*, 15680–15685.

23. Maier, G. P.; Rapp, M. V.; Waite, J. H.; Israelachvili, J. N.; Butler, A. Adaptive Synergy between Catechol and Lysine Promotes Wet Adhesion by Surface Salt Displacement. *Science* **2015**, *345*, 332–336.
24. Ahn, B. K.; Das, S.; Linstadt, R.; Kaufman, Y.; Martinez-Rodriguez, N. R.; Mirshafian, R.; Kesselman, E.; Talmon, Y.; Lipshutz, B. H.; Israelachvili, J. N.; Waite, J. H. High-Performance Mussel-Inspired Adhesives of Reduced Complexity. *Nat. Commun.* **2015**, *6*, 8663.
25. Lee, S. B.; González-Cabezas, C.; Kim, K. M.; Kim, K. N.; Kuroda, K. Catechol-Functionalized Synthetic Polymer as a Dental Adhesive to Contaminated Dentin Surface for a Composite Restoration. *Biomacromolecules* **2015**, *16*, 2265–2275.
26. Lee, B. P.; Messersmith, P. B.; Israelachvili, J. N.; Waite, J. H. Mussel-Inspired Adhesives and Coatings. *Annu. Rev. Mater. Res.* **2011**, *41*, 99-132.
27. Das, S.; Lee, B. H.; Linstadt, R. T.; Cunha, K.; Li, Y.; Kaufman, Y.; Levine, Z. A.; Lipshutz, B. H.; Lins, R. D.; Shea, J. E.; Heeger, A. J.; Ahn, B. K. Molecularly Smooth Self-Assembled Monolayer for High-Mobility Organic Field-Effect Transistors. *Nano Lett.* **2016**, *16*, 6709–6715.
28. Dupraz, A. M.; de Wijn, J. R.; v d Meer, S. A.; de Groot, K. Characterization of Silane-Treated Hydroxyapatite Powders for Use as Filler in Biodegradable Composites. *J. Biomed. Mater. Res.* **1996**, *30*, 231–238.
29. Ahn, B. K.; Lee, D. W.; Israelachvili, J. N.; Waite, J. H. Surface-Initiated Self-Healing of Polymers in Aqueous Media. *Nat. Mater.* **2014**, *13*, 867–872.
30. Yu, J.; Wei, W.; Danner, E.; Ashley, R. K.; Israelachvili, J. N.; Waite, J. H. Mussel Protein Adhesion Depends on Interprotein Thiol-Mediated Redox Modulation. *Nat. Chem. Biol.* **2011**, *7*, 586–588.
31. Bevington, J. C.; Harris, D. O. Reactivities of Acrylates and Methacrylates. *Polym. Lett.* **1967**, *5*, 799–802.
32. Pashley, D. H.; Sano, H.; Ciucchi, B.; Yoshiyama, M.; Carvalho, R. M. Adhesion Testing of Dentin Bonding Agents: A Review. *Dent. Mater.* **1995**, *11*, 117–125.
33. de Gee, A. F.; Feilzer, A. J.; Davidson, C. L. True Linear Polymerization Shrinkage of Unfilled Resins and Composites Determined with a Linometer. *Dent. Mater.* **1993**, *9*, 11–14.

34. Giachetti, L.; Russo, D. S.; Bambi, C.; Grandini, R. A Review of Polymerization Shrinkage Stress: Current Techniques for Posterior Direct Resin Restorations. *J. Contemp. Dent. Pract.* **2006**, *7*, 79–88.

Chapter 3. Bioinspired Bifunctional Block-Copolymers with superior antifouling properties

3.1. Introduction

Biofouling is known as the accumulation of undesired biomolecules and organisms on wetted surfaces, which poses significant challenges in a wide range of applications from biomedical implants to industrial and transport industry.¹⁻³ While the use of biocides is the most popular method for effectively inhibiting the accumulation of marine organisms, the toxic chemical or heavy metals present in the biocides raises considerable threat to marine environments. Therefore, improving the antifouling properties of surfaces becomes crucial to reduce the chance of life-threatening incidents and the cost of operation without harming the environment. Consequently, biocompatible polymers have been introduced as non-toxic antifouling materials, including poly(ethylene glycol),^{4,5} polyalkyloxazoline,^{6,7} polyacrylate,^{8,9} poly(2-hydroxyethyl methacrylate),¹⁰ and polyacrylamide.¹¹ Among them, PEG is widely used due to its high aqueous solubility, chain flexibility, and biocompatibility which offers antifouling and lubrication property via steric repulsion and surface hydration.^{12,13}

However, due to this unique antifouling behavior of PEG itself, immobilization of PEG onto the target surfaces has posed a significant challenge. To date, these issues were primarily addressed by surface-specific modifications, including thiol for gold surface¹⁴ and silanization.¹⁵ Alternatively, a universal surface coating strategy based on catechol moiety adapted from mussel adhesive proteins can provide a versatile adhesive property independent of the type of the surfaces. This versatility has been widely exploited in various applications, such as adhesives,^{16,17} hydrogels,^{18,19} surface primers,^{20,21} nanoparticle modification agents,^{22,23} and sensors.²⁴ Along the same line, the immobilization of PEG to the surface using catechol moiety has been suggested in different formats including terminal group modification,^{25,26} grafting with catechol functional group,^{27,28} and catechol functionalized monomer as adopted to PEG as a macroinitiator.^{29,30} Among these strategies, catechol functionalized monomer offers an accessibility to control the molecular weight, catechol contents, and location in the polymer. However, most of the previous approaches have exploited the use of rigid and hydrophobic catechol functional moiety to the flexible hydrophilic PEG backbone, which inevitably induces the segregation of the catechol functional groups.

Recently, ABA-type triblock copolymer forming a loop conformation is actively studied as advanced coating material for antifouling surface due to its large excluded volume and strong steric

hindrance. Unlike the traditional AB-type diblock copolymers forming brush conformation, it displayed enhanced antifouling and lubrication properties.^{27,31,32} Despite the successful early examples, the effects of the polymer composition and structure were rarely investigated, even though the length of the catechol units are known to affect the interaction with the surface and surface coating densities.³³ Thus, we study herein the antifouling properties of loop-like PEG-based triblock copolyethers functionalized with catechol moiety within a framework of polyethers exclusively. For that purpose, we introduce a catechol-based epoxide monomer^{34,35} into the hydrophilic PEG as the multiple anchoring point to fully realize the antifouling properties. The anchoring of the polymers on the surface was investigated by atomic force microscopy (AFM) and static contact angle measurement. The molecular-level interaction and antifouling properties of polymer coated surface are carefully evaluated using SFA and QCM-D using model protein. Finally, further antifouling properties was determined via cell attachment assay.

3.2. Materials and methods

Reagents. *p*-toluene sulfonic acid monohydrate (*p*-TsOH), lithium aluminum hydride (LiAlH₄), epichlorohydrin (ECH), tetrabutylammonium bromide (TBAB), phosphazene base *t*-Bu-P₄ solution (0.8 M in hexane), bovine serum albumin (BSA), and toluene were purchased from Sigma-Aldrich. 3, 4-Dihydroxyhydrocinnamic acid (C-COOH), 2, 2-dimethoxypropane (DMP), anhydrous methanol, aluminum oxide, poly(ethylene glycol) (PEG), and poly(ethylene glycol) monomethyl ether (*m*PEG) were purchased from Alfa-Aesar. Diethyl ether and 50% sodium hydroxide aqueous solution were obtained from Daejung. Ethyl acetate, hexane, and methanol were purchased from SK chemical. All deuterated NMR solvents such as CDCl₃ and D₂O were obtained from Cambridge Isotope Laboratories. All chemicals were analytical reagents grade and used without purification unless otherwise indicated.

Instruments. ¹H NMR spectra were recorded at 298 K with VNMRS 400 spectrometer operating at 400 MHz using CDCl₃ and D₂O solvents. All NMR spectra were measured using tetramethylsilane (TMS) as an internal standard in the NMR solvents. SEC measurement was performed using Agilent 1200 series with DMF at 40 °C with a flow rate of 1.0 mL/min using a refractive index (RI) detector. Standard PEG samples (Agilent) were used for calibration to decide the number- and weight-averaged molecular weight (M_n and M_w). Matrix-assisted laser desorption and ionization time-of-flight (MALDI-TOF) mass spectrometry were performed using and Ultraflex III MALDI mass spectrometer. Thermogravimetric analysis (TGA) was performed on a TGA Q50 analyzer (TA instruments). The surface morphologies of the priming surface were examined by an atomic force microscope (AFM,

NX-10, Park Systems, Korea). The contact angle was obtained using a Phoenix 300 goniometer (Surface Electro Optics Co. Ltd.) The surface interaction was studied using SFA 2000 (Surforce LLC, Santa Barbara, CA, USA). The real-time adsorption of polymer and protein was measured by a Q-sense E4 system (Biolin Scientific, Sweden). Cell attachment on the polymer coated surface was observed using an inverted microscope (IX73, OLYMPUS).

3.2.1. Synthesis of catechol-functionalized monomer

Acetonide protection of 3,4-dihydroxyhydrocinnamic acid. The protection of 3,4-dihydroxyhydrocinnamic acid using acetonide group was carried out by the literature procedure.²³ Due to the oxidation instability of catecholic moieties, dihydroxyl groups were protected by acetonide which shows high stability under basic condition during polymerization. 3,4-dihydroxyhydrocinnamic acid (10 g, 54.9 mmol, 1 equiv) and *p*-toluenesulfonic acid monohydrate (377 mg, 2.0 mmol, 0.04 equiv) were dissolved in 300 mL of anhydrous toluene. After equipped with a Soxhlet extractor filled with CaCl₂ and reflux condenser, the reaction solution was stirred under nitrogen atmosphere. 2,2-dimethoxypropane (17.1 mL, 139.6 mmol, 2.5 equiv) was injected dropwise and refluxed overnight. The solvent of the resulting mixture was removed using a rotary evaporator to yield a yellow liquid. The crude product was purified by silica gel column chromatography with an ethyl acetate: hexane (1:4, v/v) eluent to obtain catechol-acetonide carboxylic acid (CA-COOH) as a pale yellow solid. Yield: 64%. The product was dried in vacuum and characterized by ¹H NMR measurement. ¹H NMR (400 MHz, CDCl₃): δ [ppm] 6.60 – 6.49 (*m*, 3H), 2.79 (*t*, 2H), 2.56 (*t*, 2H), 1.58 (*s*, 6H).

Synthesis of catechol-acetonide OH (CA-OH). The reduction of CA-COOH was carried out by the literature procedure.²³ Diethyl ether was dried by sodium sulfate before use. Lithium aluminum hydride (2.39 g, 63.0 mmol, 2 equiv) in 40 mL of diethyl ether was stirred under an argon atmosphere. After that, CA-COOH (7 g, 31.5 mmol, 1 equiv) dissolved in 40 mL of diethyl ether was added dropwise and the reaction mixture was stirred for 3 h at room temperature. When the reaction is complete, unreacted lithium aluminum hydride was quenched carefully using methanol and water. Aluminum hydroxide was removed by filtration and the resulting mixture was washed 3 times with water and the remaining water was removed by sodium sulfate. The excess solvents were removed using a rotary evaporator to obtain a yellow oily product. The crude product was purified using silica gel column chromatography with an ethyl acetate/hexane (1:4 v/v) eluent to obtain pure CA-OH. Yield: 78.5%. ¹H NMR (400 MHz, CDCl₃): δ [ppm] 6.59-6.48 (*m*, 3H), 3.59 (*t*, 2H), 2.53 (*t*, 2H), 1.80 (*m*, 2H), 1.58 (*s*, 6H).

Synthesis of acetonide protected catechol bearing epoxide monomer.³⁶ A mixture of 50% aqueous NaOH (80 mL, 1.00 mol, 16 equiv), epichlorohydrin (23.3 g, 251.8 mmol, 4 equiv) and tetrabutylammonium bromide (1.01 g, 3.14 mmol, 0.05 equiv) was stirred vigorously at 0 °C. 2,2-dimethyl-1,3-benzodioxole-5-propanol²³ (13.11 g, 62.9 mmol, 1 equiv) was slowly added and stirred overnight. The excess amount of water was added to dilute reaction mixture and extracted with diethyl ether. The organic phase was dried with MgSO₄ and evaporated to obtain a pale-yellow oily product. The crude product was purified using silica gel column chromatography with an ethyl acetate/hexane (1:4 v/v) eluent to obtain CAG. CAG was distilled before polymerization to give a pure product. Yield: 81.6%. ¹H NMR (400 MHz, CDCl₃): δ [ppm] 6.59 – 6.47 (m, 3H), 3.63 (dd, J = 11.5, 3.1 Hz, 1H), 3.42 (qt, J = 9.3, 6.4 Hz, 2H), 3.31 (dd, J = 11.5, 5.8 Hz, 1H), 3.08 (td, J = 6.2, 3.3 Hz, 1H), 2.72 (t, J = 4.6 Hz, 1H), 2.57 – 2.48 (m, 3H), 1.85 – 1.63 (m, J = 13.3, 6.5 Hz, 2H), 1.58 (s, 6H). ¹³C NMR (150 MHz, CDCl₃) 150.05, 148.15, 137.59, 128.38, 120.11, 111.28, 110.70, 74.20, 73.19, 53.55, 46.99, 34.73, 34.16, and 28.37.

3.2.2. Synthesis and characterization of catechol-functionalized polymer

Synthesis of PCAG-*b*-PEG-*b*-PCAG triblock copolymers (ABA-type loop polymers). A series of a protected catechol-functionalized polymer was synthesized by anionic ring-opening polymerization with altering the mole ratio of CAG and molecular weight of PEG. Exemplified for *L10K-10. PEG (1 g, MW 10,000, 0.1 mmol, 1 equiv) was added to a flask and dried at 100 °C for 3 h. After cooling the flask to room temperature, it was purged with nitrogen and 0.3 mL of toluene was added into the flask and heated up to 60 °C. Phosphazene base, *t*-Bu-P₄ (0.25 mL, 0.2 mmol, 2 equiv) was added to the reaction mixture and stirred for 30 min. CAG monomer (0.528 g, 2 mmol) was slowly added and stirred overnight. The polymerization was quenched with the addition of benzoic acid and the resulting polymer was passed through a pad of alumina with THF. The solution was precipitated into excess cold diethyl ether and hexane to give PCAG-*b*-PEG-*b*-PCAG. Degree of polymerization was calculated from NMR data using the following equation: Number of repeating units (CAG) = [226.96 (number of repeating units for PEG macroinitiator) * 4 (number of protons of PEG)] / [29.9 (integration value) * 2 – 7 (number of protons of CAG)]. $M_n = 264.32$ (molecular weight of CAG) * 17.19 (number of CAG repeating units) + 10,000 (molecular weight of PEG) = 14,543.66 g/mol.

Removal of acetonide group. Protected block copolymer 100 mg was stirred in 0.8 mL of hydrogen chloride solution (32%) and 9.2 mL of methanol at 40 °C. The mixture was stirred under open batch to remove acetone from the reaction. After 3 h, the excess solvent was evaporated using the rotary

evaporator and the residual water removed by sodium sulfate. The concentrated product was precipitated into cold diethyl ether. Yields: quantitative.

Thermogravimetric analysis (TGA). The thermal stability of the polymer was measured by TGA. The measurement was conducted on a TG50 under nitrogen atmosphere within the temperature range 25 – 500 °C at a heating rate of 10 °C/min.

Differential scanning calorimeter (DSC). DSC was carried out under a nitrogen atmosphere in the temperature range of –80 °C to 65 °C and at a heating rate of 10 K min⁻¹ (Q200 model, TA Instruments).

3.2.3. Surface modification characterization

Static contact angle measurement. The static contact angles of water droplet on the polymer coated substrates were measured to analyze surface modification. A variety of substrates (SiO₂, polystyrene (PS), poly(ether ether ketone) (PEEK), acrylate, poly(ethylene terephthalate) (PET), TiO₂, Au, and glass) were cleaned prior to use and incubated for 1 h in 10 mg/mL polymer solution in methanol at room temperature. Next, each substrate was washed 3 times with methanol and dried with nitrogen. All samples were analyzed at least five times to obtain accurate result and the average value with the standard deviation as an error range was reported.

3.2.4. Antifouling test using model protein

Interaction force measurements between the polymer coated surfaces using an SFA. The surface forces apparatus 2000 (Surforce LLC, Santa Barbara, CA, USA) system was used to measure the interaction forces between polymer coated surfaces. The interaction forces were measured with two sets of symmetric polymer loop and brush, respectively. To prepare polymer coated surfaces, a freshly cleaved back-silvered mica (Grade #1, S&J Trading, Floral Park, NY, USA) was glued on to a cylindrical glass disk using an optical adhesive (NOA 81, Norland Products, Inc. Cranbury, NJ, USA). Then each polymer solution (10 mg/mL in methanol) was dropped onto the mica surfaces for 10 min and washed clearly with methanol to remove unbound molecules. The polymer coated surfaces were transferred into the SFA chamber with a crossed cylinder geometry and 50 μL of the corresponding buffer was injected between two opposing surfaces. And the system was equilibrated for 1 h. The two surfaces were approached by a motor which is connected to the lower surface, to reach a steric wall distance (D_{sw}) and separated. The interaction forces were measured to investigate the protein

adsorption onto polymer coated surfaces under different intervening buffers followed by (i) 10 mM phosphate-buffered saline (PBS), (ii) bovine serum albumin (BSA) solution (1 mg/mL in 10 mM PBS), (iii) BSA solution (after 1 h waiting), and (iv) 10 mM PBS. The surfaces were thoroughly rinsed with DI water before the force measurement in final, (iv) 10 mM PBS. The adhesion forces (F_{ad}) were determined as a function of the distance (D), which corresponds to the absolute distance between two opposing surfaces and the deflection of the double cantilever spring ($k = 1225.8$ N/m in this system) using a multiple beam interferometry. All force measurements were repeated at least three times and different contact points at each buffer to confirm their reproducibility.

Polymer and protein adsorption test using QCM-D. Real-time surface adsorption were measured using gold coated sensor (QSX 301). The gold sensor in a standard Q-sense flow module was equilibrated using 1X PBS buffer before polymer injection. The flow rate was 600 μ L/min and temperature were controlled at 25 $^{\circ}$ C for all the experiments. The Voigt model was adopted to calculate the mass of viscoelastic layers with Qtools software (Q-Sense, Sweden). The density of the adsorbed BSA layer was presumed to be 1200 kg/m³, the fluid density 1000 kg/m³, and the fluid viscosity 0.001 kg/ms.

Polymer grafting density measurement using QCM. The mass of polymer layer in the dry state was measured by a quartz crystal microbalance (Stanford Research System, QCM200). Each polymer solution (10 mg/mL in methanol) was dropped onto the chip and rinsed with methanol after 10 min to remove unbound molecules. The frequency shift after surface coating was measured and dry mass of polymer layer was calculated using Sauerbrey equation, $\Delta F = -C_f * \Delta m$, where ΔF is time resolved changes in resonance frequency, C_f is the sensitivity factor for crystal, and Δm is the mass difference. The grafting density σ was calculated applying the equation $\sigma = mN_A/M_n$, where N_A is the Avogadro number, and M_n is the number-average molecular weight of polymer.

3.2.5. Cell attachment test

The L929 mammalian fibroblast cell was used in the cell attachment test. Each glass substrate (1×1 cm²) was placed on the 24-well cell culture plate and exposed to UV irradiation for 30 min and washed 3 times using 70% ethanol for sterilization. After equilibration with 1X PBS and RPMI media for 30 min, L929 cells were seeded in the cell culture plate which contain the polymer coated substrates at a density of 1×10^5 cells per substrate. The cell culture plate were incubated for 24 h in 5% CO₂ at 37 $^{\circ}$ C. After 24 h, the glass substrates were washed three times with 1X PBS to remove any non-adherent cells and transferred to new cell culture plates, and examined by optical microscopy.

The bare glass substrate was used as a control group.

3.3. Results and discussion

3.3.1 Polymerization

The synthesis of CAG and PEG-initiated block copolymer was achieved as the method described in the Experimental method. The successful synthesis of CAG was confirmed via NMR (Figure 3.1-4). After the synthesis of CAG, catechol-functionalized triblock copolymers were synthesized by AROP using PEG as a macroinitiator. The use of conventional CsOH base resulted in a low conversion due to the steric effect of bulky side group in CAG monomer. Moreover, the increased reaction temperature resulted in the degradation of the acetonide protecting groups during the polymerization (Figure 3.5 and Table 3.1). Thus, we employed the metal-free phosphazene base which exhibits a high basicity and low nucleophilicity that runs the polymerization of CAG monomer at a mild temperature.³⁷ As shown in Figure 3.6, the representative ¹H NMR spectra of the triblock copolymer showed the peaks corresponding to aromatic ring (6.91-6.51 ppm) and carbon chain (2.55 ppm and 1.82 ppm) of catechol moieties and polyether backbone and PEG segment (4.04-3.24 ppm). Moreover, the acetonide protection was stable under polymerization (1.66 ppm). As a control, diblock copolymers with a brush conformation were also synthesized by AROP using methoxy-PEG (*m*PEG) as an initiator using the identical method.

The characterizations of the synthesized polymers were listed in Table 3.2. Due to the hydrophobicity of catechol block, the molecular weight measured by size exclusion chromatography (SEC) was relatively smaller than that measured in ¹H NMR. However, the increased molecular weight upon polymerization with a narrow distribution demonstrated the successful synthesis of the catechol-functionalized block copolymers (Figure 3.7). Since the molecular weight of CAG is six times of ethylene oxide which is the monomer of PEG, it is hard to distinguish the presence of CAG in the triblock copolymers under the MALDI-MS spectra (Figure 3.8). Alternatively, CAG homopolymer synthesized under the identical reaction condition revealed the successful synthesis of homopolymer of CAG with the spacing of the signals corresponds to the mass of the respective monomer as confirmed. The incorporation of catechol moieties in the polymer was also confirmed by thermogravimetric analysis (TGA) and differential scanning calorimetry (DSC) (Figure 3.9). Bare PEG, *L10K-5, *L10K-10, and CAG homopolymer (PCAG₂₀) was stable up to 300 °C. The weight percentage of the residue after thermal decomposition at 500 °C was 2.0%, 4.3%, 6.9%, and 15.2% respectively. The residue weight was increase according to the content of CAG due to the higher

thermal stability of catechol moieties. In DSC spectrum, the catechol-functionalized block copolymers show only one glass transition temperature (T_g) due to the comparatively small length of catechol block. T_g increased according to the amount of catechol content due to the rigidity of side chain. These results demonstrate that the catechol moieties were successfully incorporated into the block copolymer.

After the polymerization, the acetonide protecting group was removed by acidic treatment to reveal the free catechol functional groups. The deprotection was monitored by the disappearance of the methyl protons at 1.58 ppm in the ^1H NMR spectrum, while PEG midblock did not show any indication of degradation (Figure 3.1b and Figure 3.10). Moreover, the deprotected polymer, for example, L10K-10 displayed a rapid oxidation of catechol in pH 8.5 buffer within 12 h, again indicating the existence of free catechol group (Figure 3.11).

3.3.2. Surface characterizations

By using a simple dipping method, catechol block of each copolymer induced the adsorption of polymers on the substrate. AFM image was collected to study morphology and the nanostructure of polymer coated surfaces. Both loop and brush copolymers were successfully deposited on the silicon wafer, while protected polymer (i.e. *L10K-10) was rinsed out, revealing the critical role of the free catechol moiety for the substrate anchoring of the polymers (Figure 3.12a). The polymer coated surface demonstrates the island-like structures which is typical morphology of the polymer brush layer on the surface.³⁸ The polymer was uniformly distributed, and the small thickness of coated polymers was limited to monolayer formation. The versatile surface binding ability was also confirmed by measuring the static contact angle measurement of water droplet after coating on various substrates to examine the surface hydrophilicity. The contact angle of each surface indicated a similar range of values which demonstrated the potential of the catechol-functionalized polymer as a substrate-independent universal coating material (Figure 3.12b, 3.13).

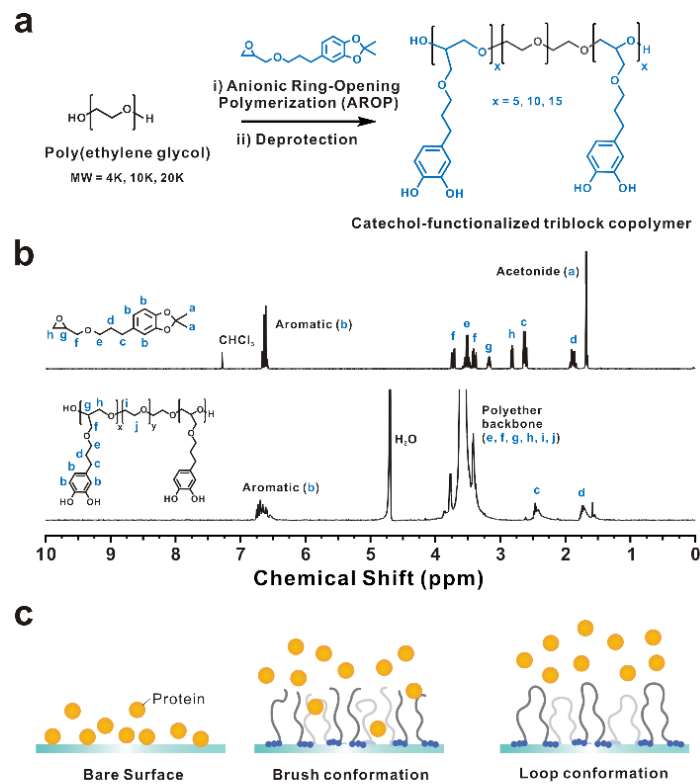


Figure 3.1. Fabrication of catechol-functionalized polymer films presenting the antifouling effect. (a) Synthesis of catechol functionalized triblock copolymers. (b) ¹H NMR spectra of CAG monomer and catechol functionalized triblock copolymer (L10K-10). (c) Schematic illustration of antifouling polymer coated surfaces

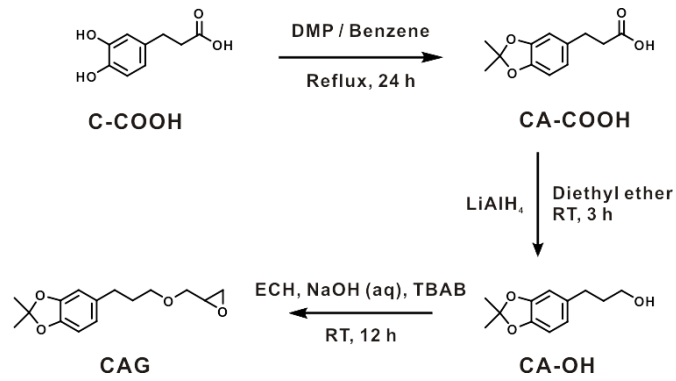


Figure 3.2. Synthesis of acetone-protected catechol functionalized monomer (CAG)

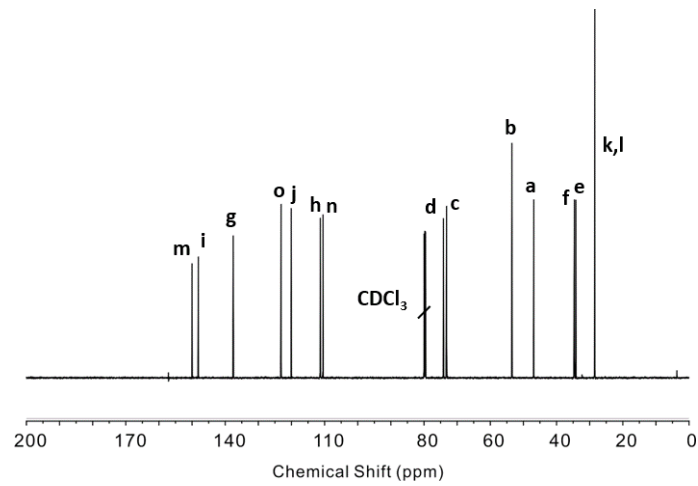


Figure 3.3. ^{13}C NMR spectrum of CAG

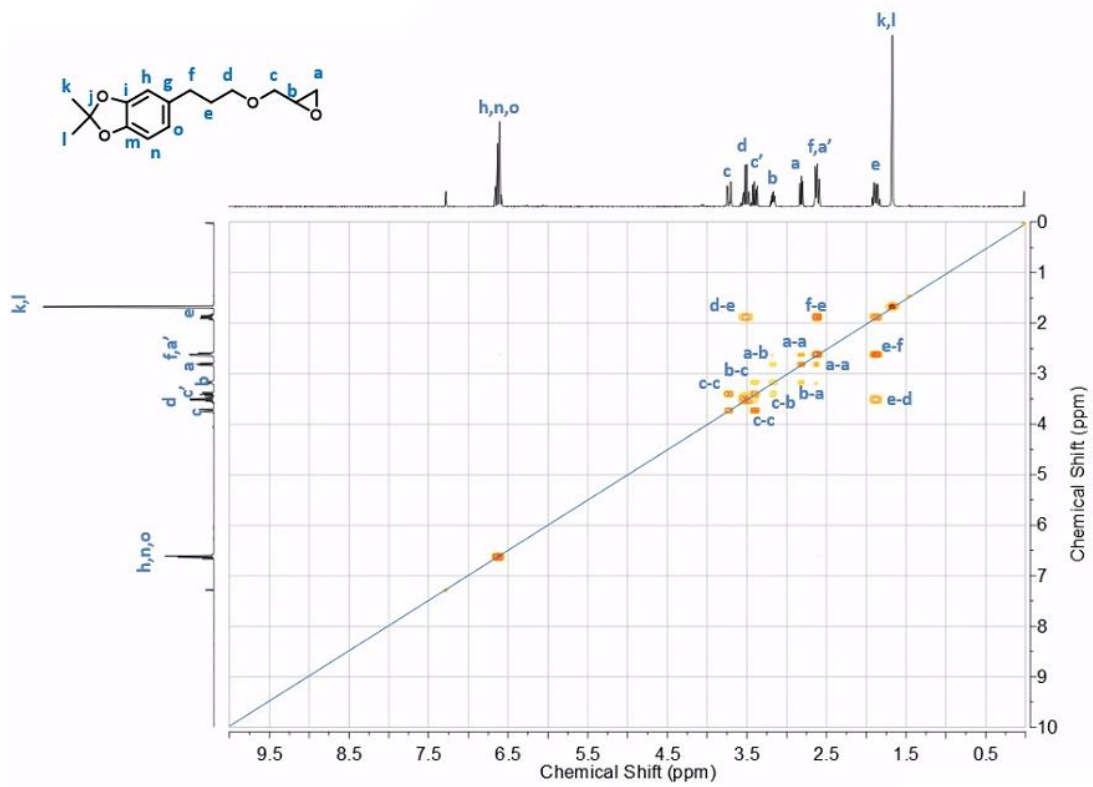


Figure 3.4. COSY NMR spectrum of CAG

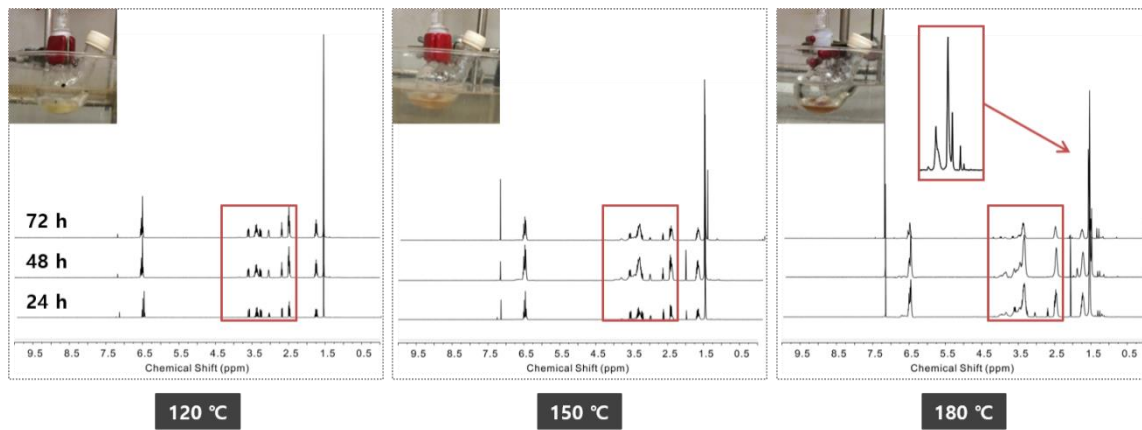


Figure 3.5. ^1H NMR spectra of homopolymerization of CAG using CsOH at high temperature

Table 3.2. Characterization of PCAG homopolymer using CsOH

Trial	Temp. (°C)	M_n (g mol $^{-1}$)	M_w (g mol $^{-1}$)	\bar{D}	DP
1	120	1210	1340	1.1	4.3
2	150	2080	2600	1.2	7.5
3	180	2780	5550	2.0	11.2

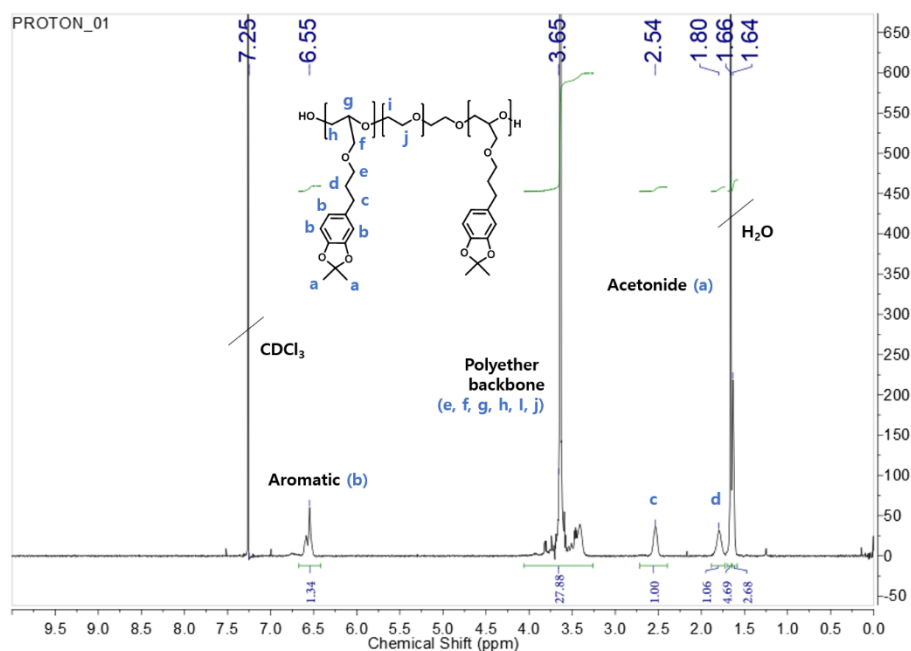


Figure 3.6. ^1H NMR spectrum of *L10K-10

Table 3.2. Characterization of the catechol-functionalized polymers.

Polymer	Composition ^a	$M_{n,\text{NMR}}^a$ (g/mol)	$M_{n,\text{SEC}}^b$ (g/mol)	D^b
*L4K-10	PCAG ₇ - <i>b</i> -PEG ₉₁ - <i>b</i> -PCAG ₇	7400	4850	1.03
*L10K-5	PCAG ₄ - <i>b</i> -PEG ₂₂₇ - <i>b</i> -PCAG ₄	11850	10900	1.10
*L10K-10	PCAG ₉ - <i>b</i> -PEG ₂₂₇ - <i>b</i> -PCAG ₉	14550	13640	1.08
*L10K-15	PCAG ₁₂ - <i>b</i> -PEG ₂₂₇ - <i>b</i> -PCAG ₁₂	17290	14940	1.32
*L20K-10	PCAG ₉ - <i>b</i> -PEG ₄₅₃ - <i>b</i> -PCAG ₉	24500	22700	1.04
*B5K-5	PEG ₁₁₄ - <i>b</i> -PCAG ₄	5930	5390	1.09
*B5K-10	PEG ₁₁₄ - <i>b</i> -PCAG ₉	7370	6890	1.12
*B5K-15	PEG ₁₁₄ - <i>b</i> -PCAG ₁₂	8960	6980	1.14

^a M_n and composition of block copolymer were determined via ^1H NMR in CDCl_3 , ^b $D(M_w/M_n)$ was measured by SEC analysis with PEG standards in DMF. [*L(X)-(Y) (protected loop polymer) or *B(X)-(Y) (protected brush polymer) in accordance with the molecular weight

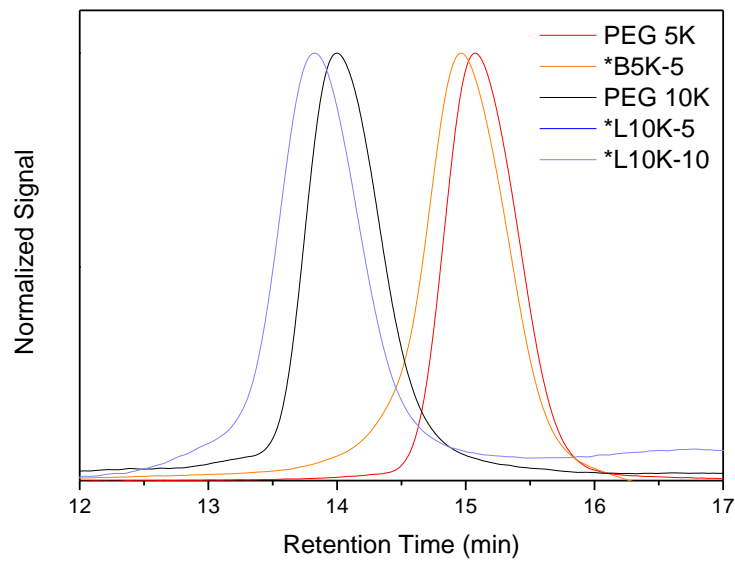


Figure 3.7. SEC trace of bare PEG and catechol functionalized polymers in DMF at 40 °C

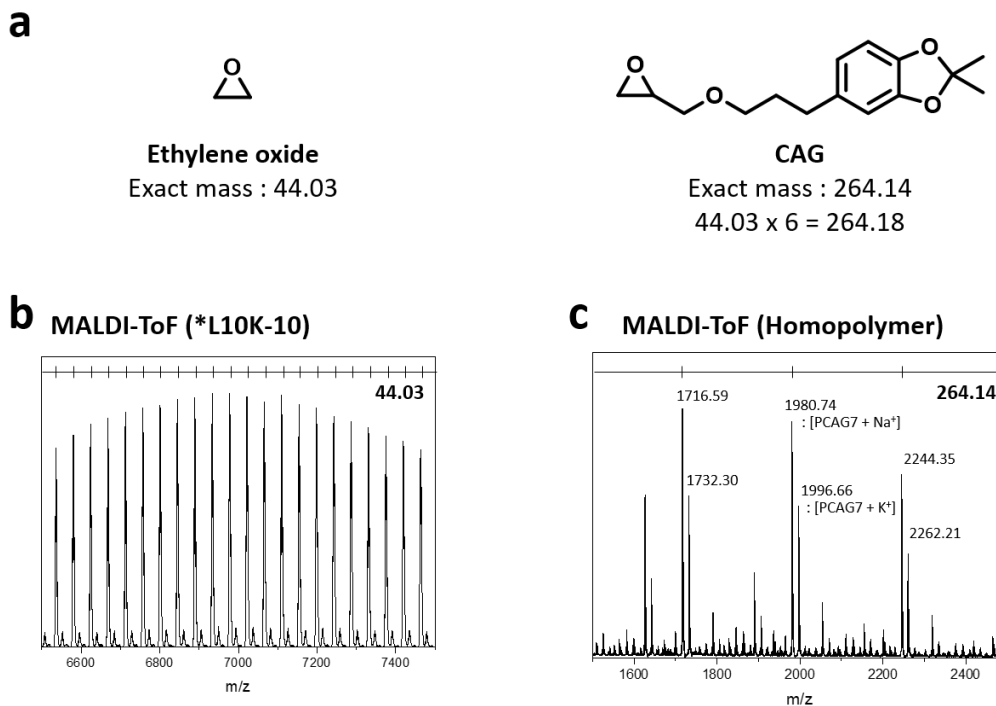


Figure 3.8. (a) The molecular weight of ethylene oxide and CAG. (b) MALDI-TOF spectrum of *L10K-10. (c) MALDI-TOF spectrum of CAG homopolymer

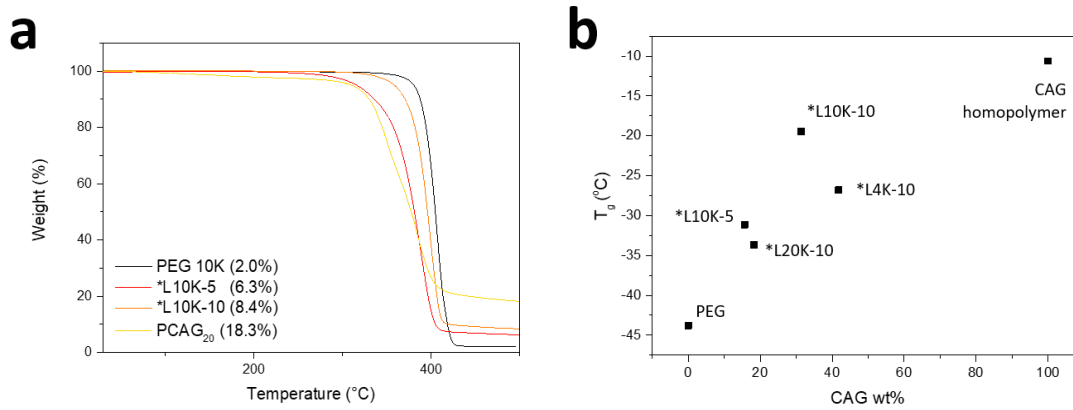


Figure 3.9. (a) TGA of catechol-functionalized triblock copolymers (b) T_g of various catechol functionalized polymers

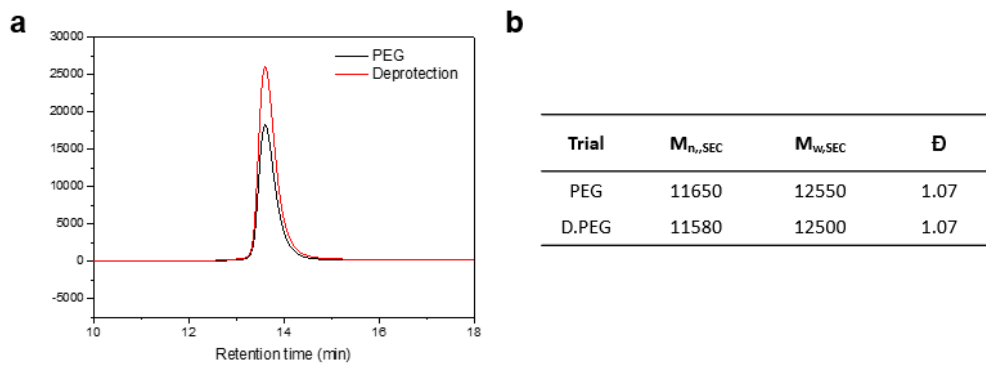


Figure 3.10. PEG hydrolysis test. (a) SEC trace and (b) molecular weight obtained by SEC

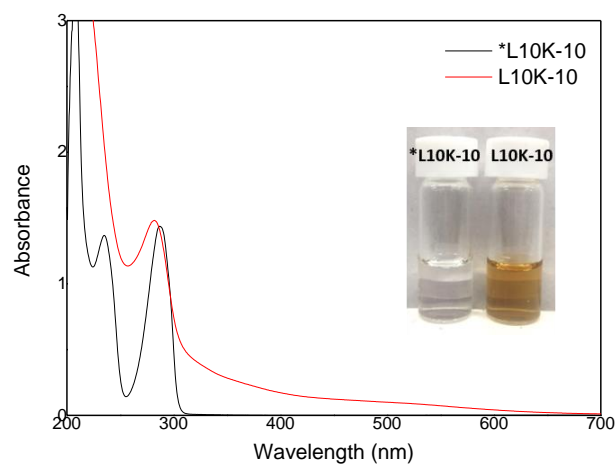


Figure 3.11. The UV-Vis spectra of protected (*L10K-10) and deprotected (L10K-10) polymer in pH 8.5 aqueous solution. Inset shows the protected polymer solution (left) and deprotected solution (right).

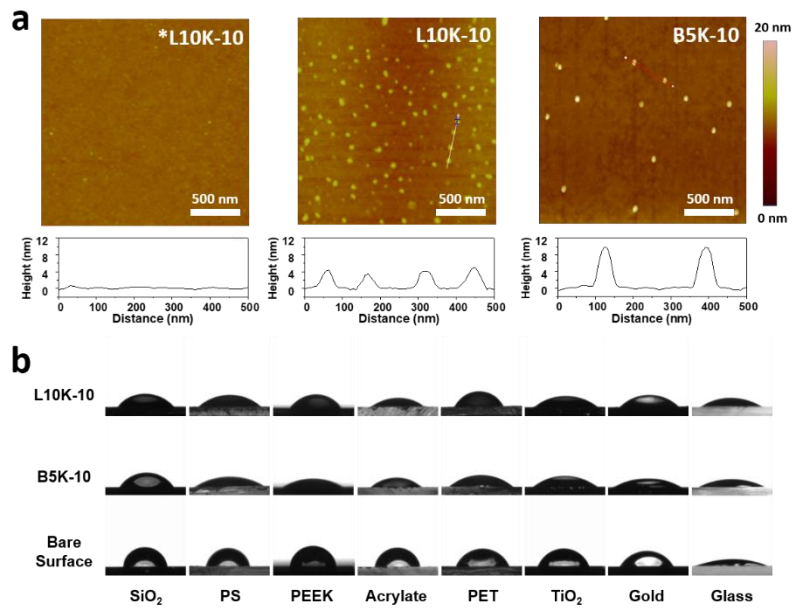


Figure 13. (a) Topographic AFM images and cross-sectional plots of *L10K-10, L10K-10, and B5K-10 coating on silicon wafer (polymer concentration: 10 mg/mL). (b) The static contact angle of bare surfaces, loop-polymer L10K-10 treated surfaces, and brush-polymer B5K-10 treated surfaces

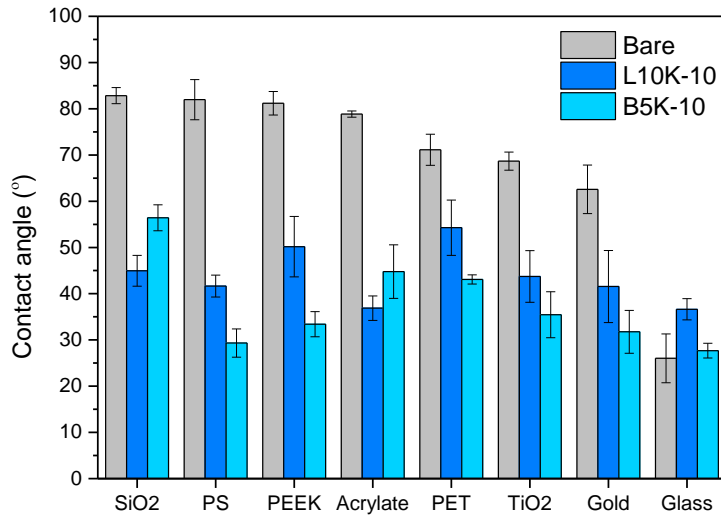


Figure 3.13. Static water contact angle after polymer coating

3.3.3 Interaction force measurement

Furthermore, the interaction forces of the polymer loop and brush coated surfaces were measured by using an SFA (Figure 3.14). SFA has been actively employed to measure the absolute distance and interaction force between two macroscopic surfaces with an ultimate resolution of 0.1 nm and 10 nN, respectively.³⁹ To investigate the antifouling effect of two polymers on the protein adsorption, bovine serum albumin (BSA) was used in this study. BSA is a well-known foulant that is commonly used as a model protein because it can adsorb easily on many different surfaces with nonspecific interactions.⁴⁰ We prepared each polymer coated surface symmetrically (loop vs. loop and brush vs. brush) and the force measurements were conducted by changing the intervening buffers in the following order: 10 mM PBS, BSA solution, and 10 mM PBS after cleaning the surfaces.

In PBS solution, both polymer loop and brush coated surfaces exhibited purely repulsive force profiles, corresponding to the ‘steric repulsion’ of polymers. The polymer loop showed a thicker steric wall distance, D_{sw} (55 nm) compared to that of the polymer brush (6 nm). This result indicated that the polymer loop showed a greater resistance to the compression compared to the polymer brush. Since both ends of polymer loop are immobilized to the surface, it has less mobility to be tilted or lay down flat upon compression, which can result in a thicker D_{sw} compared to that of the polymer brush. Considering the Debye length of 10 mM PBS is 0.76 nm, the measured decay length of the polymer loop and brush also supported the steric contribution was significant during the approach (Figure 3.15).

The interaction force between polymer loop coated surfaces right after injection of the BSA solution showed an increase in repulsion accompanied with the decrease in D_{sw} from 55 to 40 nm. The decreased D_{sw} can be interpreted as the loop polymers were collapsed by instant adsorption of the BSA onto both surfaces. However, the result after 1 h resting time showed a significant increase in D_{sw} (112 nm). The repulsion was developed from the separation distance of 190 nm, which was considerably farther than the case without the BSA due to the flocculation of BSA by the strong hydrophobic interaction.^{41,42} After rinsing the surfaces with DI water, the force measurement in PBS showed a marked decrease in repulsion and recovery of D_{sw} (55 nm), displaying a high reversibility.

Contrary to the polymer loop coated surfaces, the following force profiles were measured between polymer loop coated surfaces upon injection of BSA: (i) during the approach, BSA did not affect the repulsive force between the surfaces, and (ii) during the separation, adhesion force, F_{ad} , of -5.0 mN/m was measured. The measured adhesion force appears to be mediated by the penetration and bridging of the BSA molecules which intervened between the polymer brush gaps at the opposing surfaces.^{43,44} Due to the fast dynamics including high mobility and flexibility of the brush chain ends, the BSA has less chance to interact with the protein each other in order to aggregate. Thus, the BSA molecules

tended to be adsorbed between the polymer brush gaps rather than stacked on the surfaces, while they could be easily adsorbed and aggregated on the loop coated surfaces since there were insufficient spaces to intervene.^{32,42} The adhesion force ($F_{ad} = -3.6$ mN/m) and force-distance profile after 1 h resting time, nearly corresponded to the force run right after BSA injection. Hence, the brush coated surfaces reached the structural stability without additional aggregation of the BSA. After rinsing the surfaces clearly with DI water, the adhesion force disappeared and D_{sw} increased to 8.66 nm in PBS, showing much repulsive in-curve than initially measured in PBS during the approach. This indicated that the BSA remained in the polymer brush gaps led to a decrease in the chain mobility (which prevented polymers from tilting) even after thorough rinsing of BSA on the surfaces.

The QCM-D technique was introduced to monitor a real-time adsorption of polymer and proteins on the surface. First, the gold sensor was equilibrated using 10 mM PBS buffer and polymer solution (1 mg/mL) was applied for 30 min. The introduction of polymer generated a negative frequency shift, indicating an increase of mass on the surface. During this phase, the steep slope of ΔD vs. $\Delta F/n$ plot ($7.7 \times 10^{-7}/\text{Hz}$) suggested that the adsorbates form a viscoelastic layer with a considerable amount of energy dissipation (Figure 3.17).²⁹ The loosely bounded polymer was removed in the rinsing step and BSA solution was introduced. As shown in Figure 3.16b, the frequency was decreased while it recovered fully or partially after the rinsing step. Considering the viscoelastic nature of the polymer coated on the surface, the Voigt model was used to determine the mass of both polymer and protein (Figure 3.16c and Figure 3.16d).

As expected, the catechol-functionalized block copolymers were successfully adsorbed to the gold surface, while pristine PEG was rarely immobilized to the surface (9.5 ng/cm²). Therefore, pristine PEG itself was not effective to inhibit the binding of protein. In case of brush polymer, it effectively inhibits the protein adsorption and exhibits 8-fold lower protein uptake (59 ng/cm² for B5K-10). In addition, despite the lower grafting density of L10K-10 as shown in Table 3.3, the markedly higher suppression of protein adsorption was observed in loop polymer compared to brush polymer (approximately 0 ng/cm² except L10K-5), revealing the critical role of the topological effect in enhanced antifouling effect. Similarly, Hawker and co-workers have reported previously that the frictional force of loop polymer was reduced compared with brush polymer due to the lower interpenetration between polymer chains.²⁷ Benetti and co-workers explained that the absence of chain end significantly affect the property of surface-grafted polymer,⁴⁵ which supports the superior antifouling effect of loop polymer presented in this study.

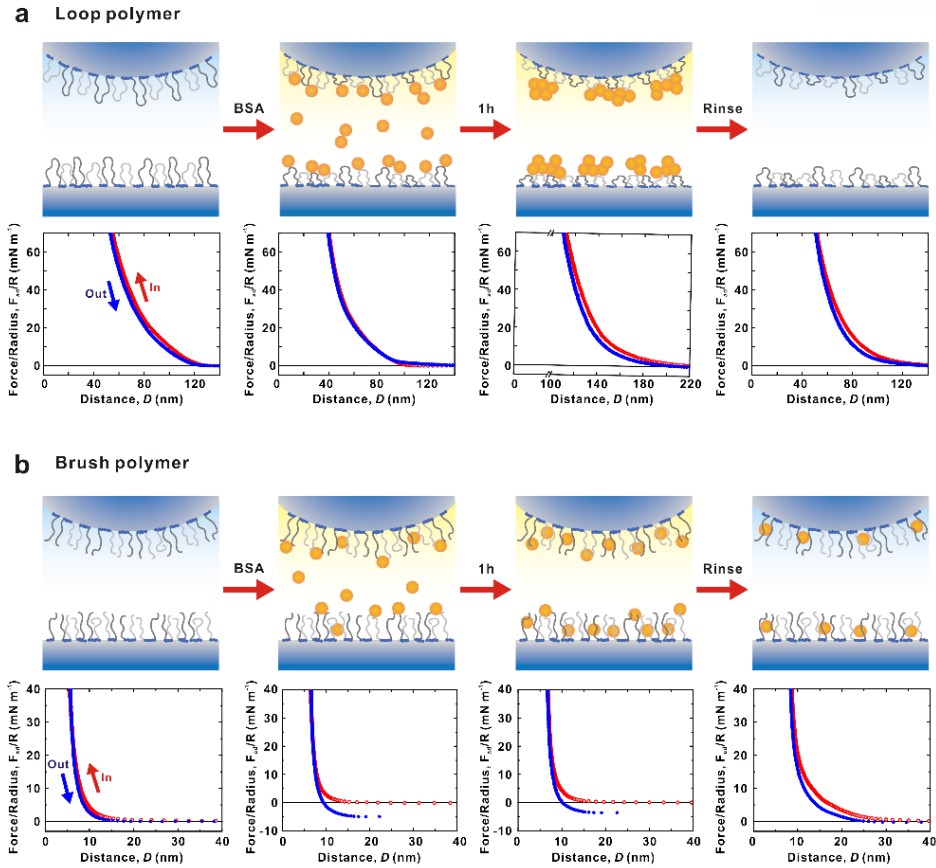


Figure 4.14 Schematics depicting antifouling study of polymer films using surface force apparatus (SFA) and force-distance profiles between two polymer films. Force-distance profiles between (a) L10K-10 and (b) B5K-10 films with different treatment sequences; 10 mM PBS, BSA solution with 1 h incubation, and 10 mM PBS rinsing.

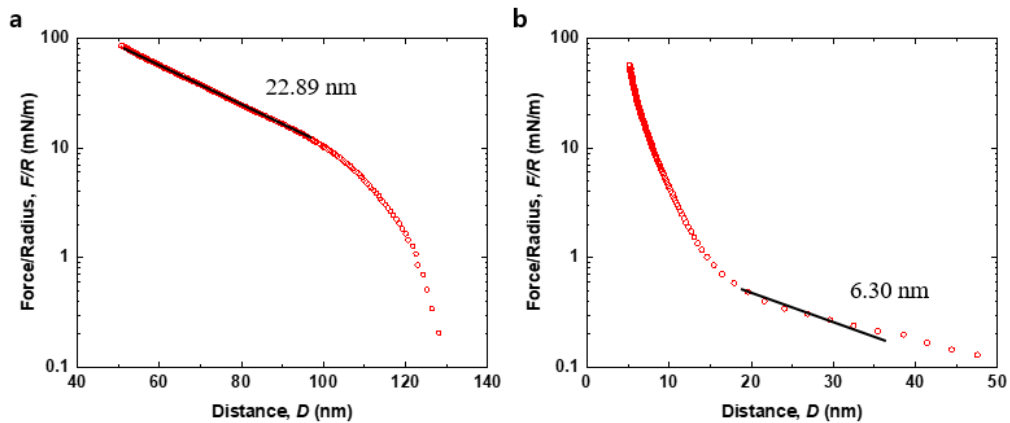


Figure 3.15. The semi-log plot of the approach curves of (a) L10K-10 and (b) B5K-10. The solid line indicates the measured decay length.

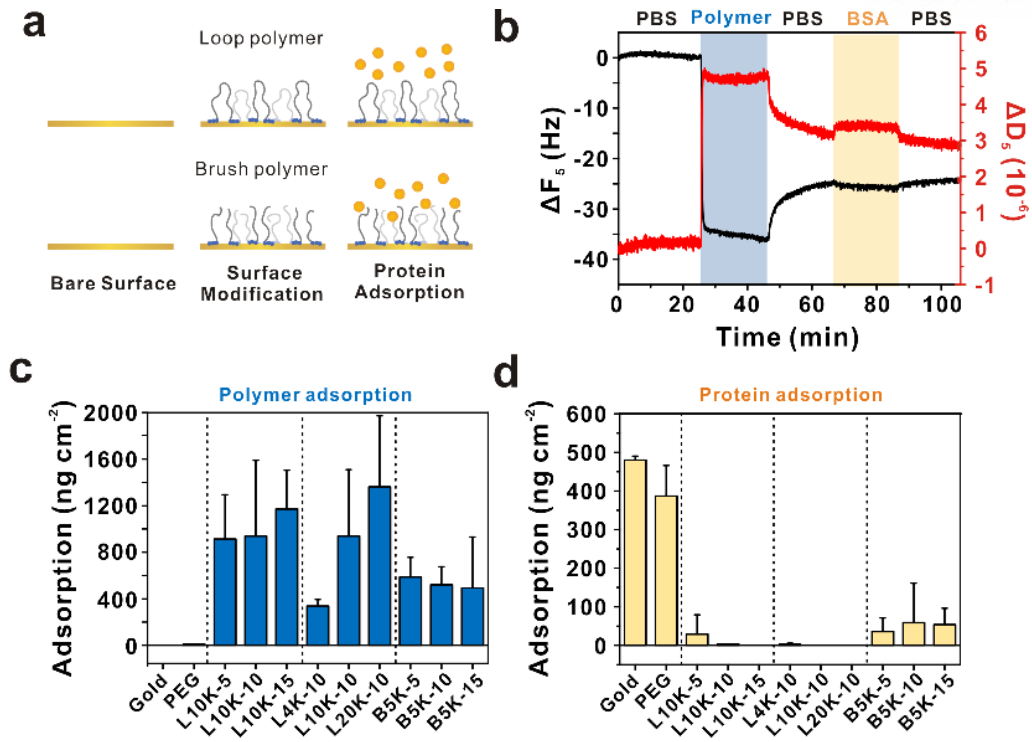


Figure 3.16. (a) Schematic illustration of antifouling test by QCM-D (b) The frequency and dissipation shift associated with the adsorption of polymer (L10K-10) and protein on gold sensor. (c) Adsorption of various polymers on bare gold surfaces. (d) Adsorption of BSA on bare and various polymers coated gold surfaces.

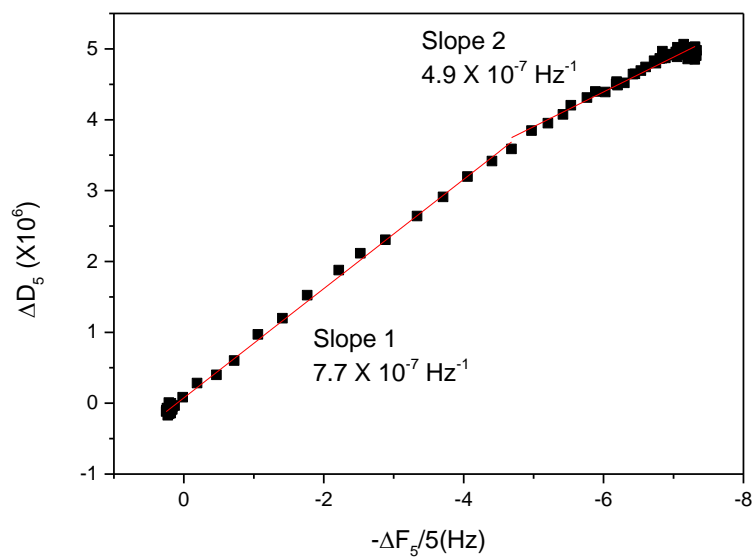


Figure 3.17. $\Delta D/\Delta F/n$ plot of the adsorption of L10K-10

Moreover, the composition effect upon the antifouling was studied using different length of PEG midblock. Even though the mass of adsorbed polymer was increased by increasing the molecular weight of PEG, for example, from 337 ng/cm² of L4K-10 to 1362 ng/cm² of L20K-10, it was not entirely proportional to the molecular weight. For comparison, dry mass and surface grafting density (σ) of polymers with the different molecular weight of PEG (L4K-10, L10K-10, and L20K-10) was measured (Table 3.3) using quartz-crystal microbalance. The polymer with a longer PEG macroinitiator shows a lower surface grafting density from 0.82 to 0.15 chains/nm² due to the higher steric hindrance, thus the increment of mass according to the molecular weight was decreased.⁴⁶ Moreover, the effect of the molecular weight of PEG was hard to compare due to the excellent antifouling properties.

A quantitative assessment of the protein adsorption and antifouling properties was also evaluated according to the number of catechol unit. In general, it was found that the increasing catechol unit enhanced the binding ability to the surface, whereas a higher number of catechol units facilitated the protein adsorption instead.^{29,33} Therefore, appropriate number of catechol unit is essential to obtain a binding ability, while maintaining the antifouling property. However, the polymer and protein adsorption with a various anchoring block length did not show a statistically significant difference. We postulate that the length of catechol block in this study is sufficient to immobilize the polymer surface, while the catechol block could not disturb the antifouling effect of PEG due to the significantly shorter length than PEG.

3.3.4 Cell attachment assay

Inhibition of cell attachment of the catechol-functionalized polymer coated surface was also confirmed with fibroblast cell. While the PEG-treated surfaces exhibit similar adhesion and proliferation with the bare glass surface (Figure 3.18), the catechol-functionalized polymer coated surface inhibit the deposition of cell and the cells were easily washed away, which demonstrated that the catechol-functionalized polymer effectively inhibited the adhesion of cell on the surface.

Table 3.3. Dry mass and surface grafting density of catechol-functionalized polymer

Polymers	Dry mass ($\mu\text{g cm}^{-2}$)	σ (chains nm^{-2})
L4K-10	1.00 ± 0.22	0.82
L10K-10	0.67 ± 0.16	0.29
L20K-10	0.58 ± 0.20	0.15
B5K-10	0.48 ± 0.26	0.41

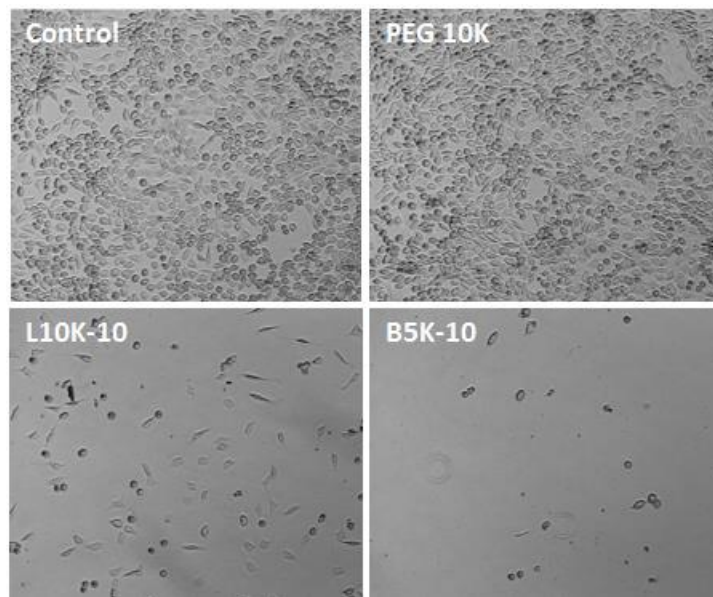


Figure 3.18. Cell attachment on each surface

3.4. Conclusion

In summary, catechol-functionalized block copolymer was prepared to compare the composition and conformation effect upon the antifouling property. The bioinspired block copolymer demonstrated that surface independent binding ability from hydrophilic to hydrophobic surfaces. The antifouling effect was evaluated by QCM and SFA, using BSA as a model protein. The composition effect was evaluated by varying the length of the PEG block and catechol block, which offers the tunable surface grafting and a diminished trade-off between surface adhesion and protein adsorption. In case of conformation, loop conformations of triblock copolymers presenting strong steric repulsion and improved antifouling effect when compared to the brush conformation of diblock copolymers. In addition, the catechol-functionalized polymer inhibits the cell attachment which demonstrates the significant potential for biomedical applications.

3.5. References

1. Bixler, G. D.; Bhushan, B. Biofouling: Lessons from Nature. *Philos. Trans. R. Soc. A Math. Phys. Eng. Sci.* **2012**, *370*, 2381–2417.
2. Ratner, B. D. The Blood Compatibility Catastrophe. *J. Biomed. Mater. Res.* **1993**, *27*, 283–287.
3. Davidson, I.; Scianni, C.; Hewitt, C.; Everett, R.; Holm, E.; Tamburri, M.; Ruiz, G. Mini-Review: Assessing the Drivers of Ship Biofouling Management – Aligning Industry and Biosecurity Goals. *Biofouling* **2016**, *32*, 411–428.
4. Goh, S. C.; Luan, Y.; Wang, X.; Du, H.; Chau, C.; Schellhorn, H. E.; Brash, J. L.; Chen, H.; Fang, Q. Polydopamine-Polyethylene Glycol-Albumin Antifouling Coatings on Multiple Substrates. *J. Mater. Chem. B* **2018**, *6*, 940–949.
5. Heo, J.; Kang, T.; Jang, S. G.; Hwang, D. S.; Spruell, J. M.; Killips, K. L.; Waite, J. H.; Hawker, C. J. Improved Performance of Protected Catecholic Polysiloxanes for Bioinspired Wet Adhesion to Surface Oxides. *J. Am. Chem. Soc.* **2012**, *134*, 20139–20145.
6. Viegas, T. X.; Bentley, M. D.; Harris, J. M.; Fang, Z.; Yoon, K.; Dizman, B.; Weimer, R.; Mero, A.; Pasut, G.; Veronese, F. M. Polyoxazoline: Chemistry, Properties, and Applications in Drug Delivery. *Bioconjug. Chem.* **2011**, *22*, 976–986.
7. Yan, W.; Divandari, M.; Rosenboom, J. G.; Ramakrishna, S. N.; Trachsel, L.; Spencer, N. D.; Morgese, G.; Benetti, E. M. Design and Characterization of Ultrastable, Biopassive and Lubricious Cyclic Poly(2-Alkyl-2-Oxazoline) Brushes. *Polym. Chem.* **2018**, *9*, 2580–2589.
8. Tanaka, M.; Mochizuki, A.; Ishii, N.; Motomura, T.; Hatakeyama, T. Study of Blood Compatibility with Poly(2-Methoxyethyl Acrylate). Relationship between Water Structure and Platelet Compatibility in Poly(2-Methoxyethylacrylate-Co-2-Hydroxyethylmethacrylate). *Biomacromolecules* **2002**, *3*, 36–41.
9. Xu, B.; Sun, X.; Wu, C.; Hu, J.; Huang, X. Construction of Catechol-Containing Semi-Fluorinated Asymmetric Polymer Brush *via* Successive RAFT Polymerization and ATRP. *Polym. Chem.* **2017**, 7499–7506.
10. Mrabet, B.; Nguyen, M. N.; Majbri, A.; Mahouche, S.; Turmine, M.; Bakhrouf, A.; Chehimi, M. M. Anti-Fouling Poly(2-Hydroxyethyl Methacrylate) Surface Coatings with Specific Bacteria Recognition Capabilities. *Surf. Sci.* **2009**, *603*, 2422–2429.
11. Liu, Q.; Singh, A.; Lalani, R.; Liu, L. Ultralow Fouling Polyacrylamide on Gold Surfaces *via* Surface-Initiated Atom Transfer Radical Polymerization. *Biomacromolecules* **2012**, *13*, 1086–1092.
12. Fruijtier-Pölloth, C. Safety Assessment on Polyethylene Glycols (PEGs) and Their Derivatives as Used in Cosmetic Products. *Toxicology* **2005**, *214*, 1–38.

13. Fahrländer, E.; Schelhaas, S.; Jacobs, A. H.; Langer, K. PEGylated Human Serum Albumin (HSA) Nanoparticles: Preparation, Characterization and Quantification of the PEGylation Extent. *Nanotechnology* **2015**, *26*, 145103.
14. Prime, K. L.; Whitesides, G. M. Adsorption of Proteins onto Surfaces Containing End-Attached Oligo(Ethylene Oxide): A Model System Using Self-Assembled Monolayers. *J. Am. Chem. Soc.* **1993**, *115*, 10714–10721.
15. Chen, J.; Wang, J.; Qi, P.; Li, X.; Ma, B.; Chen, Z.; Li, Q.; Zhao, Y.; Xiong, K.; Maitz, M. F.; *et al.* Biocompatibility Studies of Poly(Ethylene Glycol)-Modified Titanium for Cardiovascular Devices. *J. Bioact. Compat. Polym.* **2012**, *27*, 565–584.
16. Moulay, S. Dopa/Catechol-Tethered Polymers: Dioadhesives and Biomimetic Adhesive Materials. *Polym. Rev.* **2014**, *54*, 436–513.
17. Sedó, J.; Saiz-Poseu, J.; Busqué, F.; Ruiz-Molina, D. Catechol-Based Biomimetic Functional Materials. *Adv. Mater.* **2013**, *25*, 653–701.
18. Ryu, J. H.; Lee, Y.; Kong, W. H.; Kim, T. G.; Park, T. G.; Lee, H. Catechol-Functionalized Chitosan/Pluronic Hydrogels for Tissue Adhesives and Hemostatic Materials. *Biomacromolecules* **2011**, *12*, 2653–2659.
19. Li, L.; Yan, B.; Yang, J.; Huang, W.; Chen, L.; Zeng, H. Injectable Self-Healing Hydrogel with Antimicrobial and Antifouling Properties. *ACS Appl. Mater. Interfaces* **2017**, *9*, 9221–9225.
20. Shin, E.; Ju, S. W.; An, L.; Ahn, E.; Ahn, J. S.; Kim, B. S.; Ahn, B. K. Bioinspired Catecholic Primers for Rigid and Ductile Dental Resin Composites. *ACS Appl. Mater. Interfaces* **2018**, *10*, 1520–1527.
21. Sungbaek, Seo; Dong Woog, Lee; Jin Soo, Ahn; Keila, Cunha; Emmanouela, Filippidi; Sung Won, Ju; Eeseul, Shin; Byeong-Su, Kim; Zachary, A. Levine; Roberto, D. Lins; Jacob, N. Israelachvili; J. Herbert, Waite; Megan, T. Valentine; Joan, Emma, Shea; Ahn, B. K. Significant Performance Enhancement of Polymer Resins by Bioinspired Dynamic Bonding. *Adv. Mater.* **2017**.
22. Wilms, V. S.; Bauer, H.; Tonhauser, C.; Schilman, A. M.; Müller, M. C.; Tremel, W.; Frey, H. Catechol-Initiated Polyethers: Multifunctional Hydrophilic Ligands for Pegylation and Functionalization of Metal Oxide Nanoparticles. *Biomacromolecules* **2013**, *14*, 193–199.
23. Thomas, A.; Bauer, H.; Schilman, A. M.; Fischer, K.; Tremel, W.; Frey, H. The “Needle in the Haystack” Makes the Difference: Linear and Hyperbranched Polyglycerols with a Single Catechol Moiety for Metal Oxide Nanoparticle Coating. *Macromolecules* **2014**, *47*, 4557–4566.
24. Chaicham, A.; Sahasithiwat, S.; Tuntulani, T.; Tomapatanaget, B. Highly Effective Discrimination of Catecholamine Derivatives via FRET-on/off Processes Induced by the Intermolecular Assembly with Two Fluorescence Sensors. *Chem. Commun.* **2013**, *49*, 9287.
25. Liu, S.; Chen, L.; Tan, L.; Cao, F.; Bai, L.; Wang, Y. A High Efficiency Approach for a

- Titanium Surface Antifouling Modification: PEG-o-Quinone Linked with Titanium via Electron Transfer Process. *J. Mater. Chem. B* **2014**, *2*, 6758–6766.
26. Kim, H. S.; Ham, H. O.; Son, Y. J.; Messersmith, P. B.; Yoo, H. S. Electrospun Catechol-Modified Poly(Ethyleneglycol) Nanofibrous Mesh for Anti-Fouling Properties. *J. Mater. Chem. B* **2013**, *1*, 3940.
 27. Kang, T.; Banquy, X.; Heo, J.; Lim, C.; Lynd, N. A.; Lundberg, P.; Oh, D. X.; Lee, H. K.; Hong, Y. K.; Hwang, D. S.; *et al.* Mussel-Inspired Anchoring of Polymer Loops That Provide Superior Surface Lubrication and Antifouling Properties. *ACS Nano* **2016**, *10*, 930–937.
 28. Lee, H.; Lee, K. D.; Pyo, K. B.; Park, S. Y.; Lee, H. Catechol-Grafted Poly(Ethylene Glycol) for PEGylation on Versatile Substrates. *Langmuir* **2010**, *26*, 3790–3793.
 29. Patil, N.; Falentin-Daudré, C.; Jérôme, C.; Detrembleur, C. Mussel-Inspired Protein-Repelling Ambivalent Block Copolymers: Controlled Synthesis and Characterization. *Polym. Chem.* **2015**, *6*, 2919–2933.
 30. Duan, J.; Wu, W.; Wei, Z.; Zhu, D.; Tu, H.; Zhang, A. Synthesis of Functional Catechols as Monomers of Mussel-Inspired Biomimetic Polymers. *Green Chem.* **2018**, *20*, 912–920.
 31. Divandari, M.; Morgese, G.; Trachsel, L.; Romio, M.; Dehghani, E. S.; Rosenboom, J. G.; Paradisi, C.; Zenobi-Wong, M.; Ramakrishna, S. N.; Benetti, E. M. Topology Effects on the Structural and Physicochemical Properties of Polymer Brushes. *Macromolecules* **2017**, *50*, 7760–7769.
 32. Li, L.; Yan, B.; Zhang, L.; Tian, Y.; Zeng, H. Mussel-Inspired Antifouling Coatings Bearing Polymer Loops. *Chem. Commun.* **2015**, *51*, 15780–15783.
 33. Dalsin, J. L.; Lin, L.; Tosatti, S.; Vörös, J.; Textor, M.; Messersmith, P. B. Protein Resistance of Titanium Oxide Surfaces Modified by Biologically Inspired MPEG-DOPA. *Langmuir* **2005**, *21*, 640–646.
 34. Niederer, K.; Schüll, C.; Leibig, D.; Johann, T.; Frey, H. Catechol Acetonide Glycidyl Ether (CAGE): A Functional Epoxide Monomer for Linear and Hyperbranched Multi-Catechol Functional Polyether Architectures. *Macromolecules* **2016**, *49*, 1655–1665.
 35. Shin, E.; Kim, B.-S. Mussel-Inspired Polyglycerol : Synthesis and Versatile Surface Modification. *Master Thesis, Ulsan Natl. Inst. Sci. Technol.* **2015**.
 36. Güclü, D.; Rale, M.; Fessner, W. D. Modular Synthesis of Dihydroxyacetone Monoalkyl Ethers and Isosteric 1-Hydroxy-2-Alkanones. *European J. Org. Chem.* **2015**, *2015*, 2960–2964.
 37. Misaka, H.; Tamura, E.; Makiguchi, K.; Kamoshida, K.; Sakai, R.; Satoh, T.; Kakuchi, T. Synthesis of End-Functionalized Polyethers by Phosphazene Base-Catalyzed Ring-Opening Polymerization of 1,2-Butylene Oxide and Glycidyl Ether. *J. Polym. Sci. Part A Polym. Chem.* **2012**, *50*, 1941–1952.
 38. Ishida, N.; Biggs, S. Effect of Grafting Density on Phase Transition Behavior for Poly(N-

- Isopropylacryamide) Brushes in Aqueous Solutions Studied by AFM and QCM-D.
Macromolecules **2010**, *43*, 7269–7276.
39. Israelachvili, J.; Min, Y.; Akbulut, M.; Alig, A.; Carver, G.; Greene, W.; Kristiansen, K.; Meyer, E.; Pesika, N.; Rosenberg, K.; *et al.* Recent Advances in the Surface Forces Apparatus (SFA) Technique. *Reports Prog. Phys.* **2010**, *73*, 036601.
 40. Yoo, J.; Birke, A.; Kim, J.; Jang, Y.; Song, S. Y.; Ryu, S.; Kim, B.-S.; Kim, B.-G.; Barz, M.; Char, K. Cooperative Catechol-Functionalized Polypept(o)ide Brushes and Ag Nanoparticles for Combination of Protein Resistance and Antimicrobial Activity on Metal Oxide Surfaces. *Biomacromolecules* **2018**, acs.biomac.8b00135.
 41. Al-Shakhshir, R. H.; Regnier, F. E.; White, J. L.; Hem, S. L. Contribution of Electrostatic and Hydrophobic Interactions to the Adsorption of Proteins by Aluminium-Containing Adjuvants. *Vaccine* **1995**, *13*, 41–44.
 42. Yang, Z.; Galloway, J. A.; Yu, H. Protein Interactions with Poly(Ethylene Glycol) Self-Assembled Monolayers on Glass Substrates: Diffusion and Adsorption. *Langmuir* **1999**, *15*, 8405–8411.
 43. Sheth, S. R.; Leckband, D. Measurements of Attractive Forces between Proteins and End-Grafted Poly(Ethylene Glycol) Chains. *Proc. Natl. Acad. Sci. U. S. A.* **1997**, *94*, 8399–8404.
 44. Bosker, W. T. E.; Iakovlev, P. A.; Norde, W.; Cohen Stuart, M. A. BSA Adsorption on Bimodal PEO Brushes. *J. Colloid Interface Sci.* **2005**, *286*, 496–503.
 45. Benetti, E. M.; Divandari, M.; Ramakrishna, S. N.; Morgese, G.; Yan, W.; Trachsel, L. Loops and Cycles at Surfaces: The Unique Properties of Topological Polymer Brushes. *Chem. - A Eur. J.* **2017**, *23*, 12433–12442.
 46. Morgese, G.; Trachsel, L.; Romio, M.; Divandari, M.; Ramakrishna, S. N.; Benetti, E. M. Topological Polymer Chemistry Enters Surface Science: Linear versus Cyclic Polymer Brushes. *Angew. Chemie - Int. Ed.* **2016**, *55*, 15583–15588.

Chapter 4. Synergistic adhesion properties of catechol and amine functionalized polyether

4.1 Introduction

Mussel is attracted its adhesive properties to adhere to rough and wet surfaces. Even though synthetic adhesives lose their properties underwater, mussels strongly bind to various surfaces in seawater and endure strong waves. Therefore, the adhesion mechanism of mussel foot protein (mfp) has been extensively studied during the past decades. The unique feature of this interfacial protein is their high contents of catecholic amino acid, L-3,4-dihydroxyphenylalanine (DOPA), which is synthesized by posttranslational modification of tyrosine. DOPA, especially catechol moiety has pivotal role for the cross-linking of the reaction of cohesive curing and adhesive surface bonding.

In actuality, mfp contains a high portion of cationic amino acids as well as DOPA (i.e. mfp-5 contains cationic acid up to 28%), which are frequently in adjacent positions.¹ Recently, Waite et al. revealed that cationic group of mussel protein displaces positively charged salt ion from the anionic surface.^{2,3} This study showed that lysine is a key of wet adhesion which prepare the surface to form interfacial bonds for catechol moieties. Moreover, different research groups also showed that incorporation of the cationic group improves the adhesive property in simulated seawater or saline.⁴ However, most of the studies remained in the single molecular system although synergistic wet-adhesion of catechol and amine can offer the great potential to high-performance underwater adhesive materials.

Our approach to providing the extended study about the role of amine and catechol is incorporating primary amine and catechol to the polymer system, which allows the mimic of neighboring lysine residue and Dopa. Furthermore, we adopted the functional groups to epoxide monomer and polymerized using anionic ring opening polymerization. The resulting polymer has a polyether backbone, which renders water solubility and flexibility.⁵ Random copolymers with the various ratio of catechol and amine were prepared and surface interaction with different pH as demonstrated.

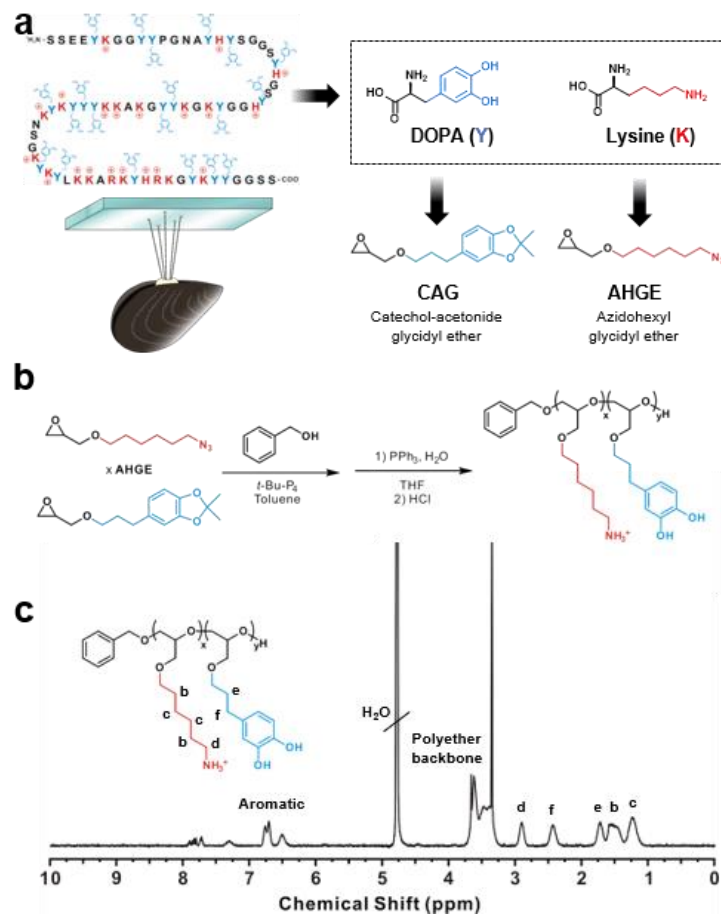


Figure 4.1. (a) Primary sequence of mfp-5 and Structure of mussel-inspired functional epoxide monomers. (b) Synthesis of amine and catechol functionalized copolymer. (c) ^1H NMR spectra of amine and catechol functionalized copolymer (AC1)

4.2. Materials and methods

Reagents. *p*-toluene sulfonic acid monohydrate (*p*-TsOH), lithium aluminum hydride (LiAlH₄), epichlorohydrin (ECH), tetrabutylammonium bromide (TBAB), phosphazene base *t*-Bu-P₄ solution (~0.8 M in hexane), 6-chloro-1-hexanol, triphenylphosphine, and toluene were obtained from Sigma-Aldrich. 3, 4-Dihydroxyhydrocinnamic acid (C-COOH), 2, 2-dimethoxypropane (DMP), sodium azide, anhydrous methanol, and aluminum oxide were obtained from Alfa-Aesar. Diethyl ether and 50% sodium hydroxide aqueous solution were obtained from Daejung. Ethyl acetate, hexane, and methanol were purchased from SK chemical. All deuterated NMR solvents in this experiment (CDCl₃, D₂O) were obtained from Cambridge Isotope Laboratories. All chemicals were analytical reagents grade and used without purification unless otherwise indicated.

Instruments. ¹H NMR spectra were measured at 400 MHz (298K) with VNMRS 400 spectrometer. All spectra were recorded using tetramethylsilane (TMS) as an internal standard. SEC measurements (Agilent 1200 series) were performed using DMF solvent as an eluent at 40 °C with a constant flow rate of 1.0 mL/min using a refractive index (RI) detector. For calibration, the poly(methyl methacrylate) standard were used to calculate the number- and weight-averaged molecular weight (*M_n* and *M_w*). Matrix-assisted laser desorption and ionization time-of-flight (MALDI-TOF) mass spectrometry were performed using LRF 20 (Bruker Daltonics). The surface interaction was studied using SFA 2000 (Surforce LLC, Santa Barbara, CA, USA).

Synthesis of catechol acetone glycidyl ether (CAG). See experimental details in Part 3.

Synthesis of 6-azido-1-hexanol. A round bottom flask was filled with 6-chloro-1-hexanol (109.8 mmol, 1 equiv), 22 mL of water and sodium azide (164.7 mmol, 1.5 equiv), and stirred overnight under reflux condition. The desired product was extracted to organic layer using ethyl acetate and washed with water, brine, and dried over Na₂SO₄ and the excess solvent was evaporated under reduced pressure to give a yellowish liquid. Yield: 98%. ¹H NMR (400 MHz, CDCl₃): δ [ppm] 3.65 (t, *J* = 6.5 Hz, 2H), 3.27 (t, *J* = 6.9 Hz, 2H), 1.67 – 1.53 (m, 4H), 1.49 – 1.32 (m, *J* = 4.6, 3.8, 1.8 Hz, 5H). ¹³C NMR (101 MHz, CDCl₃): δ [ppm] 62.66, 51.42, 32.56, 28.84, 26.56, 25.38.

Synthesis of azido hexyl glycidyl ether (AHGE). Tetrabutylammonium hydrogensulfate (TBAHSO₄) (3.44 mmol, 0.05 equiv) and epichlorohydrin (343.85 mmol, 5 equiv) were added to an aqueous KOH solution (40%) at 0 °C. The reaction mixture was stirred for 30 min and 6-azido-1-hexanol (68.77 mmol, 1 equiv) was slowly added to flask. The reaction was stirred overnight and

extracted with ethyl acetate and washed with water, brine, and dried over Na₂SO₄ and evaporated using rotary evaporator. The crude product was purified using silica gel column chromatography with an ethyl acetate/hexane (1:3 v/v) eluent to obtain AHGE. AHGE was distilled before polymerization to give the pure product. Yield: 55%. ¹H NMR (400 MHz, CDCl₃): δ [ppm] 3.72 (dd, *J* = 11.5, 3.0 Hz, 1H), 3.58 – 3.41 (m, 2H), 3.37 (dd, *J* = 11.5, 5.8 Hz, 1H), 3.27 (t, *J* = 6.9 Hz, 2H), 3.19 – 3.08 (m, *J* = 5.8, 4.1, 2.9 Hz, 1H), 2.80 (dd, *J* = 5.0, 4.2 Hz, 1H), 2.61 (dd, *J* = 5.0, 2.7 Hz, 1H), 1.65 – 1.54 (m, 4H), 1.45 – 1.34 (m, 4H). ¹³C NMR (101 MHz, CDCl₃): δ [ppm] 71.57, 71.45, 51.44, 50.94, 44.32, 29.61, 28.85, 26.61, 25.75. ESI-MS (*m/z*): [M+Na]⁺ calcd for C₉H₁₇N₃O₂Na, 199.13; found, 222.04

Synthesis of azide-catechol copolymers. A series of the azide-catechol functionalized polymer was prepared using anionic ring-opening polymerization with altering the mole ratio of AHGE and CAG. Exemplified for AC1. A flask was purged with nitrogen and benzyl alcohol (0.3 mmol, 1 equiv) was added into the flask. Phosphazene base, t-Bu-P₄ (0.3 mmol, 1 equiv) and 2 mL of toluene was added stirred for 30 min. The flask heated up to 60 °C, CAG monomer (1.5 mmol, 5 equiv) and AHGE monomer (4.5 mmol, 15 equiv) was slowly added and the mixture was stirred overnight. The polymerization was quenched with excess amount of benzoic acid and the resulting polymer was purified using alumina column with THF. The solution was precipitated into excess cold hexane to give P(AHGE-*co*-CAG).

Deprotection of azide and protected catechol functionalized copolymers. AC1 (100 mg, 0.30 mmol of azide, 1 equiv) was dissolved in 1 mL of THF and the solution was degassed by N₂ bubbling for 20 min. Triphenylphosphine (0.60 mmol, 2 equiv) was completely dissolved in the solution. Water (0.05 mL) was added to the mixture and the solution was stirred for 12 h at room temperature. THF was removed using rotary evaporator and 1.0 M HCl solution was added to acidify and remove acetonide group of the polymer. The mixture was stirred for 3 h at 40 °C. Then the solution was washed 3 times with diethyl ether to remove residual triphenylphosphine and triphenylphosphine oxide. The aqueous phase was lyophilized to give viscous polymer.

Surface force apparatus. The SFA 2000 (Surforce LLC, Santa Barbara, CA, USA) was used in this study. The experiment was conducted in an environment pH 3 and pH 7 DI water titrated with HCl and NaOH. The surface is prepared in a sample with a back-silvered thin mica sheet attached to a cylindrical disk (*R* = 2 cm). Catechol-amine surface was prepared by drop-casting 0.1 mg/mL polymer solution dissolved in pH 3 buffer on smooth mica surface for 10 minutes and then washing with pH 3 buffer. The experiment was carried out at room temperature and at each pH condition, the buffer was injected between the two surfaces and equilibrated for 1 hour.

The interaction between the two surfaces can be measured as a function of the distance (D) between the two surfaces and the Derjaguin approximation, $W = F / 2\pi R$, is used because D approaches much smaller than R . The measured adhesion F_{ad} was converted to adhesion energy per area W_{ad} between two flat surfaces based on the Johnson-Kendall-Roberts (JKR) theory, $W_{ad} = F_{ad} / 1.5\pi R$.

The two surfaces were contacted for 2 minutes and 1 hour and then separated to investigate changes in surface adhesion with each pH environment and contact time. Experiments were carried out at pH 3 and repeated after the buffer was changed to pH 7 buffer.

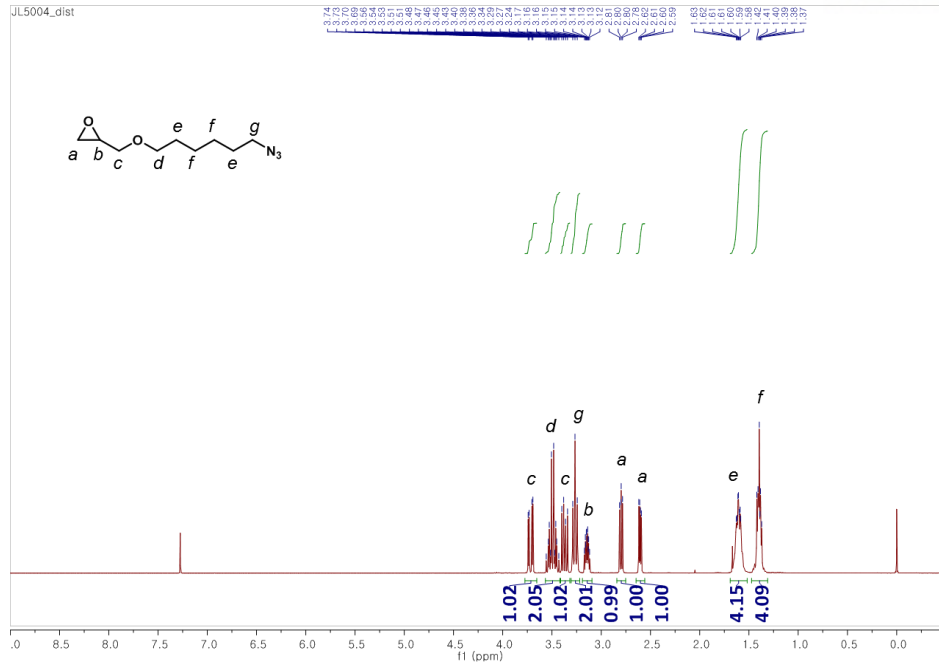


Figure 4.2. ^1H NMR spectrum of AHGE

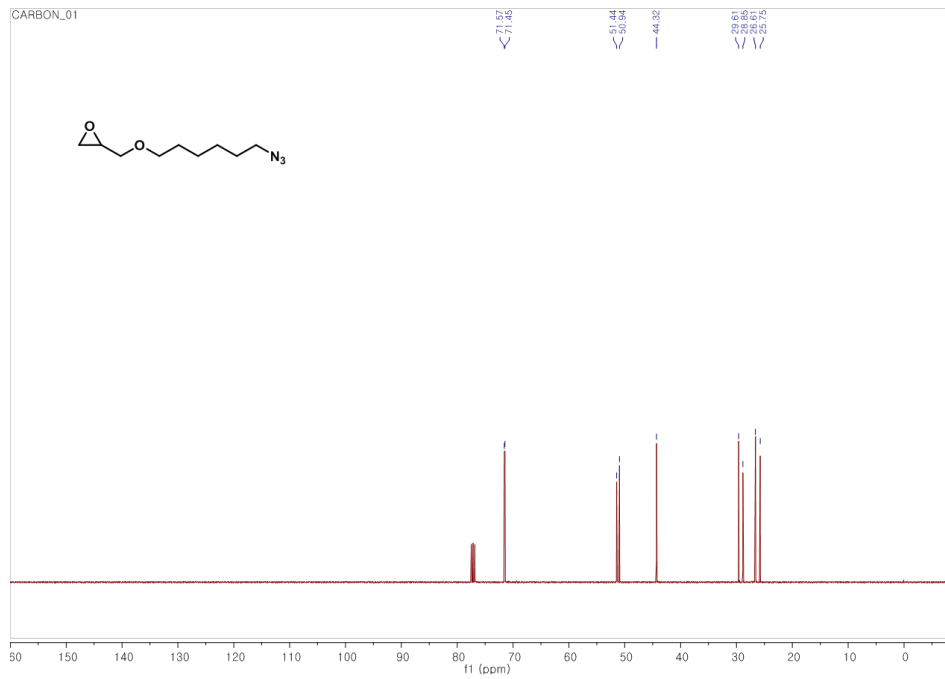


Figure 4.3. ^{13}C NMR spectrum of AHGE

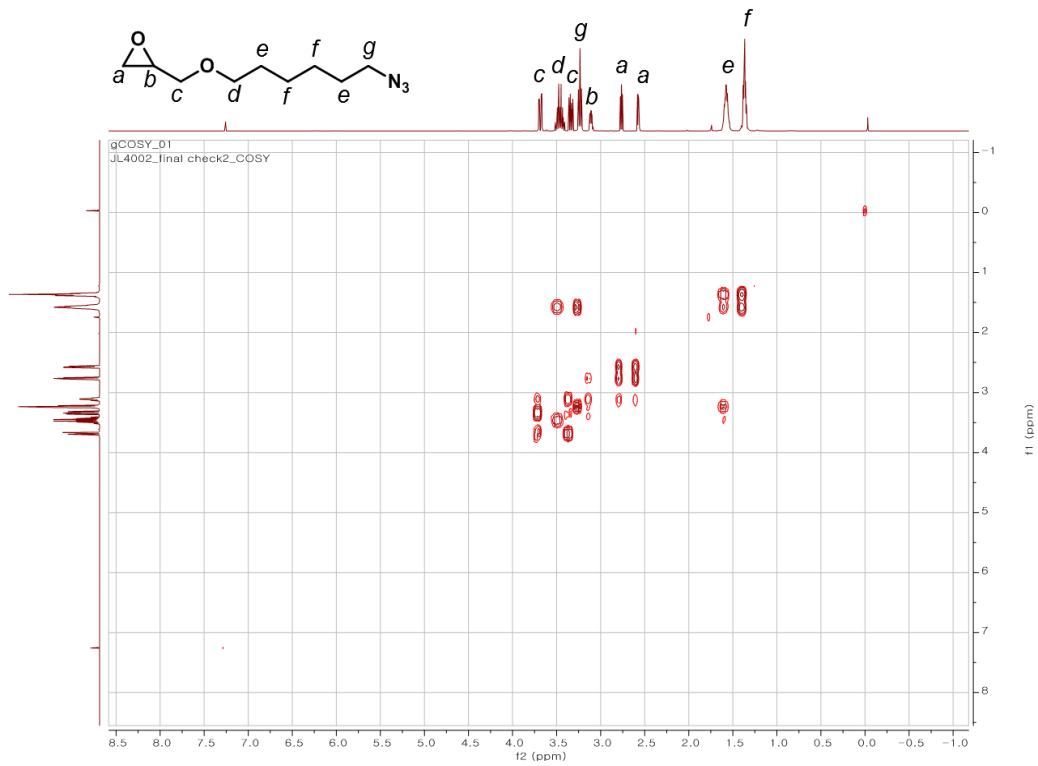


Figure 4.4. ^1H - ^1H COSY NMR spectrum of AHGE in CDCl_3

4.3. Results and discussion

4.3.1 Polymerization

In order to explore the synergistic adhesion of lysine and DOPA, lysine inspired monomer (azidohexyl glycidyl ether, AHGE) and catechol inspired monomer (catechol acetonide glycidyl ether, CAG) was prepared (Figure 4.1a). Azide group and acetonide protected catechol was incorporated to epoxide due to the reactivity of amine and catechol under basic condition. The successful synthesis of AHGE and CAG was convinced via ^1H - and ^{13}C -NMR (Figure 4.2-4.4). The azide and protected catechol functionalized random copolymer (poly[AHGE-*co*-CAG], *AC) was synthesized using AROP of AHGE and CAG. As shown in Figure 4.5, *AC show resonance peaks of protected catechol, azide and polyether backbone. The degree of polymerization was fixed to 20 to eliminate the effect of molecular weight such as wetting, viscosity, and chain entanglement.⁶ Five polymers were synthesized by controlling the composition of AHGE and CAG. From *AC0 to *AC4, the catechol contents increase from 0 to 100%.

The resulting copolymers were characterized by ^1H NMR spectroscopy, size exclusion chromatography (SEC) and matrix-assisted laser desorption/ionization time-of-flight (MALDI-TOF). The average molecular weight of the polymer was around 5,000 and dispersity fell between 1.2 and 1.5. The azide functional group of the resulting polymer was reduced to a primary amine by Staudinger reduction and hydrogen chloride was treated to protonate amine and remove acetonide protecting group of catechol (Figure 4.1c). Unfortunately, AC4 was insoluble in water due to the hydrophobicity of the catechol side chain. Hence the subsequent experiments were conducted using AC0 to AC3.

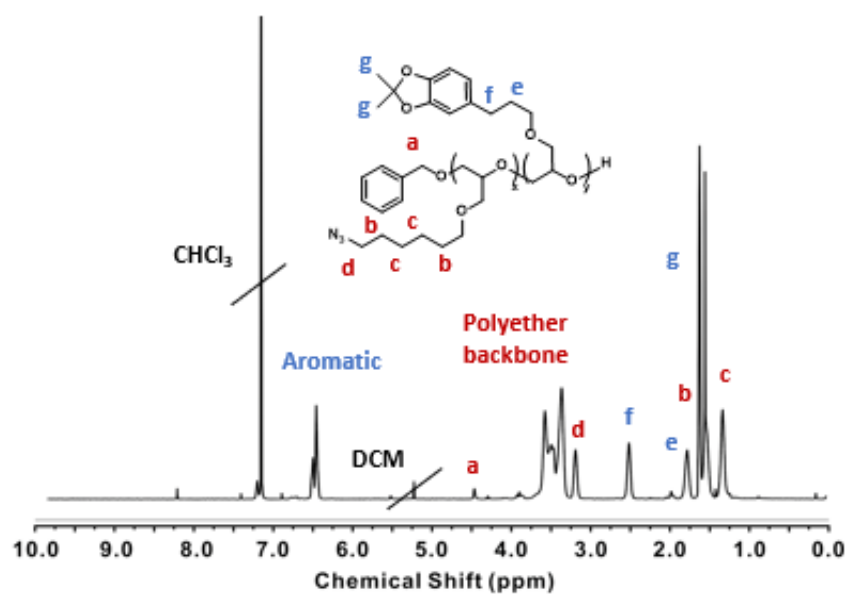


Figure 4.5. ^1H NMR spectrum of AC1 before deprotection

Table 4.1 Characterization of azide and protected catechol-functionalized polymers

Polymer	AHGE	CAG	$M_{n,\text{NMR}}^a$	$M_{n,\text{SEC}}^b$	$\text{DP}_{\text{NMR}} (\text{A/C})^a$	\bar{D}^b
AC0	20	0	4890	5800	24.0/0.0	1.24
AC1	15	5	5400	4190	16.1/5.2	1.30
AC2	10	10	4550	3560	9.8/9.3	1.44
AC3	5	15	4870	5010	5.5/16.6	1.25
AC4	0	20	5820	5290	0.0/21.6	1.28

$^aM_{n,\text{NMR}}$ and composition of the copolymer were determined via ^1H NMR in CDCl_3 , $^bM_{n,\text{SEC}}$ and $\bar{D}(M_w/M_n)$ was measured by SEC analysis with PMMA standards in DMF.

4.3.2. Surface interaction measurement

The interaction forces of the polymer were investigated by using a surface force apparatus (SFA). SFA has been used to measure the absolute distance and interaction force between two macroscopic surfaces with resolutions of 0.1 nm and 10 nN, respectively.⁷

In nature, mussel foot protein secreted under acidic pH during mussel plaque formation to limit Dopa oxidation.⁸ The AC polymer also deposited on the mica surface with pH 3 buffer to minimize the auto-oxidation. To probe the effect of polymer composition on cohesion behavior, the polymer solution in pH 3 buffer was symmetrically deposited on both mica surfaces. Due to the steric hindrance of the side chain, part of the catechol moieties in the adsorbed polymer is bound to a mica surface, and unbound catecholic functional groups are capable of bonding to other surfaces or forming multiple layers. Cohesion between two polymers was mediated by cation- π interaction between catechol and amine, π - π interaction between catechol and catechol and H-bonding interaction (Figure 4.6a).⁹⁻¹¹ The representative force-distance curves of AC1 are shown in Figure 4.6b. The polymer films adsorbed at pH 3 exhibited a thin hard wall thickness of ~ 5 nm. The cohesion at pH 3 was E_{ad} 29.0 mJ/m² and increased to 34.7 mJ/m² after 1 h contact time because longer contact allows better interfacial equilibration.

When the intervening buffer was changed to pH 7, the stronger cohesion was obtained. In pH 7, cohesion was increased after 1 h which indicates that there is no defect on the polymer layer during the experiment. Moreover, AC1 exhibited significantly higher attraction force after pH elevation (41.7 mJ/m²). Previous research shows that mfp-5 and mfp3 exhibit a significant reduction in adhesion even when distributed at pH 5.5 due to the Dopa oxidation.^{12,13} However, two symmetric AC1 films already deposited under acidic condition and reduced Coulombic repulsion due to the increment of pH may be responsible.¹⁴

The cohesion of AC polymers with different contact time and pH is shown in Figure 4.6c. AC1 which has 25 mol% catechol exhibited the strongest cohesion at both pH 3 and pH 7. The cohesion was not proportional to catechol contents which demonstrate that the existence of amine with proper composition is required. Interestingly, the effect of pH was maximized when the catechol content is 50 mol%, while AC0 without catechol did not show a significant increase. The result suggests that the primary amine group of AC polymer was expected to be crosslinked with oxidized catechol via Michael addition reaction.^{15,16} When the intervening buffer was changed to pH 2 buffer, the cohesion was not fully reduced ($E_{ad} \sim 19.7$ mJ/m²) which indicates that the cohesion of AC is not only affected by non-covalent crosslinking.

Whereas the cohesion interaction was mediated by two polymer layers, adhesion force was measured between the polymer layer and mica surface as an asymmetric test. A bidentate H-bond of

the catecholic hydroxyl group or amine group with the surface oxygen atom of mica and electrostatic interaction of amine seems the reasonable chemical basis for interaction (Figure 4.6a).¹⁷ The adhesion of AC1 was also contact time-dependent, the adhesion was E_{ad} 11.9 mJ/m² increased to 17.3 mJ/m² after 1 h contact time. After the pH of the intervening buffer was elevated to pH 7, adhesion was improved and still exhibit increment after 1 h contact time (23.8 mJ/m²).

The adhesion of AC polymers with different contact time and pH is shown in Figure 4.6d. The adhesion at pH 3 with various composition tend to be different from the symmetric test. There was no additive effect and adhesion slightly improved when the content of catechol is increased. However, the pH increment effectively enhances the adhesion when the catechol and amine were incorporated simultaneously. Therefore, AC1 exhibited the strongest adhesion at pH 7.

Although adhesion of AC1 at pH 7 is 2-fold lower than the interaction energy of cohesion test, the value was comparable to the adhesion of mfp-5.¹² Furthermore, the amine-catechol functionalized polymer exhibited strong wet-cohesion (at least 10-fold greater than mfp-5 even under pH 3) which demonstrate the potential as a high-performance wet-adhesive.

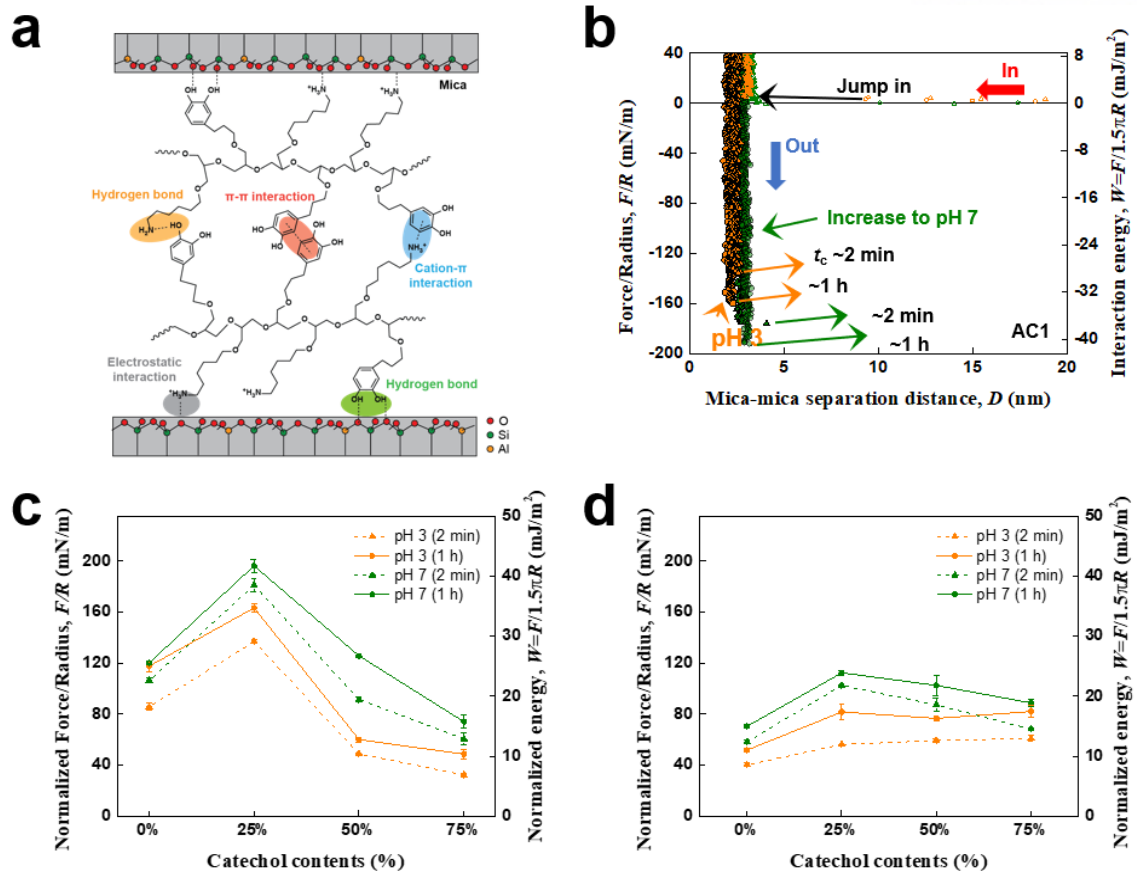


Figure 4.6. (a) Schematic representation of adhesion and cohesion mechanism of amine and catechol functionalized polymer with mica substrate. (b) Representative force-distance curves of AC1 (0.1 mg mL⁻¹). Effect of pH and contact time on Interaction energy of AC polymers with different catechol contents in (c) symmetric mode and (d) asymmetric mode.

0.1 mg/ml in pH 3 solution, 10 m coating
Force measured at pH 3 → pH 7 → pH 2

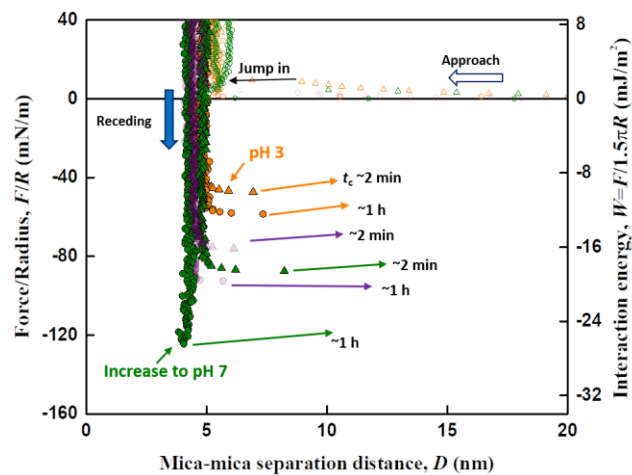


Figure 4.7. Representative force-distance curves of AC1 (0.1 mg mL⁻¹) with different pH.

4.4. Conclusion

In conclusion, catechol and amine functionalized polymer was prepared to study the synergistic adhesion of DOPA and lysine. The protected catechol and azide functionalized epoxide monomer were synthesized and polymerized using AROP. The surface interaction of copolymers with different amine-catechol ratio was measured by SFA. Through optimizing the ratio between catechol and amine, the polymer film deposited onto mica exhibits both strong adhesion and cohesion. Moreover, the elevated pH after deposition enhances the surface interaction that is rarely found phenomena in previous studies. This study provides the insight to design mussel-inspired synthetic adhesive material.

4.5. References

1. Waite, J. H.; Qin, X. Polyphosphoprotein from the Adhesive Pads of *Mytilus Edulis*. *Biochemistry* **2001**, *40*, 2887–2893.
2. Maier, G. P.; Rapp, M. V.; Waite, J. H.; Israelachvili, J. N.; Butler, A. Adaptive Synergy between Catechol and Lysine Promotes Wet Adhesion by Surface Salt Displacement. *Science (80-.)*. **2015**, *349*, 628–632.
3. Rapp, M. V.; Maier, G. P.; Dobbs, H. A.; Higdon, N. J.; Waite, J. H.; Butler, A.; Israelachvili, J. N. Defining the Catechol-Cation Synergy for Enhanced Wet Adhesion to Mineral Surfaces. *J. Am. Chem. Soc.* **2016**, *138*, 9013–9016.
4. White, J. D.; Wilker, J. J. Underwater Bonding with Charged Polymer Mimics of Marine Mussel Adhesive Proteins. *Macromolecules* **2011**, *44*, 5085–5088.
5. Klein, R.; Wurm, F. R. Aliphatic Polyethers: Classical Polymers for the 21st Century. *Macromol. Rapid Commun.* **2015**, *36*, 1147–1165.
6. Wei, W.; Yu, J.; Gebbie, M. A.; Tan, Y.; Martinez Rodriguez, N. R.; Israelachvili, J. N.; Waite, J. H. Bridging Adhesion of Mussel-Inspired Peptides: Role of Charge, Chain Length, and Surface Type. *Langmuir* **2015**, *31*, 1105–1112.
7. Israelachvili, J.; Min, Y.; Akbulut, M.; Alig, A.; Carver, G.; Greene, W.; Kristiansen, K.; Meyer, E.; Pesika, N.; Rosenberg, K.; *et al.* Recent Advances in the Surface Forces Apparatus (SFA) Technique. *Reports Prog. Phys.* **2010**, *73*, 036601.
8. Rodriguez, N. R. M.; Das, S.; Kaufman, Y.; Israelachvili, J. N.; Waite, J. H. Interfacial PH during Mussel Adhesive Plaque Formation. *Biofouling* **2015**, *31*, 221–227.
9. Gallivan, J. P.; Dougherty, D. A. A Computational Study of Cation- π Interactions vs Salt Bridges in Aqueous Media: Implications for Protein Engineering. *J. Am. Chem. Soc.* **2000**, *122*, 870–874.
10. Waite, J. H. Reverse Engineering of Bioadhesion in Marine Mussels. *Ann. N. Y. Acad. Sci.* **1999**, *875*, 301–309.
11. Schnurrer, J.; Lehr, C. M. Mucoadhesive Properties of the Mussel Adhesive Protein. *Int. J. Pharm.* **1996**, *141*, 251–256.
12. Hammer, M. U.; Danner, E. W.; Kan, Y.; Waite, J. H.; Israelachvili, J. N. Adhesion of Mussel Foot Protein Mefp-5 to Mica: An Underwater Superglue. *Biochemistry* **2012**, *51*, 6511–6518.
13. Yu, J.; Wei, W.; Danner, E.; Israelachvili, J. N.; Waite, J. H. Effects of Interfacial Redox in Mussel Adhesive Protein Films on Mica. *Adv. Mater.* **2011**, *23*, 2362–2366.
14. Seo, S.; Das, S.; Zalicki, P. J.; Mirshafian, R.; Eisenbach, C. D.; Israelachvili, J. N.; Waite, J. H.; Ahn, B. K. Microphase Behavior and Enhanced Wet-Cohesion of Synthetic

- Copolyampholytes Inspired by a Mussel Foot Protein. *J. Am. Chem. Soc.* **2015**, *137*, 9214–9217.
15. Zhang, chao; Xiang, L.; Zhang, J.; Gong, L.; Han, L.; Xu, Z.-K.; Zeng, H. Tough and Alkaline-Resistant Mussel-Inspired Wet Adhesion with Surface Salt Displacement via Polydopamine-Amine Synergy. *Langmuir* **2019**, acs.langmuir.9b00559.
 16. Yang, J.; Saggiomo, V.; Velders, A. H.; Stuart, M. A. C.; Kamperman, M. Reaction Pathways in Catechol/Primary Amine Mixtures: A Window on Crosslinking Chemistry. *PLoS One* **2016**, *11*, 1–17.
 17. Lu, Q.; Danner, E.; Waite, J. H.; Israelachvili, J. N.; Zeng, H.; Hwang, D. S. Adhesion of Mussel Foot Proteins to Different Substrate Surfaces. *J. R. Soc. Interface* **2013**, *10*.

Chapter 5. Summary

Due to the fascinating adhesion property of mussel, there are various synthetic materials bearing the catechol functional group inspired by mussel foot protein. However, the binding mechanism of mussel foot protein is not fully understood, and the development of wet-adhesive synthetic materials is still challenging. Therefore, this thesis describes the synthesis of catechol-functionalized materials and their applications.

First, the catechol functionalized bifunctional molecule was adopted to dental applications. The catechol moieties can bind to hydrophilic substrates with hydrogen bond while other chain end crosslinked with (meth)acrylate-based polymers. The dental materials using catechol functionalized molecule exhibited comparable mechanical strength with a commercial product, which demonstrates the potential of catechol as dental applications. Second, the catechol group was incorporated to epoxide monomer and polymerized using PEG as initiator. The catechol functionalized monomer enables to control the molecular weight and catechol contents in resulting polymers and successfully immobilized PEG on the various substrate. Finally, the catechol-amine functionalized polymer was synthesized. Synergistic wet-adhesion of Dopa and lysine was demonstrated using polyether system with various catechol contents. The catechol-amine functionalized polymer shows strong wet-adhesion which exceed the interaction energy of mussel foot protein.

The mussel-inspired materials, especially catechol incorporated system have the potential for future adhesive. Besides the biomedical applications covered in this thesis, we anticipate that the catechol-based materials can be applied to other fields.

Lists of publications

1. **Eeseul Shin,**[†] Chanoong Lim,[†] Joonhee Lee, Jinwoo Park, Dong Woog Lee,* and Byeong-Su Kim* "Synergistic adhesion of catechol and amine" *Manuscript in preparation*
2. **Eeseul Shin,**[†] Chanoong Lim,[†] Minseong Kim, Jinwoo Park, Uk Jung Kang, Dongseok Kim, Chunggi Baig,* Dong Woog Lee,* and Byeong-Su Kim* "Bioinspired Bifunctional Block-Copolymers with superior antifouling properties" *Manuscript in preparation*
3. Ayaka Seto, Rika Kajiwara, Jaeun Song, **Eeseul Shin,** Byeong-Su Kim, Hisayoshi Kofujita, Yoshiyuki Oishi, and Yuji Shibasaki* "Preparation of glycoside polymer micelles with antioxidant polyphenolic cores using alkylated poly(arbutin)s" *RSC Advances* **2019**, *9*, 7777
4. **Eeseul Shin,**[†] Sung Won Ju,[†] Larry An, Eungjin Ahn, Jin-Soo Ahn,* Byeong-Su Kim,* and B. Kollbe Ahn* "Bioinspired Catecholic Primers for Rigid and Ductile Dental Resin Composites" *ACS Applied Materials & Interfaces* **2018**, *10*, 1520-1527
5. Sungbaek Seo, Dong Woog Lee, Jin Soo Ahn, Keila Cunha, Emmanouela Filippidi, Sung Won Ju, **Eeseul Shin,** Byeong-Su Kim, Zachary A. Levine, Roberto D. Lins, Jacob N. Israelachvili, J. Herbert Waite, Megan T. Valentine, Joan Emma Shea, and B. Kollbe Ahn* "Significant performance enhancement of polymer resins by bioinspired dynamic bonding" *Advanced Materials* **2017**, *29*, 1703026
6. Suhyun Son, Haeree Park, **Eeseul Shin,** Yuji Shibasaki, and Byeong-Su Kim* "Architecture-Controlled Synthesis of Redox-Degradable Hyperbranched Polyglycerol Block Copolymers and the Structural Implications of Their Degradation" *Journal of Polymer Science, Part A: Polymer Chemistry* **2016**, *54*, 1752-1761
7. Yun Kyung Jung, **Eeseul Shin,** and Byeong-Su Kim* "Cell Nucleus-Targeting Zwitterionic Carbon Dots" *Scientific Reports* **2015**, *5*, 18807
8. Suhyun Son, **Eeseul Shin,** and Byeong-Su Kim* "Redox-Degradable Biocompatible Hyperbranched Polyglycerols: Synthesis, Copolymerization Kinetics, Degradation, and Biocompatibility" *Macromolecules* **2015**, *48*, 600-609
9. Daeun Kim, Yuri Choi, **Eeseul Shin,** Yun Kyung Jung, and Byeong-Su Kim* "Sweet nanodot for biomedical imaging: carbon dot derived from xylitol" *RSC Advances* **2014**, *4*, 23210-23213
10. Suhyun Son, **Eeseul Shin,** and Byeong-Su Kim* "Light-Responsive Micelles of Spiropyran Initiated Hyperbranched Polyglycerol for Smart Drug Delivery" *Biomacromolecules* **2014**, *15*, 628-634
11. Yun Kyung Jung, Taemin Lee, **Eeseul Shin,** and Byeong-Su Kim* "Highly Tunable Aptasensing Microarrays with Graphene Oxide Multilayers" *Scientific Reports* **2013**, *3*, 3367

Acknowledgements

석사 학위를 마치고 박사 학위를 이어가면서 두 번째 감사의 글을 쓰게 되었습니다. 먼저 박사 학위 동안에도 따뜻한 눈으로 지켜봐 주신 김병수 교수님께 깊은 감사를 드립니다. 여전히 부족한 점이 많지만, 학위 과정 동안 교수님의 가르침 덕에 다시없을 경험들을 하였고 성장할 수 있었습니다. 그리고 바쁘신 와중에도 시간 내주셔서 좋은 말씀 남겨 주신 이동욱 교수님, 박영석 교수님, 차채녕 교수님, 홍익대학교 최수형 교수님께도 감사의 말씀 올립니다. 특히 공동 연구를 진행하며 큰 가르침을 주고 계시는 이동욱 교수님, 짧은 시간이지만 많은 격려와 도움을 주신 Iwate University의 Yuji Shibasaki 교수님, 그리고 University of Central Florida 의 Kollbe Ahn 교수님께도 감사드립니다.

또한 학위 과정 동안 누구보다 많은 시간을 함께 했던 KBS group 여러분께도 감사드립니다. 지금은 랩을 떠나셨지만 대학원 생활 내내 정신적 지주가 되어 주신 선배님들, 유리 언니, 은용 오빠, 태민오빠 감사드립니다. 그리고 멋진 동기들인 응진 오빠와 캡틴 구민수, 함께 기쁨과 고생을 나뉘온 준희 오빠와 민주, 수고가 많은 방장 민성이와 (아마도) 차기 방장 태형이, 먼 곳에 있는 은별이, 항상 투닥대도 사이 좋아 보이는 동석이, 영주, 소희, 그리고 새내기 일오와 기환이에게도 고마움을 전합니다. 랩을 떠나면 지금처럼 함께할 순 없겠지만 모두 좋은 곳에 가서 즐겁게 지내면 좋겠습니다.

그리고 박사 과정 동안에도 동결 건조한 쿠키다스 같았던 저를 응원해주고 힘이 되어준 친구들, 특히 같이 학위 과정을 거치며 깊은 대화를 나누었던 동기들도 고맙습니다. 무엇보다도 학위 과정 뿐만 아니라 제 모든 인생에서 버팀목이 되어 주신 부모님과 자주 만나진 못해도 세상에 둘도 없는 남매인 아람이와 한철이, 서울에 와서도 외롭지 않게 챙겨 주시는 외할머니와 외할아버지께도 큰 사랑을 보냅니다.

